The Application of Statistical Mechanics on the Study of Selfish Behaviors in Transportation Networks and Energy Landscapes in Models of Combinatorial Optimization Problems

by

Po Ho Fai

A Thesis Submitted to

The Education University of Hong Kong

in Partial Fulfillment of the Requirements for

the Degree of Doctor of Philosophy

September, 2021

Statement of Originality

I, Po Ho Fai, hereby declare that I am the sole author of the thesis and the material presented in this thesis is my original work. All material taken from other sources is explicitly acknowledged as such. I further declare that I have followed the Education University of Hong Kong's policies and regulations on academic honesty, copyright and plagiarism in writing the thesis and no material in this thesis has been submitted for a degree at this or other universities.

Most of the content in Chapter 2 (except Section 2.5) and Chapter 3 was published during my Ph.D. study in the following paper: Po, H. F., Yeung, C. H., and Saad, D. 2021. Futility of being selfish in optimized traffic. *Physical Review E*, *103*(2), 022306.

Most of the content in Chapter 4 was included during my Ph.D. study in the following paper: Po, H. F., and Yeung, C. H. 2021. Complete realization of energy landscape and non-equilibrium trapping dynamics in spin glass and optimization problem. *(submitted to Physical Review Letters and under review), arXiv preprint arXiv:2106.05330*.

Abstract

Knowledge and techniques from statistical physics have been extensively applied in many areas of study, including complex networks and optimization problems. In this thesis, we study two interdisciplinary problems using methods from statistical physics, underlining the broad applicability of statistical methods.

The first corresponds to a problem in transportation systems, in which selfish users exist and choose alternative routes to minimize their individual costs instead of using the optimal paths provided. The dynamics of selfish routing have been extensively studied and yet their impact on an initially optimized transportation network have not yet been discussed. We apply the cavity method in spin glass theory with probabilistic modeling to reveal the rerouting behaviors of selfish users as well as their impacts. We also extend to the case of multiple rounds of selfish rerouting, to study the Nash equilibrium of the system via simulation.

The second problem corresponds to the study of the energy landscapes of complex disordered systems. These systems exhibit glassy behaviors which are believed to be characterized by the energy landscapes. However, most existing methods describing the energy landscapes have omitted important features. We introduce a method to reveal the complete energy landscape of complex disordered systems, taking spin glasses and $K-$Satisfiability problems as examples. The energy landscape is used to derive the non-equilibrium dynamics of these systems analytically, which is computationally infeasible by simulations. Physical pictures of the glassy behaviors of these systems are also discussed.

Keywords: Statistical physics, transportation optimization, Nash equilibrium, complex disordered systems, energy landscapes

Acknowledgments

I would like to express my thanks to my supervisor, Dr. Yeung Chi Ho, for his support and patient guidance. Without him, I would not be able to enjoy the delicious taste of the process of researching. I learned a lot from him, not only innovative insights and techniques in doing research, but most importantly his enthusiasm, patience and good attitude as a researcher and a teacher. Dr. Yeung gave me many opportunities to present at international conferences and collaborate with other great researchers including Prof. David Saad and Prof. Kwok Yee Michael Wong. Dr. Yeung supported me significantly in my studies and my career, and I would like to thank him again for his guidance.
I would like to thank Prof. David Saad, Prof. Kwok Yee Michael Wong, Dr. Zeng An, and Dr. Yi-Zhi Xu for giving me the chance to work with them. I am very thankful to the Education University of Hong Kong for creating a supportive research environment, and especially to all members of the Graduate School for helping me significantly whenever I needed. I would also like to thank my colleagues and friends for their support and discussions.
I would like to thank my family for their constant support, understanding and encouragement. Finally, I would like to thank my wife, Zoe, for her support and encouragement over these years and many more.

List of publications/research outputs

1. Po, H. F., Yeung, C. H., Zeng, A., and Wong, K. M. 2017. Evolving power grids with self-organized intermittent strain releases: An analogy with sandpile models and earthquakes. *Physical Review E*, *96*(5), 052312.

2. Po, H. F., Yeung, C. H., and Saad, D. 2021. Futility of being selfish in optimized traffic. *Physical Review E*, *103*(2), 022306.

3. Po, H. F., and Yeung, C. H. 2021. Complete realization of energy landscape and non-equilibrium trapping dynamics in spin glass and optimization problem. *(submitted to Physical Review Letters and under review), arXiv preprint arXiv:2106.05330*.

4. Xu, Y.-Z., Po, H. F., Yeung, C. H., and Saad, D. 2021a. Scalable node-disjoint and edge-disjoint multi-wavelength routing. *(submitted to Physical Review X and under review). arXiv preprint arXiv:2107.00609*.

Table of Contents

List of Figures

Chapter 1: Introduction

Modern developments in statistical physics have led to its application in areas outside conventional physical systems, bringing significant impacts. For instance, in the fields of complex systems and social science, knowledge and techniques from statistical mechanics are used to study the blackout sizes in power grids via scaling theory and self-organized criticality (Cao, Ding, Wang, Bao, and Han 2009; Nesti, Sloothaak, and Zwart 2020; Po, Yeung, Zeng, and Wong 2017), to identify optimal paths in transportation networks (Yeung 2019; Yeung and Saad 2012; Yeung, Saad, and Wong 2013) and routing optimization in optical communication networks (Xu, Po, Yeung, and Saad 2021b), and to understand the dynamics and optimization of epidemic spreading (Lokhov, Mézard, Ohta, and Zdeborová 2014; Lokhov and Saad 2017; Pastor-Satorras and Vespignani 2001). In computer science and applied mathematics, combinatorial optimization problems such as $K-$Satisfiability problems and graph coloring (Gabrié, Dani, Semerjian, and Zdeborová 2017; Krzakała, Montanari, Ricci-Tersenghi, Semerjian, and Zdeborová 2007; Marino, Parisi, and Ricci-Tersenghi 2016; Mézard and Zecchina 2002; Ricci-Tersenghi and Semerjian 2009; Zdeborová and Krząkała 2007), effective algorithms as well as phase diagrams of the solution space are produced by drawing an analogy with spin glass systems.

In this thesis, we study two interdisciplinary problems using knowledge and techniques from statistical mechanics. In the first part of the thesis, we study a problem in transportation systems where selfish users choose alternative routes to minimize their individual costs, instead of using the optimal paths provided. Due to the extensive number of routing possibilities, it is highly challenging to identify the paths of the optimal configuration as well as the rerouting decisions of selfish users. Methods originally aimed at studying spin glasses are applied to study the problem and lead to a clear physical picture about selfish users' rerouting and their impacts on the system. In the second part of the thesis, we study the energy landscape of complex disordered systems. That these systems exhibit glassy behaviors has been extensively studied. We introduce methods to completely reveal the energy landscape of these glassy systems, and are able to identify the minima of the systems and preserve connectivity between states. Furthermore, we derive the non-equilibrium dynamics of these systems analytically. We show how the techniques and knowledge derived from statistical physics can be broadly applied to problems in different areas.

1.1 Transportation optimization: motivation and introduction

Traffic congestion is a serious problem in metropolitan areas worldwide, which is costly in both monetary and environmental terms. For instance, in Europe, traffic congestion is costing nearly €100 billion annually, or about 1% of the EU's GDP (Directorate-General for Mobility and Transport 2021). Therefore, easing congestion is important and can bring huge benefits to the society. Alleviating congestion through infrastructure upgrades is costly and often infeasible in established metropolitan areas. Alternatively, coordinating traffic through optimized routes coupled with variable road-charges or financial inducements is one of the most feasible and promising approaches to mitigate congestion (Bayati et al. 2008b; Dobrin and Duxbury 2001; Noh and Rieger 2002).

Although optimization algorithms have been derived for identifying optimal routes to achieve a global objective that is beneficial to the whole system, some individuals often have to sacrifice and travel on a slightly longer path (Yeung 2019; Yeung and Saad 2012; Yeung et al. 2013). Therefore, even though optimally coordinated routes may be provided, it is trivial to observe that some selfish individuals may choose alternative routes which drive the system away from the optimum (Prato 2009; Shiftan, Bekhor, and Albert 2011). Such dynamics of individual route decisions have been studied in game theory and operations research. For instance, mathematical models are constructed to study dynamical selfish routing (Anshelevich and Ukkusuri 2009; Fischer and Vöcking 2004), and to reveal the impact of economic incentives on suppressing selfish behaviors (Cole, Dodis, and Roughgarden 2006). Selfish routing and the resulting Nash equilibria in capacitated networks have also been investigated (Correa, Schulz, and Stier-Moses 2004). However, most of these studies focus on the dynamics of individual route decisions only, while the impact of selfish routing on an initially optimized transportation network has not yet been discussed, nor has any analytical solution to the problem been devised. Such analysis can reveal the potential benefits of global coordination of routes, which is important for future transportation systems in which route coordination is possible via self-driving vehicles and information technology.

In Chapter 2, we introduce the model of a transportation network, where users are initially provided with the optimized routes from their starting points to a common destination, while some do not follow the suggested routes and choose alternatives to minimize their own individual costs. We employ the cavity method developed for studying spin glasses (Mézard and Zecchina 2002) and probabilistic modeling to reveal the impact of selfish rerouting on the system. In Chapter 3, we extend the model to the case of multiple rounds of selfish rerouting and study the Nash equilibrium of such problems via simulation.

1.2 Energy landscapes of complex disordered systems: motivation and introduction

An energy landscape corresponds to the graph of the energy function of a physical system which associates each possible variable configuration with an energy. Since most physical systems consist of many variables, the energy landscapes of these physical systems are high-dimensional surfaces and thus are extremely intricate to visualize. For instance, for a spin system with N spins, the configuration space is in N dimensions and there are a total of 2^N possible variable configurations(corresponding to spin “up” or spin “down” for each). Similar to physical systems, the energy landscape of optimization problems can be understood as the graph of the cost functions. The energy landscapes serve an important role in characterizing the emergent behavior of these systems. For instance, in spin systems, spins glasses are believed to be characterized by the existence of a large number of local minima in the energy landscapes, while ferromagnetic spin systems are characterized by energy landscapes without local minima (Mézard, Parisi, and Virasoro 1987b; Nishimori 2001). Similarly, the algorithm hard and algorithm easy phases in combinatorial optimization problems distinguishing how hard the system can be solved are also characterized by the number of local minima in the energy landscapes (Krzakała et al. 2007; Zdeborová and Krząkała 2007). Therefore, methods that can reveal and analyze the complete energy landscape are crucial in the study of these systems.

Since the energy landscapes are high-dimensional surfaces, revealing their structure completely is highly challenging. While various approaches are used to investigate the energy landscapes of complex systems, some features of the landscape are omitted so that the realization is feasible. For instance, disconnectivity graphs (DGs) represents the energy landscapes by showing the set of all minima and the lower energy barriers between any two minima (Becker and Karplus 1997), which have been extensively applied to study problems in spin glasses (Biswas and Katzgraber 2020), protein folding (Krivov and Karplus 2004) and machine learning (Ballard et al. 2017). Nevertheless, DGs only show the connectivity between minima by the path with the lowest energy barriers, and the exact connectivity between states is omitted. Another approach commonly used is multidimensional scaling (MDS), which maps all variable configurations in the N-dimensional configuration space to an assigned dimension (usually 2 or 3) and preserves the distance or similarity between any two states (Mead 1992). However, some important features including the connectivity, energy difference, as well as the energy barrier between states, are omitted, thus the landscape is oversimplified by MDS. A method that can reveal the complete energy landscape showing the exact connectivity between states remains unexplored.

In Chapter 4, we introduce a method to show the complete energy landscape of complex disordered systems, using spin glasses and $K-$Satisfiability problems as examples. The obtained energy landscapes are then used to reveal the non-equilibrium dynamics analytically, at any given temperature for any given time, which is computationally infeasible by simulation. The energy landscapes and the non-equilibrium dynamics obtained are studied, and a complete physical picture of the long-time dynamics is presented.

Chapter 2: Selfish behavior on optimized transportation networks

2.1 Model formulation

Consider a transportation network $\mathbb{G} = (\mathbb{V}, \mathbb{E})$ comprising the set of nodes $\mathbb{V}$ and the set of links $\mathbb{E}$. The set $\mathbb{V}$ consists of N nodes, denoted as $i = 1, \ldots, N$. Every node $i \in \mathbb{V}$ on the network connects to a set of neighboring nodes $\mathcal{N}_i$. For every link $(ij) \in \mathbb{E}$ connecting the nodes i and $j \in \mathcal{N}_i$, we define w_{ij} as the weight of the link, representing how costly it is for traveling through (ij), such as the physical traveling distance. Since we are focusing on the physical properties of a transportation system, we assume $w_{ij} = 1\ \forall (ij) \in \mathbb{E}$ for simplicity. Now, consider that there exist M vehicles, denoted as $\nu = 1, \ldots, M$, traveling on the transportation network, and the density of vehicles for the network is defined as $\alpha = \frac{M}{N}$. Every vehicle ν is traveling to an arbitrary universal destination node $\mathcal{D}$ from its starting node $\mathcal{O}$ that is randomly selected. We define σ^{ν}_{ij} as the path configuration of the vehicle ν on the link between nodes i and j, where: $\sigma^{\nu}_{ij} = 1$ if the vehicle ν is traveling from node i to node j; $\sigma^{\nu}_{ij} = -1$ if the vehicle ν is traveling from node j to node i, and; $\sigma^{\nu}_{ij} = 0$ when ν is not traveling on the link (ij). It is trivial that $\sigma^{\nu}_{ij} = -\sigma^{\nu}_{ji}$. The vector of the routing decisions made by all vehicles is then defined by $\boldsymbol{\sigma} = \left\{\sigma^{\nu}_{ij}\right\}_{\nu,(ij)}$.

Yeung and Saad 2012 proved that, over an optimized transportation network, drivers always travel in the same direction, i.e. either $\sigma^{\nu}_{ij} \geq 0$ or $\sigma^{\nu}_{ij} \leq 0\ \forall \nu$, for any link $(ij) \in \mathbb{E}$. Since we are studying selfish routing behavior over an optimized transportation network, we can assume all vehicles are heading in the same direction on a certain link. The directed total traffic flow from node i to node j on the transportation network, defined as the total number of vehicles traveling on link (ij), is denoted as I_{ij}, where

$$I_{ij} = \sum_{\nu} \sigma_{ij}^{\nu}, \tag{1}$$

so that vehicles are traveling from i to j if $I_{ij} > 0$ and j to i if $I_{ij} < 0$. The total volume of traffic from node i to j is $\left|I_{ij}\right| = \sum_{\nu} |\sigma_{ij}^{\nu}| = \left|\sum_{\nu} \sigma_{ij}^{\nu}\right|$. Similar to the real-life situation in which traffic congestion usually occurs when vehicles' paths are overlapping and sharing the same road, the social cost of traffic is defined as $\mathcal{H}(\boldsymbol{\sigma}|\gamma)$, given by

$$\mathcal{H}(\boldsymbol{\sigma}|\gamma) = \frac{1}{M} \sum_{(ij)} \left|I_{ij}\right|^{\gamma} = \frac{1}{M} \sum_{(ij)} \left(\sum_{\nu} \left|\sigma_{ij}^{\nu}\right| \right)^{\gamma}. \tag{2}$$

The exponent γ defines the preference of the transportation network. When $\gamma > 1$, the cost increases with the traffic flow nonlinearly, meaning the system prevents a link being shared by multiple vehicles. When $\gamma = 1$, the two summations in Eq.(2) are interchangeable, and the social cost $\mathcal{H}(\boldsymbol{\sigma}|\gamma)$ becomes

$$\mathcal{H}(\boldsymbol{\sigma}|1) = \frac{1}{M} \sum_{(ij)} \left(\sum_{\nu} \left|\sigma_{ij}^{\nu}\right| \right) = \frac{1}{M} \sum_{\nu} \left(\sum_{(ij)} \left|\sigma_{ij}^{\nu}\right| \right), \tag{3}$$

meaning that the social cost is minimized when all users are minimizing their individual traveling path lengths. We remark that the cost function in Eq.(2) can be replaced by other nonlinear costs to fit the needs of different applications, such as the Bureau of Public Roads (BPR) latency function that is used frequently for studying realistic transportation networks (Lien, Mazalov, Melnik, and Zheng 2016; United States. Bureau of Public Roads 1964). We will present how the social cost $\mathcal{H}(\boldsymbol{\sigma}|\gamma)$ and the corresponding path configuration can be minimized using a message-passing algorithm proposed by Yeung and Saad 2012 in Section 2.3.

Now, assume that the social travel cost $\mathcal{H}(\boldsymbol{\sigma}|\gamma)$ is minimized, and the corresponding configuration of route for every vehicle ν is identified and suggested to all vehicles. The optimized path for the vehicle ν is defined as $\sigma_{ij}^{\nu *}$. If the optimized path for ν is traveling from node i to node j, then $\sigma_{ij}^{\nu *} = 1$ and $\sigma_{ji}^{\nu *} = -1$, and $\sigma_{ij}^{\nu *} = 0$ otherwise. The vector of the optimized routing strategies for all vehicles is then defined as $\boldsymbol{\sigma}^*$, where

$$\boldsymbol{\sigma}^* = \underset{\boldsymbol{\sigma}}{\operatorname{argmin}}\, \mathcal{H}\left(\boldsymbol{\sigma}|\gamma\right). \tag{4}$$

Next, the optimized directed total traffic flow from node i to j, denoted as I_{ij}^*, is given by $I_{ij}^* = \sum_\nu \sigma_{ij}^{\nu *}$. To study how selfish routing behavior impacts an optimized network, one must first define the utility function for individual users. Consider that a fraction f_s of M vehicles are selfish, i.e. the number of selfish users is $f_s M$. For any vehicle ν that is selfish, it aims to minimize its own individual costs by traveling through another route $\tilde{\boldsymbol{\sigma}}^\nu = \left\{\tilde{\sigma}_{ij}^\nu\right\}_{(ij)}$. We define the individual travel cost as $\mathcal{H}_\nu\left(\tilde{\boldsymbol{\sigma}}|\boldsymbol{\sigma}^*, \gamma\right)$, given by

$$\mathcal{H}_\nu\left(\tilde{\boldsymbol{\sigma}}^\nu|\boldsymbol{\sigma}^*, \gamma\right) = \sum_{(ij)} \left|\tilde{\sigma}_{ij}^\nu\right| \left(1 + \left|I_{ij}^* - \sigma_{ij}^{\nu *}\right|\right)^{\gamma - 1}. \tag{5}$$

The quantity $\left|I_{ij}^* - \sigma_{ij}^{\nu *}\right|$ represents the induced traffic condition due to the other users. The individual travel cost implies that, for the selfish vehicle ν, it is provided with the recommended traffic condition as well as the induced traffic, and this information is used to minimize its own cost. The exponent in Eq.(5) is defined as $\gamma - 1$ so that the sum of individual costs is equivalent to the social cost in Eq.(2), which will be discussed below. Similar to Eq.(3), when $\gamma = 2$, the individual travel cost represents the total traffic flow experienced by ν over the route it decided.

We remark that both the social cost and the individual cost for every vehicle can also be defined separately without satisfying the above conditions for other specific needs. The individual travel cost is defined in this manner because Eq.(5) can relate the social cost $\mathcal{H}$ in Eq.(2) with the individual cost $\mathcal{H}_\nu$ for convenience of treatment. Now, if we consider that all vehicles are following the suggested optimal paths, i.e. $\tilde{\sigma}^{\nu}_{ij} = \sigma^{\nu*}_{ij}, \forall \nu, (ij)$, then we have

$$\left|\tilde{\sigma}^{\nu}_{ij}\right| \left(1 + \left|I^{*}_{ij} - \sigma^{\nu*}_{ij}\right|\right)^{\gamma-1} = \begin{cases} \left|I^{*}_{ij}\right|^{\gamma-1} & , \quad \text{if } \left|\sigma^{\nu*}_{ij}\right| = 1; \\ 0 & , \quad \text{if } \left|\sigma^{\nu*}_{ij}\right| = 0. \end{cases}, \tag{6}$$

$$\Rightarrow \left|\tilde{\sigma}^{\nu}_{ij}\right| \left(1 + \left|I^{*}_{ij} - \sigma^{\nu*}_{ij}\right|\right)^{\gamma-1} = \left|\tilde{\sigma}^{\nu}_{ij}\right| \left|I^{*}_{ij}\right|^{\gamma-1}. \tag{7}$$

Using Eq.(7), and by summing the individual costs for all vehicles, we have

$$\begin{aligned} \sum_{\nu} \mathcal{H}_\nu(\boldsymbol{\sigma}^{\nu*}|\boldsymbol{\sigma}^{*}, \gamma) &= \sum_{\nu} \sum_{(ij)} \left|\tilde{\sigma}^{\nu}_{ij}\right| \left|I^{*}_{ij}\right|^{\gamma-1} \\ &= \sum_{(ij)} \sum_{\nu} \left|\tilde{\sigma}^{\nu}_{ij}\right| \left|I^{*}_{ij}\right|^{\gamma-1} = \sum_{(ij)} \left|I^{*}_{ij}\right|^{\gamma} = \mathcal{H}(\boldsymbol{\sigma}|\gamma). \end{aligned} \tag{8}$$

Therefore, the above equations show that if all vehicles are following the suggested optimal routes, the sum of all individual costs $\mathcal{H}_\nu$ is equal to the social cost $\mathcal{H}$. If there exist some vehicles that are not following the suggested routes, the social cost would be either unchanged or increased, due to the fact that the social cost is minimized under the suggested configuration.

To analyze the impact of selfish routing strategies, we have to quantify their impact on the social cost in the next step. It is important to note that the preference of the route recommending system can be different from the real social cost; for example, for maintenance proposes, the transportation system wants to minimize the total number of roads that are in use. Therefore, we separate them by assigning γ_r and γ as the exponent in Eq.(2), representing the preference of the recommending system and the real social cost respectively, where γ_r and γ not necessarily the same. We measure the fractional change of the social cost $\mathcal{H}$ induced by the rerouting caused by selfish drivers, defined as

$$\Delta\mathcal{H}(\gamma_r,\gamma) = \frac{\mathcal{H}\left(\tilde{\boldsymbol{\sigma}}^*(\gamma_r)|\gamma\right) - \mathcal{H}\left(\boldsymbol{\sigma}^*(\gamma_r)|\gamma\right)}{\mathcal{H}\left(\boldsymbol{\sigma}^*(\gamma_r)|\gamma\right)}, \tag{9}$$

where the vector $\boldsymbol{\sigma}^*(\gamma_r)$ is the recommended route configurations that minimize $\mathcal{H}(\boldsymbol{\sigma}|\gamma_r)$, provided that the real social traffic cost is characterized by $\mathcal{H}(\boldsymbol{\sigma}|\gamma)$. Other than $\boldsymbol{\sigma}^*(\gamma_r)$, the vector $\tilde{\boldsymbol{\sigma}}^*(\gamma_r)$ denotes the selfish rerouting strategies for all vehicles that optimize their own individual travel costs $\mathcal{H}_\nu\left(\tilde{\boldsymbol{\sigma}}^{\nu*}|\boldsymbol{\sigma}^*,\gamma_r\right)$ by considering the recommended traffic configuration $\boldsymbol{\sigma}^*(\gamma_r)$, i.e. $\tilde{\boldsymbol{\sigma}}^*(\gamma_r) = \{\tilde{\boldsymbol{\sigma}}^{\nu*}(\gamma_r)\}_{\nu=1,\ldots,M}$. Note that there are two types of users on the transportation network, the first type who are compliant and follow the recommended routes provided, and the other type of users who are selfish and follow the routes that can optimize their individual costs. Therefore,

$$\tilde{\boldsymbol{\sigma}}^{\nu*}(\gamma_r) = \begin{cases} \boldsymbol{\sigma}^{\nu*}(\gamma_r), & \text{for compliant vehicles,} \\ \operatorname{argmin}_{\tilde{\boldsymbol{\sigma}}^{\nu}} \mathcal{H}_\nu(\tilde{\boldsymbol{\sigma}}^{\nu}|\boldsymbol{\sigma}^*(\gamma_r),\gamma), & \text{for selfish vehicles.} \end{cases} \tag{10}$$

In this chapter, we aim to study the impact caused by selfish routing decisions, including the factional change in social cost, and isolated individual costs for both compliant and selfish vehicles. We remark that the model discussed is applicable for any values of $\gamma_r, \gamma \geq 1$. Nevertheless, since we are focusing on the physical properties of the transportation system, we mainly study the following two different scenarios of recommended traffic: (1) $(\gamma_r, \gamma) = (1, 2)$. This scenario represents that originally, all vehicles are suggested to pick their shortest path, $\boldsymbol{\sigma}^*(1)$; (2) $(\gamma_r, \gamma) = (2, 2)$. This scenario represents that originally, all vehicles are suggested to pick the routes that minimize the social cost $\mathcal{H}(\boldsymbol{\sigma}|2)$ that prevent link-sharing. In both scenarios, the social cost is characterized by $\mathcal{H}(\boldsymbol{\sigma}|2)$ to discourage overlapping of traffic, while the individual travel costs are characterized by $\mathcal{H}_\nu(\tilde{\boldsymbol{\sigma}}^{\nu*}|\boldsymbol{\sigma}^*(\gamma_r), 2)$ for different γ_r. After recommended routes are provided to the selfish users, they are rerouting to new paths $\tilde{\boldsymbol{\sigma}}^\nu$ to minimize their own individual costs $\mathcal{H}_\nu(\tilde{\boldsymbol{\sigma}}^{\nu*}|\boldsymbol{\sigma}^*(\gamma_r), 2)$.

To compute the quantities measuring the impacts caused by selfish routing, we apply tools and techniques from statistical physics that are used to study spin glass systems. In Section 2.2, we first introduce the cavity method which was originally introduced for studying spin glasses (Mézard, Parisi, and Virasoro 1987a). In Section 2.3, we present the approach developed in Yeung and Saad 2012 in detail, showing how the analytical solution of the transportation system that minimizes $\mathcal{H}$ can be found. In Section 2.4, we derive a new two-stage cavity method based on the framework in Section 2.3, where the first stage of the method is identifying the optimal configuration of paths to recommend to users, and the second stage corresponds to identifying the rerouting decisions made by selfish vehicles. Following the two-stage cavity method, we describe the selfish routing behavior of selfish vehicles by probabilistic modeling. In Section 2.5, we modify the newly developed framework from Section 2.4 to derive an exhaustive analytic approach that can describe the precise routing behaviors of all users before and after rerouting.

2.2 Ordinary cavity method

The cavity method was first presented by Mézard et al. 1987a, originally for studying spin glass systems. The method is adapted very well to treelike graph structures, i.e. sparse graphs in which only large loops exist, such as random regular graphs (Bollobás 2001) and Erdős–Rényi graphs (Erdös and Rényi 1959). The cavity method carries out rigorous probabilistic analysis by reproducing a self-consistence recurrence relation for a system with $N + 1$ nodes based on the same system with N nodes, assuming that when N is large enough, the correlations between any two nodes vanish, i.e. the two nodes are statistically independent. Remarkably, the cavity method provides a framework that is able to compute statistical properties for many disordered systems, such as condensed matter and optimization problems. Although the replica method (Nishimori 2001) provides a more elegant and rigorous mathematical formulation, the cavity method has unique advantages. First, since concrete probabilistic modeling is done through the derivation of the cavity method, not just macroscopic physical quantities (e.g. energy and entropy) can be measured, the method itself can be considered as a tool and method for rigorous probabilistic analysis for complex systems.

Another important advantage is that, contrary to the replica approach, the derivation of the cavity method firstly describes mathematically how the energy of a node depends on its neighbors and other variables, and the macroscopic quantities are found by performing quenched averaging over the disorder afterward. This allows us to define message-passing algorithms inspired by the derivation process of the cavity method. This important advantage makes the cavity method not only able to produce theoretical results, but also produce algorithms that are applicable to a single instance of problems, such as the message-passing algorithms similar to belief propagation discovered in computer science and survey propagation algorithms in solving the K-satisfiability problems, which have been proven to be very effective (Mézard et al. 1987a).

In the following sections, we make use of these advantages of the cavity method to produce theoretical solutions, carry out concrete probabilistic analysis, and produce a practical algorithm for transportation networks. In Section 2.3, we first apply the conventional cavity method to optimize the social travel cost $\mathcal{H}$ and simplify it into a more specific cavity method at zero temperature.

Then we develop two different cavity methods for studying selfish routing behavior based on this specific cavity method in Section 2.4 and Section 2.5.

2.3 Cavity method to optimize social travel cost

An optimization framework for identifying the optimal traffic condition has been proposed by Yeung and Saad 2012. To provide a clearer picture of how the frameworks in Section 2.4 and Section 2.5 are derived, we first present the original framework in this section.

Consider a transportation model as described above, while no selfish routing will occur after the optimal configuration is found. This routing optimization problem is first mapped into a resource allocation problem, where resources are transferring from a set of nodes to a universal sink. In this case, every node i is assigned with a transportation load Λ_i, where

$$\Lambda_i = \begin{cases} 1, & \text{if } \exists \nu \text{ s.t. } \mathcal{O}_\nu = i; \\ -\infty, & \text{if } \mathcal{D} = i; \\ 0, & \text{otherwise.} \end{cases} \tag{11}$$

In other words, every vehicle is transferring a positive unit of load from its origin to the common destination, which can be understood as a universal sink. To ensure all paths to the universal sink for each user are valid and identified, we have to restrict all traffic flow to integer values, i.e. $I_{ij} \in \mathbb{Z}, \forall (ij)$. Moreover, to ensure the identified paths are connected from their origin to the sink, the net resources on any node i except the destination, denoted as $R_i, \forall i \neq \mathcal{D}$, have to be conserved, where

$$R_i = \Lambda_i + \sum_{j \in \mathcal{N}_i} I_{ji} = 0. \tag{12}$$

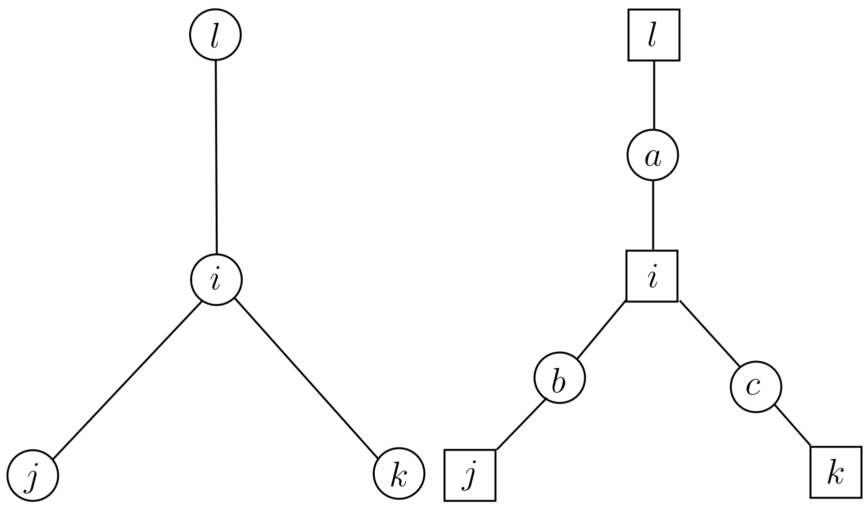

Figure 1. (a) The original transportation network. (b) The corresponding factor graph of the original transportation network shown in (a).

Next, we assume that the networks we study are sparse, and that only large loops exist and with treelike structures. Therefore, for any node i, when it is removed from the network, the neighbors of i become statistically independent. We remark that although a treelike structure is assumed, the analytical results obtained on non-tree structures are in good agreement with the simulation results, as discussed in Bayati et al. 2008a and Yeung, Wong, and Li 2014. We next employ the cavity method to optimize the system. Conventionally, the variables are usually defined over nodes in the cavity method. Nevertheless, the current flow I_{ij} is defined over links in our model setup. To tackle this problem, we switch the role of nodes and links in the corresponding factor-graph of the transportation network. In particular, as shown in Fig. 1(b), the variable node a represents the link connecting physical junctions i and l, while the function node i represents the physical junction. For clear presentation, we also note that the traffic flow $I_{il} = I_{i\to a} = I_{a\to l}$ for the variable node a connecting i and l. We denote $\partial' i$ and $\partial' a$ as the set of neighbors of the node i and node a, respectively, in the corresponding factor-graph of the transportation network. Employing the cavity method with inverse temperature β, we define $m_{i\to a}(I_{i\to a})$ as the message sent from node a

to node i, as a function of $I_{i\to a}$, given as

$$m_{i\to a}(I_{i\to a}) = \sum_{\{I_{b\to i}\}_{b\in\partial' i\backslash a}} e^{-\beta|I_{i\to a}|^{\gamma}} \delta\left(\Lambda_i + \sum_{b\in\partial' i\backslash a} I_{b\to i} - I_{i\to a}\right) \prod_{b\in\partial' i\backslash a} m_{b\to i}\left(I_{b\to i}\right), \tag{13}$$

and $m_{b\to i}(I_{b\to i})$ as the message sent from node b to node i, where

$$m_{b\to i}(I_{b\to i}) = \prod_{j\in\partial' b\backslash i} m_{j\to b}\left(I_{j\to b}\right) = m_{j\to b}\left(I_{j\to b}\right). \tag{14}$$

Note that the messages $m_{i\to a}$ and $m_{a\to l}$ are identical, we can combine them into one message $m_{i\to l}$ and remove all the variable nodes in the factor graph. The message passing equation then becomes

$$m_{i\to l}(I_{il}) = \sum_{\left\{I_{j\to i}\right\}_{j\in\partial' i\backslash l}} \left[e^{-\beta|I_{il}|^{\gamma}} \delta\left(\Lambda_i + \sum_{j\in\partial' i\backslash l} I_{ji} - I_{il}\right) \prod_{j\in\partial' i\backslash l} m_{j\to i}\left(I_{ji}\right)\right]. \tag{15}$$

Since we are focusing on optimal configurations only, we can employ the cavity method at zero temperature and further simplify Eq. (15) by $m_{i\to l}(I_{il}) = e^{-\beta E(I_{il})}$ and take β to infinity. We define $E_{i\to l}(I_{il})$ as the optimized energy function terminated at node i to node l, as a function of the traffic flow I_{il} on the link (il). Next, a recurrence relation can be formulated relating the energy $E_{i\to l}(I_{il})$ (the parent) at node i to the energies $E_{j\to i}(I_{ji})$ (the descendants) of the neighbors $j \in \mathcal{N}_i$ except the parent l, given by

$$E_{i\to l}\left(I_{il}\right) = \min_{\left\{\left\{I_{ji}\right\}_{j\in\mathcal{N}_i\backslash l}|R_i=0\right\}} \left[|I_{il}|^{\gamma} + \sum_{j\in\mathcal{N}_i\backslash l} E_{j\to i}(I_{ji})\right]. \tag{16}$$

Intuitively speaking, any given node i is provided with the marginal energies of its descendant nodes j except the parent node l, and tries to minimize the traveling cost and propagate to the parent node

l by finding the optimal combination of the set of traffic flows $\left\{I_{ji}\right\}_{j\in\mathcal{N}_i\backslash l}$ of its descendant, given the constraint that $R_i = 0$. Noting that the energy function $E_{i\to l}(I_{il})$ is convex due to the convexity of $|I|^\gamma$ for all $\gamma \geq 1$, the computation of Eq. (16) can be further simplified. Making use of the convexity of the energy function, we define the change of energy $\Delta_i^\pm(I_{il}) = E_{i\to l}(I_{il} \pm 1) - E_{i\to l}(I_{il})$ and we have

$$\Delta_i^\pm(I_{il}) = |I_{il} \pm 1|^\gamma - |I_{il}|^\gamma + \min_{j\in\mathcal{N}_i\backslash l}\left\{\Delta_j^\pm\left[I_{ji}^*(I_{il})\right]\right\}, \text{where}$$
$$I_{ji}^*(I_{il}) = \begin{cases} I_{ji}^*(I_{il}) \pm 1 \quad , & j = \operatorname{argmin}_{j\in\mathcal{N}_i\backslash l}\left\{\Delta_j^\pm\left[I_{ji}^*(I_{il})\right]\right\} \\ I_{ji}^*(I_{il}) \quad , & \text{otherwise.} \end{cases} \tag{17}$$

Therefore, instead of finding all combinations of the set of traffic flows $\left\{I_{ji}\right\}_{j\in\mathcal{N}_i\backslash l}$, we just need to find the value of $\min_{j\in\mathcal{N}_i\backslash l}\left\{\Delta_j^\pm\left[I_{ji}^*(I_{il})\right]\right\}$. Hence, the computational complexity of finding the energy function $E_{i\to l}(I_{il})$ is $O(\langle k\rangle M)$. We further note that the quantity $E_{i\to l}(I_{il})$ is extensive, meaning that the values of the energies depend on the size of the system, which will be difficult to find by iterations. Therefore, we have to modify $E_{i\to l}(I_{il})$ and define a new intensive quantity $E_{i\to l}^V(I_{il})$, where

$$E_{i\to l}^V(I_{il}) = E_{i\to l}(I_{il}) - E_{i\to l}(0), \tag{18}$$

which can be easily computed after all energy functions $E_{i\to l}(I_{il})$ are found by Eq.(16).

The next step is to solve the systems analytically and obtain theoretical results. In the thermodynamic limit as $N \to \infty$, the correlation between nodes vanish and they become independent of each other. Therefore, when a link (ij) is chosen, the energy $E_{i\to l}^V(I_{il})$ should follow a functional probability distribution $P\left[E^V(I)\right]$, and to solve the system we have to first solve $P\left[E^V(I)\right]$. In the thermodynamic limit, in principle we can write a self-consistent equation, using Eq.(16) and Eq.(18), given by

$$P\left[E^V(I)\right] = \int dk \frac{P(k)k}{\langle k\rangle} \int d\Lambda P(\Lambda) \prod_{j=1}^{k-1} \int dE_j^V P\left[E_j^V(I)\right] \delta\left(E^V(I) - \mathcal{R}\left[\left\{E_j^V\right\}, \Lambda, I\right]\right), \tag{19}$$

where we denote $\mathcal{R}$ as the right hand side of Eq.(18), which can be evaluated by the recurrence relation derived in Eq.(16); $P(k)$ is the probability distribution of the nodes degree k over the network; $\langle k\rangle = \int P(k)kdk$ represents the average degree of nodes, for instance in the random regular graph, $P(k) = \langle k\rangle = C$, for some $C \in \mathbb{Z}$; $P(\Lambda)$ is the probability distribution of the transportation load, for instance over a network of $N = 100$ and $M = 10$, we have $P(\Lambda = -\infty) = 0.01$ and $P(\Lambda = 1) = 0.1$. To obtain the converged functional probability distribution $P\left[E^V(I)\right]$, one can employ a procedure known as population dynamics (Mézard and Zecchina 2002) to iterate Eq.(19), which is a set of iterative steps defining a stochastic process. Theoretically, $P\left[E^V(I)\right]$ should be a population of infinite size, where the functional equation describing it would be extremely complicated and impractical. Therefore, to make the distribution feasible to compute, we approximate $P\left[E^V(I)\right]$ as a pool with Ξ functions $E^V(I)$ in which the function forms can be randomly drawn, and here we choose $E^V(I) = I^\gamma$ for all functions. The procedure of population dynamics is to iterate Eq.(19) until the distribution is converged. At each step of the iteration, we perform the following processes:

(i) Randomly select the degree k from the probability distribution $\frac{P(k)k}{\langle k\rangle}$.

(ii) Randomly select the transportation load Λ from the probability distribution $P(\Lambda)$.

(iii) Randomly draw $k-1$ functions $E^V(I)$ from the distribution $P\left[E^V(I)\right]$.

(iv) Compute a new energy function $E^V(I)$, using

$$E^V(I) = \mathcal{R}\left(\left\{E_j^V\right\}, \Lambda, I\right), \tag{20}$$

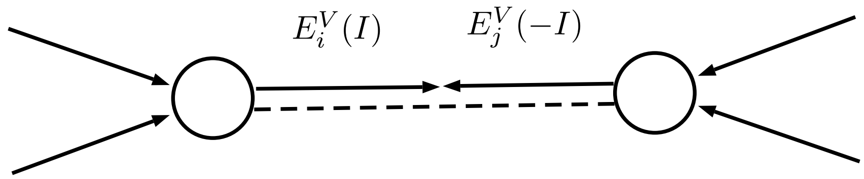

Figure 2. The combination of the trees characterized by the cavity energies. The dotted line represents the traffic flow that we aim to find.

where the functions in the set $\left\{E_j^V\right\}$ on the right hand side are the functions drawn in (iii).

(v) Randomly select a function from $P\left[E^V(I)\right]$, and replace it with the function $E^V(I)$ that is newly evaluated in (iv).

The above procedure is repeated until the approximated distribution $P\left[E^V(I)\right]$ is converged. We remark that since our transportation system of interest has been proven to be in the replica symmetric phase in Yeung and Saad 2012, where the ground state of the system presence as a single state, the equilibrium state of $P\left[E^V(I)\right]$ would not be affected by the initial condition of the functions.

With the converged functional distribution, one is allowed to compute any macroscopic physical quantities that we are interested in analytically. Since the cavity energy $E_i^V(I_i)$ characterizes the energy of a tree structure sent to its parent node, we can compute the optimal configuration of traffic flow of any link (ij) by merging two duplicated trees, as shown in Fig. 2. Therefore, the optimal configuration of flow I^* of any link (ij) is given by $\operatorname{argmin}_I\left[E_i^V(I)+E_j^V(-I)-|I|^\gamma\right]$, where the term $|I|^\gamma$ in the argmin function is to cancel the double counting of the energy. Hence, the average energy of the system $\langle E\rangle$ describing the average social cost over the optimal configuration can be found by

$$\langle E \rangle = \sum_{I^*} P(I^*)\, |I^*|^\gamma \,, \text{ where} \tag{21}$$

$$P(I^*) = \int dE_i^V P\left[E_i^V(I)\right] \int dE_j^V P\left[E_j^V(I)\right] \sum_{I^*} \delta\left(I^* - \underset{I}{\text{argmin}}\left[E_i^V(I) + E_j^V(-I) - |I|^\gamma\right]\right). \tag{22}$$

In this section, we have provided the derivation of the optimization framework for studying optimal traffic flow where selfish users and rerouting behaviors do not exist. The derivation gives a basic understanding of the cavity method and its practical application to a complex system. This gives a clearer picture of how the framework is derived in the following sections, as it consists of multiple steps and might be hard to follow.

2.4 Two-stage cavity method and probabilistic modeling of selfish routing

Consider the case in which we not only aim to find the optimal configuration that minimizes the social traffic cost of the system, but also the impact of selfish rerouting. Note that the framework we discussed in the last section does not consider individual travel routes. Therefore, in this case, we first introduce an extra variable to single out a vehicle μ and study its route switching behavior from the optimal path configuration suggested. We then use the probability distribution that describes the selfish rerouting strategies to estimate the case when there are multiple selfish drivers.

Similar to Eq.(11), we define $\mathbf{\Lambda}_i = (\Lambda_i^\mu, \Lambda_i^{\setminus\mu})$ to be the vector of transportation load on node i, where Λ_i^μ and $\Lambda_i^{\setminus\mu}$ are the transportation loads for the isolated vehicle μ and the other vehicles on the node

i, respectively. The transportation resource $\mathbf{\Lambda}_i$ is then given by

$$\mathbf{\Lambda}_i = \begin{cases} (1,0), & \text{if } \mathcal{O}_\mu = i; \\ (0,1), & \text{if } \exists \nu \neq \mu \text{ s.t.} \mathcal{O}_\nu = i; \\ (-\infty,-\infty), & \text{if } \mathcal{D} = i; \\ (0,0), & \text{otherwise.} \end{cases} \tag{23}$$

Then, as in Eq.(12), we define $\boldsymbol{R} = (R_i^\mu, R_i^{\backslash\mu})$ as the vector of the net resources on node i, given by

$$R_i^\mu = \Lambda_i^\mu + \sum_{j\in\mathcal{N}_i} \sigma_{ji}^\mu, \tag{24}$$

$$R_i^{\backslash\mu} = \Lambda_i^{\backslash\mu} + \sum_{j\in\mathcal{N}_i} I_{ji}^{\backslash\mu} = \Lambda_i^{\backslash\mu} + \sum_{j\in\mathcal{N}_i}\sum_{\nu\neq\mu} \sigma_{ji}^\nu, \tag{25}$$

where R_i^μ and $R_i^{\backslash\mu}$ are the net resources for the isolated vehicle μ and the other vehicles on the network, respectively; $I_{ji}^{\backslash\mu}$ and σ_{ji}^μ are the traffic flow except μ and the path of μ, respectively. We then restrict all flow σ and I to be integer valued and the vector of resources $\boldsymbol{R}_i = (R_i^\mu, R_i^{\backslash\mu}) = (0,0)$ for all $i \neq \mathcal{D}$, so the paths from the origins to the destination can be identified and are connected.

In the initial stage, the path configuration that minimizes the social cost $\mathcal{H}(\boldsymbol{\sigma}|\gamma_r)$ is identified and recommended to all vehicles. Next, based on the suggested configuration provided, the vehicle μ reroutes in order to minimize its own individual traffic cost $\mathcal{H}_\mu(\tilde{\boldsymbol{\sigma}}^\mu|\boldsymbol{\sigma}^*,\gamma)$. To model the above process mathematically, similar to Section 2.3, we assume the networks studied are sparse graphs such that only large loops exist and in treelike structures. For any node i, we define $E_{i\to l}\left(\sigma_{il}^\mu, I_{il}^{\backslash\mu}\right)$ as the optimized energy terminated at node i, describing the marginal energy from i to l, as a function of the traffic flow σ_{il}^μ and $I_{il}^{\backslash\mu}$ on the link (il). The energy is defined differently by introducing a new parameter to separate the contribution by the routing decisions of the user μ to the energy from the other users on the link (il). We can then formulate the recurrence relation among $E_{i\to l}\left(\sigma_{il}^{\mu}, I_{il}^{\setminus\mu}\right)$ and $E_{j\to i}\left(\sigma_{ji}^{\mu}, I_{ji}^{\setminus\mu}\right)$ for all descendant neighbors $j \in \mathcal{N}_i \setminus l$, given by

$$E_{i\to l}\left(\sigma_{il}^{\mu}, I_{il}^{\setminus\mu}\right) = \min_{\left\{\sigma_{ji}^{\mu}, I_{ji}^{\setminus\mu} \middle| \boldsymbol{R}_i=(0,0)\right\}} \left[\left(|\sigma_{il}^{\mu}| + |I_{il}^{\setminus\mu}|\right)^{\gamma_r} + \sum_{j\in\mathcal{N}_i\setminus l} E_{j\to i}\left(\sigma_{ji}^{\mu}, I_{ji}^{\setminus\mu}\right)\right], \tag{26}$$

recalling that the exponent γ_r defines the preference of the recommending system to identify the suggested optimal paths, offered to all users.

Eq.(26) only describes how the isolated vehicle μ and the other vehicles identify the optimal path configuration. Therefore, we have to introduce another energy function $\tilde{E}_{i\to l}(\tilde{\sigma}_{il}^{\mu}, \sigma_{il}^{\mu*}, I_{il}^{\setminus\mu*})$ that characterizes the selfish behavior of the singled-out vehicle μ. This function describes the strategy of the vehicle μ that is replacing its recommended path configuration $\sigma_{il}^{\mu*}$ by $\tilde{\sigma}_{il}^{\mu}$, by considering the recommended traffic $I_{il}^{\setminus\mu*}$ resulting from all vehicles except μ that optimize the social cost $\mathcal{H}(\boldsymbol{\sigma}|\gamma_r)$. To achieve this, we have to identify the set of recommended traffic conditions on the links connecting to any given node i by using Eq.(26). For any set $(\sigma_{il}^{\mu*}, I_{il}^{\mu*})$, the corresponding optimal traffic of the set $\left\{(\sigma_{ji}^{\mu*}, I_{ji}^{\setminus\mu*})\right\}_{j\in\mathcal{N}_i\setminus l}$ from the neighbors j of node i except the parent l can be expressed by

$$\left\{(\sigma_{ji}^{\mu*}, I_{ji}^{\setminus\mu*})\right\}_{j\in\mathcal{N}_i\setminus l} = \operatorname*{argmin}_{\left\{\sigma_{ji}^{\mu}, I_{ji}^{\setminus\mu} \middle| \boldsymbol{R}_i=(0,0)\right\}} \left[\left(|\sigma_{il}^{\mu}| + |I_{il}^{\setminus\mu}|\right)^{\gamma_r} + \sum_{j\in\mathcal{N}_i\setminus l} E_{j\to i}\left(\sigma_{ji}^{\mu}, I_{ji}^{\setminus\mu}\right)\right]. \tag{27}$$

Therefore, the set $\left\{(\sigma_{ji}^{\mu*}, I_{ji}^{\setminus\mu*})\right\}_{j\in\mathcal{N}_i\setminus l}$ can be understood as a function of $(\sigma_{il}^{\mu*}, I_{il}^{\mu*})$, while for clear presentation, we simply write this function as a variable, and these can be found in parallel with the energy $E_{i\to l}\left(\sigma_{il}^{\mu}, I_{il}^{\setminus\mu}\right)$ as Eq.(26) and Eq.(27) are two identical equations except one is finding the minimal energy while another is looking for the arguments that give that energy. Subsequently, the

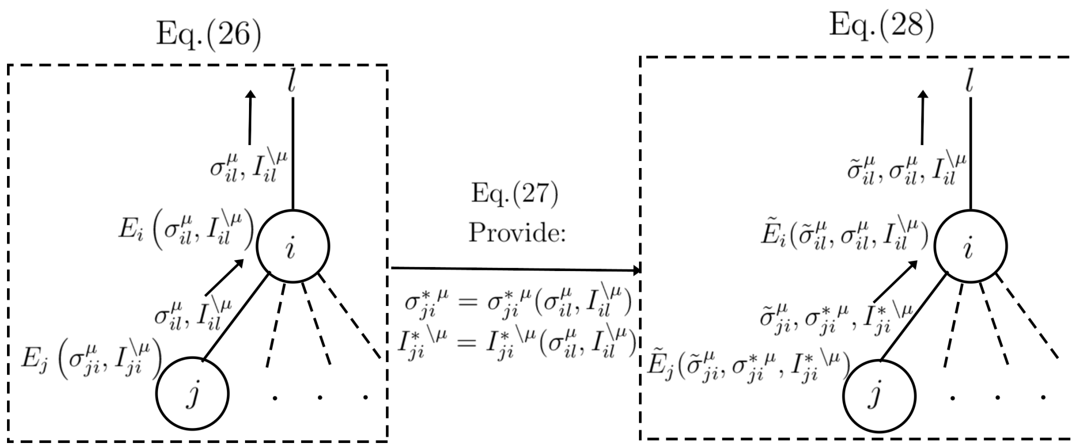

Figure 3. A two-layered diagram to illustrate (1) the recurrence relation in Eq.(26) and Eq.(28) about how the ancestor depends on its descendants, and (2) how Eq.(28) depends on Eq.(26). Both recurrent relations are iterated in parallel until the joint probability distribution $P\left[E^V, \tilde{E}^V\right]$ is converged.

energy $\tilde{E}_{i\to l}(\tilde{\sigma}_{il}^{\mu}, \sigma_{il}^{\mu*}, I_{il}^{\backslash\mu*})$ can be written down as a recurrent relation with the descendants' energies $\tilde{E}_{j\to i}(\tilde{\sigma}_{ji}^{\mu}, \sigma_{ji}^{\mu*}, I_{ji}^{\backslash\mu*})$ for all $j \in \mathcal{N}_i \setminus l$, describing the singled-out user μ switching from recommended route σ_{il}^{μ} to the route $\tilde{\sigma}_{il}^{\mu}$ that optimized its own individual traffic cost, given by

$$\tilde{E}_{i\to l}(\tilde{\sigma}_{il}^{\mu}, \sigma_{il}^{\mu*}, I_{il}^{\backslash\mu*}) = \min_{\left\{\left\{\tilde{\sigma}_{ji}^{\mu}\right\}_{j\in\mathcal{N}_i\setminus l}\middle|R_i^{\mu}=0\right\}} \left[\left|\tilde{\sigma}_{il}^{\mu}\right|\left(1+\left|I_{il}^{\backslash\mu*}\right|\right)^{\gamma-1} + \sum_{j\in\mathcal{N}_i\setminus l} \tilde{E}_{j\to i}(\tilde{\sigma}_{ji}^{\mu}, \sigma_{ji}^{\mu*}, I_{ji}^{\backslash\mu*})\right]. \tag{28}$$

To conclude, the process of this two-stage message passing framework is illustrated in Fig. 3, and in brief summary is described as follows: (1) In Eq.(26) we minimize the social travel cost that favors the recommendation system $\mathcal{H}(\boldsymbol{\sigma}|\gamma_r)$ for all vehicles. (2) For any given values of $\left(\sigma_{il}^{\mu*}, I_{il}^{\backslash\mu*}\right)$, the corresponding optimal path decisions $\left\{(\boldsymbol{\sigma}_{ji}^{\mu*}, I_{ji}^{\backslash\mu*})\right\}_{j\in\mathcal{N}_i\setminus l}$ of all neighbors j of the terminated node i except l is obtained by Eq.(27). (3) The information in (2) is provided to the singled-out vehicle μ to optimize its own individual traffic cost $\mathcal{H}_{\mu}(\tilde{\boldsymbol{\sigma}}^{\mu}|\boldsymbol{\sigma}^*, \gamma)$ and the selfish routing energy $\tilde{E}$ is computed by Eq.(28). Since Eq.(26) and Eq.(28) are extensive, we have to define two intensive quantities corresponding to E and $\tilde{E}$, given as

$$E^V_{i\to l}\left(\sigma^\mu_{il}, I^{\backslash\mu}_{il}\right) = E_{i\to l}\left(\sigma^\mu_{il}, I^{\backslash\mu}_{il}\right) - E_{i\to l}(0,0), \tag{29}$$

$$\tilde{E}_{i\to l}(\tilde{\sigma}^\mu_{il}, \sigma^{\mu*}_{il}, I^{\backslash\mu*}_{il}) = \tilde{E}_{i\to l}(\tilde{\sigma}^\mu_{il}, \sigma^{\mu*}_{il}, I^{\backslash\mu*}_{il}) - \tilde{E}_{i\to l}(0,0,0), \tag{30}$$

where the energies E^V and $\tilde{E}^V$ are computed by iterations based on Eq.(26) and Eq.(28), respectively.

In the thermodynamic limit as $N \to \infty$, it is assumed that the correlation between any 2 nodes vanishes and thus they are statistically independent of each other. Then, the analytical solution of the selfish rerouting strategy of the singled-out vehicle μ can be obtained by finding the joint functional probability distribution $P\left[\tilde{E}^V(\tilde{\sigma}^\mu_{il}, \sigma^{\mu*}, I^{\backslash\mu*}), E^V\left(\sigma^\mu, I^{\backslash\mu}\right)\right]$. For a clear presentation, we omit the arguments of both energy functions and denote this joint distribution as $P\left[\tilde{E}^V, E^V\right]$. Similar to Eq.(19), using Eqs. (26)-(30), the self-consistent equation for $P\left[\tilde{E}^V, E^V\right]$ can be written as

$$\begin{aligned} P\left[\tilde{E}^V, E^V\right] &= \int dk \frac{P(k)k}{\langle k\rangle} \int d\mathbf{\Lambda} P(\mathbf{\Lambda}) \prod_{j=1}^{k-1} \int dE^V_j d\tilde{E}^V_j P\left[\tilde{E}^V_j, E^V_j\right] \\ &\times \delta\left(E^V(\sigma^\mu, I^{\backslash\mu}) - \mathcal{R}'\left[\left\{E^V_j\right\}, \mathbf{\Lambda}, \sigma^\mu, I^{\backslash\mu}\right]\right) \\ &\times \delta\left(\tilde{E}^V(\tilde{\sigma}^\mu, \sigma^{\mu*}, I^{\backslash\mu*}) - \mathcal{R}''\left[\left\{\tilde{E}^V_j\right\}, \mathbf{\Lambda}, \tilde{\sigma}^\mu, \sigma^{\mu*}, I^{\backslash\mu*}\right]\right), \end{aligned} \tag{31}$$

where $\mathcal{R}'$ and $\mathcal{R}''$ refer to the right hand side of Eq.(29) and Eq.(30), respectively, which can be computed by the recurrence relation defined in Eq.(26) and Eq.(28). Noted that $P(k)$ and $\langle k\rangle = \int P(k)kdk$ represent the probability distribution and average of the nodes of degree k over the network, and $P(\mathbf{\Lambda})$ is the probability distribution of the transportation resources. Next, we can solve the converged distribution $P\left[\tilde{E}^V, E^V\right]$ numerically by employing population dynamics, for which the details were discussed in the previous section.

We remark that the computational complexity of the two-stage framework we introduce here is approximately $O\left(\langle k\rangle\left(8M-5\right)\right)$, allowing us to analyze the dynamics of the target vehicle over large systems. It is because when we are iterating Eq.(29) and Eq.(30) simultaneously, the optimal configuration of the path extracted serves as the decision in the former stage and the self-rerouting serves as the latter stage. This not only provides a tool to study selfish rerouting, but also generalizes the cavity method as a tool for studying dynamical systems. Note that we have only done one step ahead of selfish rerouting in the dynamics, and our framework can be extended to cases that consider more steps.

2.4.1 Single user case: Probability of selfish rerouting

Recall that our goal is to derive the physical quantities relating to the impact caused by selfish routing decisions, and after deriving the self-consistent equation, we are able to compute $p(\tilde{\sigma}^{\mu*}, \sigma^{\mu*}, I^{*})$, measuring the probability of the traffic behavior of the singled-out vehicle μ, where μ is switching from the original suggested route $\sigma^{\mu*}$ to another route $\tilde{\sigma}^{\mu*}$, on a link on which the total recommended traffic flow is I^{*}. For example, $p(1,0,5)$ is the probability of the vehicle μ switching its path to a link with the total flow of 5, where originally it was not on that link. Using the probability

$P\left[\tilde{E}^V, E^V\right]$ obtained in Eq.(31), we can express $p(\tilde{\sigma}^{\mu*}, \sigma^{\mu*}, I^*)$ by

$$p(\tilde{\sigma}^{\mu*}, \sigma^{\mu*}, I^*) = \int dE_1^V d\tilde{E}_1^V P\left[\tilde{E}_1^V, E_1^V\right] \int dE_2^V d\tilde{E}_2^V P\left[\tilde{E}_2^V, E_2^V\right] \sum_{I^{\setminus\mu*}} \Big\{ \delta\left(I^* - \left(\sigma^{\mu*} + I^{\setminus\mu*}\right)\right)$$
$$\times\, \delta\left(\left(\sigma^{\mu*}, I^{\setminus\mu*}\right) - \operatorname*{argmin}_{\sigma, I}\left[E_1^V(\sigma, I) + E_2^V(-\sigma, -I) - |\sigma + I|^{\gamma_r}\right]\right)$$
$$\times\, \delta\left(\tilde{\sigma}^{\mu*} - \operatorname*{argmin}_{\tilde{\sigma}}\left[\tilde{E}_1^V(\tilde{\sigma}, \sigma^{\mu*}, I^{\setminus\mu*}) + \tilde{E}_2^V(-\tilde{\sigma}, -\sigma^{\mu*}, -I^{\setminus\mu*}) - |\tilde{\sigma}|\left|1 + I^{\setminus\mu*}\right|^{\gamma_r - 1}\right]\right)\Big\}, \tag{32}$$

where the probability is evaluated by measuring the energy change caused by the given set of routing strategies.

2.4.2 Single user case: Cost of rerouting

After obtaining the probability of the routing behavior of the vehicle μ, we can obtain the probability of the traffic flow $P(I^*)$ by marginalizing $p(\tilde{\sigma}^{\mu*}, \sigma^{\mu*}, I^*)$. Thus, the probability of the initial recommended total traffic flow I^* on a link is given by

$$P(I^*) = \sum_{\tilde{\sigma}^{\mu*}, \sigma^{\mu}*} p(\tilde{\sigma}^{\mu*}, \sigma^{\mu*}, I^*). \tag{33}$$

The optimal social traffic cost $\mathcal{H}(\boldsymbol{\sigma}^*(\gamma_r)|\gamma)$ of the initial system with the suggested configurations $\boldsymbol{\sigma}^*(\gamma_r)$ can then be computed by

$$\mathcal{H}(\boldsymbol{\sigma}^*(\gamma_r)|\gamma) = \sum_{I^*} P(I^*)\,|I^*|^{\gamma}\,. \tag{34}$$

We recall that γ_r is the exponent reflecting the preference of the recommending system, for computing the recommended traffic configurations and the resulting total traffic flow I^* using Eq.(26), while the exponent γ is the exponent that defines the realistic social cost in Eq.(2). Similar to Eq.(34), we can compute the updated social cost $\mathcal{H}(\tilde{\boldsymbol{\sigma}}^*(\gamma_r)|\gamma)$ for the case in which only a single selfish vehicle exists on the network and is rerouted from the initial suggested route, which is given by

$$\mathcal{H}(\tilde{\boldsymbol{\sigma}}^*(\gamma_r)|\gamma) = \sum_{\tilde{\sigma}^{\mu*},\sigma^{\mu*},I^*} p(\tilde{\sigma}^{\mu*}, \sigma^{\mu*}, I^*)\,(|I^* - \sigma^{\mu*}| + |\tilde{\sigma}^{\mu*}|)^{\gamma}\,. \tag{35}$$

Note that the traffic flow $(|I^* - \sigma^{\mu*}| + |\tilde{\sigma}^{\mu*}|)$ represents the updated traffic flow after the vehicle has taken its selfish rerouting strategy, where $|I^* - \sigma^{\mu*}|$ is the background initial total traffic flow excluding the route of vehicle μ, while the term $|\tilde{\sigma}^{\mu*}|$ represents the updated selfish rerouting decision made by μ. With $\mathcal{H}(\boldsymbol{\sigma}^*(\gamma_r)|\gamma)$ and $\mathcal{H}(\tilde{\boldsymbol{\sigma}}^*(\gamma_r)|\gamma)$ computed by Eq.(34) and Eq.(35) respectively, we are allowed to compute the fractional change in social cost, $\Delta\mathcal{H}(\gamma_r, \gamma)$, as defined in Eq.(9), for a transportation system in which only one selfish vehicle exists.

2.4.3 Multiple user case: Cost of rerouting

To study the case in which multiple selfish users exist on the transportation system, we assume that all selfish vehicles' decisions are independent of each other, and represent their driving behavior by the selfish driving behavior of the singled-out user μ we measured in Eq.(32). Given that a link consists of n users and there are t selfish users, where the rerouting probability is given by p, the total combinations of such a situation is the binomial distribution

$$\mathcal{B}(n, p, t) = C^n_t p^t (1 - p)^{n-t}, \tag{36}$$

where $C_t^n = \frac{n!}{t!(n-t)!}$ is the binomial coefficient. We next define the conditional probability $P(\tilde{I}^*|I^*)$ as the probability when the resulting total traffic flow on a link after selfish rerouting is $\tilde{I}^*$, and when the original total traffic flow on the link is I^*. We further define $\tilde{m}_s^*$ as the number of selfish vehicles that exist on the link, after all selfish vehicles have already taken their selfish rerouting strategies by considering the initial recommended configurations. Next, we evaluate the probability $P(\tilde{I}^*, \tilde{m}_s^*|I^*)$, depending on the number of rerouting strategies, as

$$P(\tilde{I}^*, \tilde{m}_s^*|I^*) = \sum_{m_s=\max(0,Mf_s-(M-I^*))}^{\min(Mf_s,I^*)} \left[\frac{C_{m_s}^{Mf_s} C_{I^*-m_s}^{M(1-f_s)}}{C_{I^*}^M} \sum_{r=0}^{m_s} \mathcal{B}\left(m_s, r, \frac{p(0,1,I^*)}{p(0,1,I^*)+p(1,1,I^*)}\right) \right.$$
$$\left. \times \sum_{s=0}^{Mf_s-m_s} \mathcal{B}\left(Mf_s - m_s, s, \frac{p(1,0,I^*)}{p(1,0,I^*)+p(0,0,I^*)}\right) \delta_{\tilde{I}^*, I^*+(s-r)} \delta_{\tilde{m}_s^*, m_s+(s-r)} \right]. \tag{37}$$

The probability derived in Eq.(37) appears complicated but is relatively easy to understand. The term $\frac{C_{m_s}^{Mf_s} C_{I^*-m_s}^{M(1-f_s)}}{C_{I^*}^M}$ is the probability that there are m_s selfish users on a link on which the total traffic flow is I^*, and: (1) the denominator is the total combination in which I^* users are on the link among all M users, and; (2) the numerator is the total of combinations of choosing m_s and $I^* - m_s$ vehicles on the link among all Mf_s selfish users and $M(1-f_s)$ compliant users. The probability $\frac{p(0,1,I^*)}{p(0,1,I^*)+p(1,1,I^*)}$ is the conditional probability that an arbitrary selfish vehicle leaves the link, given that it is on the link in the initial recommendation. Similarly, $\frac{p(1,0,I^*)}{p(1,0,I^*)+p(0,0,I^*)}$ is the conditional probability that an arbitrary selfish vehicle switches into the link, given that it is not on the link in the initial recommendation. Therefore, the binomial probability $\mathcal{B}\left(m_s, r, \frac{p(0,1,I^*)}{p(0,1,I^*)+p(1,1,I^*)}\right)$ is the probability that among m_s selfish vehicles that are initially on the link, there are r of them not traveling on the link after selfish rerouting. Similarly, the binomial probability $\mathcal{B}\left(Mf_s - m_s, s, \frac{p(1,0,I^*)}{p(1,0,I^*)+p(0,0,I^*)}\right)$ is the probability that of the remaining $Mf_s - m_s$ selfish users who are initially not traveling on the link, s of them are switching in and traveling on the link after selfish rerouting. Therefore, the probability $P(\tilde{I}^*, \tilde{m}_s^*|I^*)$ we derived in Eq.(37) has considered all combinations of path changing by assigning the appropriate weighted factors as explained above. We remark that we measure $P(\tilde{I}^*, \tilde{m}_s^*|I^*)$ instead of simply measuring $P(\tilde{I}^*|I^*)$ so that we can identify the number of selfish vehicles remaining on the link after selfish rerouting and allowing us to compute the averaged traveling cost over the selfish and compliant users after rerouting, as described below.

Since we have already obtained the probability $P(\tilde{I}^*, \tilde{m}_s^*|I^*)$, we can compute the probability $P(\tilde{I}^*|I^*)$ by marginalizing $P(\tilde{I}^*, \tilde{m}_s^*|I^*)$ over $\tilde{m}_s^*$, given by

$$P(\tilde{I}^*|I^*) = \sum_{\tilde{m}_s^*=1}^{Mf_s} P(\tilde{I}^*, \tilde{m}_s^*|I^*). \tag{38}$$

Hence, after obtaining $P(\tilde{I}^*|I^*)$, the global traffic cost $\mathcal{H}(\tilde{\boldsymbol{\sigma}}^*(\gamma_r), \gamma)$ after rerouting can be found by

$$\mathcal{H}(\tilde{\boldsymbol{\sigma}}^*(\gamma_r), \gamma) = \sum_{\tilde{I}^*} \left|\tilde{I}^*\right|^{\gamma} \sum_{I^*} P\left(\tilde{I}^*\middle| I^*\right) P\left(I^*\right). \tag{39}$$

Other than the global traffic cost, we can also compute the other major quantities of interest, in order to study the impact of rerouting specifically on selfish and compliant users. Thus, the travel cost averaged over the selfish users is evaluated by

$$\mathcal{H}_{\text{selfish}}\left(\tilde{\boldsymbol{\sigma}}^*(\gamma_r)|\gamma\right) = \frac{1}{Mf_s} \sum_{\tilde{I}^*, \tilde{m}_s^*} \left[\tilde{m}_s^* \left|\tilde{I}^*\right|^{\gamma-1} \sum_{I^*} P(\tilde{I}^*, \tilde{m}_s^*|I^*) P(I^*)\right], \tag{40}$$

and the travel cost averaged over the compliant users is evaluated by

$$\mathcal{H}_{\text{compliant}}\left(\tilde{\boldsymbol{\sigma}}^*(\gamma_r)|\gamma\right) = \frac{1}{M(1-f_s)} \sum_{\tilde{I}^*,\tilde{m}_s^*} \left[\left(\left|\tilde{I}^*\right| - \tilde{m}_s^* \right) \left|\tilde{I}^*\right|^{\gamma-1} \sum_{I^*} P(\tilde{I}^*, \tilde{m}_s^* | I^*) P(I^*) \right]. \tag{41}$$

Note that after reordering Eq.(40) and Eq.(41), we have

$$\begin{aligned} M f_s \mathcal{H}_{\text{selfish}}\left(\tilde{\boldsymbol{\sigma}}^*(\gamma_r)|\gamma\right) + M(1-f_s)\mathcal{H}_{\text{compliant}}\left(\tilde{\boldsymbol{\sigma}}^*(\gamma_r)|\gamma\right) &= \sum_{\tilde{I}^*,\tilde{m}_s^*} \left[\left|\tilde{I}^*\right|^{\gamma} \sum_{I^*} P(\tilde{I}^*, \tilde{m}_s^* | I^*) P(I^*) \right] \\ &= \mathcal{H}(\tilde{\boldsymbol{\sigma}}^*(\gamma_r), \gamma), \end{aligned} \tag{42}$$

showing the trivial result that the sum of the averaged costs of selfish and compliant users is indeed the total cost of the system. Thus, we can compute the fractional change $\Delta\mathcal{H}(\gamma_r, \gamma)$, $\Delta\mathcal{H}_{\text{selfish}}(\gamma_r, \gamma)$ and $\Delta\mathcal{H}_{\text{compliant}}(\gamma_r, \gamma)$, of the global traffic cost, selfish users and compliant users respectively, as defined in Eq.(9).

2.4.4 Cost of rerouting after incorporating distance into cavity equations

In the above derivation, we provided a generalized framework on how the cavity method can be used to provide a vigorous probability analysis and measure quantities beyond the averaged energy, which can be extended and applied to other disordered and complex systems. We remark that the above calculation of probabilities is not enough for predicting $\Delta\mathcal{H}(\gamma_r, \gamma)$, $\Delta\mathcal{H}_{\text{selfish}}(\gamma_r, \gamma)$ and $\Delta\mathcal{H}_{\text{compliant}}(\gamma_r, \gamma)$ with sufficient accuracy, and our hypothesis on this issue is that we have omitted some crucial parameters that are highly correlated with the probabilities of interest. We further observe that the derivations in Section 2.4.3 are assuming all links in the network are homogeneous, while an assumption of heterogeneity should be adopted. For instance, for any given link on the network with initial total traffic flow $I^* = 0$, if it is closer to the universal destination, there would be a higher probability that the corresponding total traffic flow $\left|\tilde{I}^*\right| > 0$ after rerouting. This is because, for the links that are closer to the destination, most vehicles do not need to reroute to a longer path in order to switch to the link which is more favorable to the users compare to the links that are far from the destination. Therefore, in order to improve the equations we derived, we incorporate the distance of a link from the universal destination into the derivation.

To facilitate the derivation, we define d_i as the minimum distance between the node i and the common destination. For any network, the minimum distance between any two nodes is defined as the minimum number of links required to construct a connected path between them. Therefore, a node i with $d_i = 0$ is indeed the universal destination $\mathcal{D}$. In simulations, one is allowed to use Dijkstra's method (Barbehenn 1998) to find the minimal distance of nodes, nevertheless, it is not applicable in the cavity method as there is no fixed graph structure. Instead, we incorporate d_i into the cavity energies defined in Eq.(26) and Eq.(28), where the variable d_i corresponds to the distance in the message-passing process and is given by

$$d_i = \begin{cases} 0, & \text{if } \mathcal{D} = i, \text{i.e. } \Lambda_i = -\infty \\ 1 + \min_{j \in \mathcal{N}_i \backslash l} \left\{ d_j \right\} & \text{otherwise} \end{cases}, \text{ where} \tag{43}$$

d_i can be further simplified as $d_i = (1 - \delta_{i,\mathcal{D}}) \left(1 + \min_{j \in \mathcal{N}_i \backslash l} \left\{ d_j \right\}\right)$. We remark that in the iteration process of message-passing, Eq.(26), Eq.(28) and Eq.(43) are updating in parallel, and hence the self-consistent equation in Eq.(31) will be modified and becomes

$$
\begin{aligned}
P\left[\tilde{E}^V, E^V, D\right] = \int dk \frac{P(k)k}{\langle k \rangle} \int d\mathbf{\Lambda} P(\mathbf{\Lambda}) \prod_{j=1}^{k-1} \int dE_j^V d\tilde{E}_j^V dD P\left[\tilde{E}_j^V, E_j^V, D\right] \\
\times \delta\left(E^V(\sigma^\mu, I^{\setminus\mu}) - \mathcal{R}^*\left[\left\{E_j^V\right\}, \mathbf{\Lambda}, \sigma^\mu, I^{\setminus\mu}\right]\right) \\
\times \delta\left(\tilde{E}^V(\tilde{\sigma}^\mu, \sigma^{\mu*}, I^{\setminus\mu*}) - \mathcal{R}^{**}\left[\left\{\tilde{E}_j^V\right\}, \mathbf{\Lambda}, \tilde{\sigma}^\mu, \sigma^{\mu*}, I^{\setminus\mu*}\right]\right) \\
\times \delta\left(D - (1 - \delta_{i,\mathcal{D}})\left(1 + \min_{j \in \mathcal{N}_i \setminus l}\left\{d_j\right\}\right)\right).
\end{aligned}
\tag{44}
$$

Similarly, we can modify Eq.(32) to include the minimum distance D^* to the common destination, in order to compute the joint probability of rerouting $p(\tilde{\sigma}^{\mu*}, \sigma^{\mu*}, I^*, D^*)$, given by

$$
\begin{aligned}
p(\tilde{\sigma}^{\mu*}, \sigma^{\mu*}, I^*, D^*) = \int dE_1^V d\tilde{E}_1^V dD_1 P\left[\tilde{E}_1^V, E_1^V, D_1\right] \int dE_2^V d\tilde{E}_2^V dD_2 P\left[\tilde{E}_2^V, E_2^V, D_2\right] \sum_{I^{\setminus\mu*}} \left\{\delta\left(I^* - \left(\sigma^{\mu*} + I^{\setminus\mu*}\right)\right)\right. \\
\times \delta\left(\left(\sigma^{\mu*}, I^{\setminus\mu*}\right) - \underset{\sigma, I}{\operatorname{argmin}}\left[E_1^V(\sigma, I) + E_2^V(-\sigma, -I) - |\sigma + I|^{\gamma_r}\right]\right) \\
\left. \times \delta\left(\tilde{\sigma}^{\mu*} - \underset{\tilde{\sigma}}{\operatorname{argmin}}\left[\tilde{E}_1^V(\tilde{\sigma}, \sigma^{\mu*}, I^{\setminus\mu*}) + \tilde{E}_2^V(-\tilde{\sigma}, -\sigma^{\mu*}, -I^{\setminus\mu*}) - |\tilde{\sigma}|\left|1 + I^{\setminus\mu*}\right|^{\gamma_r - 1}\right]\right)\right\} \\
\times \delta\left(D^* - \min(D_1, D_2)\right).
\end{aligned}
\tag{45}
$$

With $p(\tilde{\sigma}^{\mu*}, \sigma^{\mu*}, I^*, D^*)$ established, we can obtain $P(I^*, D^*)$ by marginalization as

$$
P(I^*, D^*) = \sum_{\tilde{\sigma}^{\mu*}, \sigma^{\mu*}} p(\tilde{\sigma}^{\mu*}, \sigma^{\mu*}, I^*, D^*). \tag{46}
$$

Next, the conditional probability in Eq.(37) is modified to obtain $P(\tilde{I}^*, \tilde{m}_s^* | I^*, D^*)$, given by

$$P(\tilde{I}^*, \tilde{m}_s^* | I^*, D^*) = \sum_{m_s=\max(0, Mf_s-(M-I^*))}^{\min(Mf_s, I^*)} \left[\frac{C_{m_s}^{Mf_s} C_{I^*-m_s}^{M(1-f_s)}}{C_{I^*}^{M}} \sum_{r=0}^{m_s} \mathcal{B}\left(m_s, r, \frac{p(0,1,I^*,D^*)}{p(0,1,I^*,D^*) + p(1,1,I^*,D^*)} \right) \right.$$
$$\left. \times \sum_{s=0}^{Mf_s-m_s} \mathcal{B}\left(Mf_s - m_s, s, \frac{p(1,0,I^*,D^*)}{p(1,0,I^*,D^*) + p(0,0,I^*,D^*)} \right) \delta_{\tilde{I}^*, I^*+(s-r)} \delta_{\tilde{m}_s^*, m_s+(s-r)} \right], \tag{47}$$

which will also allow us to eventually compute $P(\tilde{I}^* | I^*, D^*)$.

Thus, we can find the quantities of interest in order to measure the impact caused by selfish rerouting. The social traffic cost of the whole system after selfish rerouting and including distance as a variable is given by

$$\mathcal{H}(\tilde{\boldsymbol{\sigma}}^*(\gamma_r)|\gamma) = \sum_{\tilde{I}^*} \left|\tilde{I}^*\right|^{\gamma} \sum_{I^*, D^*} P\left(\tilde{I}^* \middle| I^*, D^*\right) P\left(I^*, D^*\right); \tag{48}$$

the travel cost averaged over the selfish users is evaluated by

$$\mathcal{H}_{\text{selfish}}\left(\tilde{\boldsymbol{\sigma}}^*(\gamma_r)|\gamma\right) = \frac{1}{Mf_s} \sum_{\tilde{I}^*, \tilde{m}_s^*} \left[\tilde{m}_s^* \left|\tilde{I}^*\right|^{\gamma-1} \sum_{I^*, D^*} P(\tilde{I}^*, \tilde{m}_s^* | I^*, D^*) P(I^*, D^*) \right]; \tag{49}$$

and the travel cost averaged over the compliant users is

$$\mathcal{H}_{\text{compliant}}\left(\tilde{\boldsymbol{\sigma}}^*(\gamma_r)|\gamma\right) = \frac{1}{M(1-f_s)} \sum_{\tilde{I}^*, \tilde{m}_s^*} \left[\left(\left|\tilde{I}^*\right| - \tilde{m}_s^* \right) \left|\tilde{I}^*\right|^{\gamma-1} \sum_{I^*, D^*} P(\tilde{I}^*, \tilde{m}_s^* | I^*, D^*) P(I^*, D^*) \right]. \tag{50}$$

Therefore, we can specifically investigate different kinds of vehicles, including vehicles on average, selfish vehicles and compliant vehicles, and see whether they benefit or lose in cost after rerouting. The results will be discussed in Section 2.6.

2.4.5 Algorithm inspired by the cavity method

Remarkably, not only rigorous probability analysis can be carried out using the cavity method, but an effective algorithm can be obtained for optimizing and investigating individuals' behavior over single instances. To do this, we can iterate Eq.(29) and Eq.(30) over the fixed network topology of a particular instance until convergence is reached for both energies E^V and $\tilde{E}^V$. Then for any link (ij) over the network, the optimal configurations to identify paths, $\tilde{\sigma}_{ij}^{\mu*}, \sigma_{ij}^{\mu*}$ and $I_{ij}^{\backslash\mu*}$ can be found by

$$\left\{\sigma_{ij}^{\mu*}, I_{ij}^{\backslash\mu*}\right\} = \underset{\{\sigma, I\}}{\operatorname{argmin}} \left[E_{i\to j}^V(\sigma, I) + E_{j\to i}^V(-\sigma, -I) - |\sigma + I|^{\gamma_r}\right], \text{ and} \tag{51}$$

$$\tilde{\sigma}_{ij}^{\mu*} = \underset{\tilde{\sigma}}{\operatorname{argmin}} \left[\tilde{E}_{i\to j}^V\left(\tilde{\sigma}, \sigma_{ij}^{\mu*}, I_{ij}^{\backslash\mu*}\right) + \tilde{E}_{j\to i}^V\left(-\tilde{\sigma}, -\sigma_{ji}^{\mu*}, -I_{ji}^{\backslash\mu*}\right) - |\tilde{\sigma}|\left|1 + I_{ij}^{\backslash\mu*}\right|^{\gamma_r - 1}\right]. \tag{52}$$

In simulations, it is common that the solutions of Eq.(51) and Eq.(52) exhibit degeneracy, meaning that there exist multiple solutions that can achieve the optimal state of the system. Degeneracy in the ground state might be highly complicated, for instance, it is difficult to identify the corresponding paths of vehicles when there are multiple values of the optimal flow of a link. To break the degeneracy, for any link (ij) we can assign a randomly selected quenched bias ϵ_{ij}, by adding $\epsilon_{ij}\left|\sigma_{ij}^{\mu} + I_{ij}^{\backslash\mu*}\right|$ to $E_{i\to j}^V\left(\sigma_{ij}^{\mu}, I_{ij}^{\backslash\mu*}\right)$ and adding $\epsilon_{ij}\left|\tilde{\sigma}_{ij}^{\mu*}\right|\left|1 + I_{ij}^{\backslash\mu*}\right|$ to $\tilde{E}_{i\to j}^V\left(\tilde{\sigma}_{ij}^{\mu*}, \sigma_{ij}^{\mu*}, I_{ij}^{\backslash\mu*}\right)$, while the iteration and merging process remains the same. By adding the biases, the convergence of the iteration process will be in a particular state without degeneracy. The convergence to a single state is due to the following: Assuming there exists a set of states at minimum energy, by adding the quenched bias which is very small in value into the cost function, these states are no longer at the same energy, but differ by infinitesimal values from which one of these states would be identified as the ground state.

2.5 Two-stage exhaustive cavity method and analytical solutions for selfish routing

As discussed in Section 1.1, it is crucial to develop a precise optimization framework and study why the cavity method presented in Section 2.4 failed to provide accurate predictions of quantities of interest. In this section, we adopt the same mathematical model defined in Section 2.1, and develop a two-stage exhaustive optimization framework that is not only capable of measuring macroscopic quantities relating to traffic conditions, but also able to measure microscopic quantities such as the detail of the path configurations of all vehicles on the network. Similar to the cavity method in Section 2.4, the first stage in the exhaustive optimization framework aims to identify the exact paths of all users in the optimal configuration that optimize $\mathcal{H}(\boldsymbol{\sigma}|\gamma_r)$ and recommended to all vehicles. In the second stage, we randomly select a group of selfish vehicles and every vehicle μ in the group optimizes its own individual traffic cost $\mathcal{H}_\mu(\tilde{\boldsymbol{\sigma}}^\mu|\tilde{\boldsymbol{\sigma}}^*, \gamma)$ by switching to another path. To facilitate the derivation, the transportation resource on node i is defined as $\boldsymbol{\Lambda}_i = \left\{\Lambda_i^\mu\right\}_\mu$, where Λ_i^μ is defined as the transportation load for the user μ in i, in particular,

$$\Lambda_i^\mu = \begin{cases} 1, & \text{if } O_\mu = i; \\ -\infty, & \text{if } \mathcal{D} = i; \\ 0, & \text{otherwise.} \end{cases} \tag{53}$$

Next, similar to Eq.(12), we define the vector of the net sources of all users on node i as $\boldsymbol{R} = \{R_i^\mu\}_\mu$, therefore, we have

$$R_i^\mu = \Lambda_i^\mu + \sum_{j \in \mathcal{N}_i} \sigma_{ji}^\mu, \quad \forall \mu \tag{54}$$

where R_i^μ is the net resource for the vehicle μ on the transportation network. Similar to the previous two-stage cavity method, the paths σ_{il}^μ are restricted to be integers for all links (ij) and vehicles μ. Then, $\forall i \neq \mathcal{D}$, we restrict $\boldsymbol{R} = \mathbf{0}$, i.e. $R_i^\mu = 0, \forall \mu, \forall i$, to ensure that all paths identified from origin to destination are connected.

Assuming the networks are sparse, that are in treelike structure and only large loops exist, we employ the cavity method at zero temperature. For all nodes i, we define the optimized energy function of the tree structures terminated at i as $E_{i\to l}(\boldsymbol{\sigma}_{il})$, where $\boldsymbol{\sigma}_{il} = \left\{\sigma_{il}^\mu\right\}_\mu$ is the vector of routing decisions for all users μ on the link (il). In contrast to the definition in Section 2.4, this approach measures the exact path decisions of every user instead of the total traffic flow I, allowing us to identify the contribution of energy by every vehicle. The recurrence relation among the energies $E_{i\to l}(\boldsymbol{\sigma}_{il})$ and $E_{j\to i}(\boldsymbol{\sigma}_{ji}), \forall j \in \mathcal{N}_i \setminus l$, can then be given by

$$E_{i\to l}(\boldsymbol{\sigma}_{il}) = \min_{\left\{\{\boldsymbol{\sigma}_{ji}\}_{j\in\mathcal{N}_i\setminus l}|\boldsymbol{R}_i=\mathbf{0}\right\}} \left[\left(\sum_\mu \left|\sigma_{il}^\mu\right|\right)^{\gamma_r} + \sum_{j\in\mathcal{N}_i\setminus l} E_{j\to i}\left(\boldsymbol{\sigma}_{ji}\right)\right], \tag{55}$$

where the exponent γ_r identifies the recommended optimal paths by the recommending system.

After identifying the exact optimal path recommendations for all vehicles, we study the selfish rerouting behaviors of the selfish vehicles. We first assume that all vehicles are selfish and introduce $\left\{\tilde{E}_{i\to l}^\mu\left(\tilde{\sigma}_{il}^\mu, \boldsymbol{\sigma}_{il}^*\right)\right\}_\mu$ as the set of energy functions for all vehicles μ. Similar to the case in Section 2.4, the energy $\tilde{E}_{i\to l}^\mu$ describes the energy for a user μ to switch to another choice of path $\tilde{\sigma}_{il}^\mu$ from the original decision σ_{il}^μ, in order to optimize its own individual traffic cost $\mathcal{H}_\mu$ by considering the background traffic condition $\boldsymbol{\sigma}_{il}^*$ that optimize $\mathcal{H}(\boldsymbol{\sigma}|\gamma_r)$. Using Eq.(55), for any optimal traffic condition $\boldsymbol{\sigma}_{il}^*$ on the link (il), the corresponding set of optimal traffic condition $\left\{\boldsymbol{\sigma}_{ji}^*\right\}_{j\in\mathcal{N}_i\setminus l}$ of all descendant neighbors j of the node i except the parent node l, which can be understood as functions

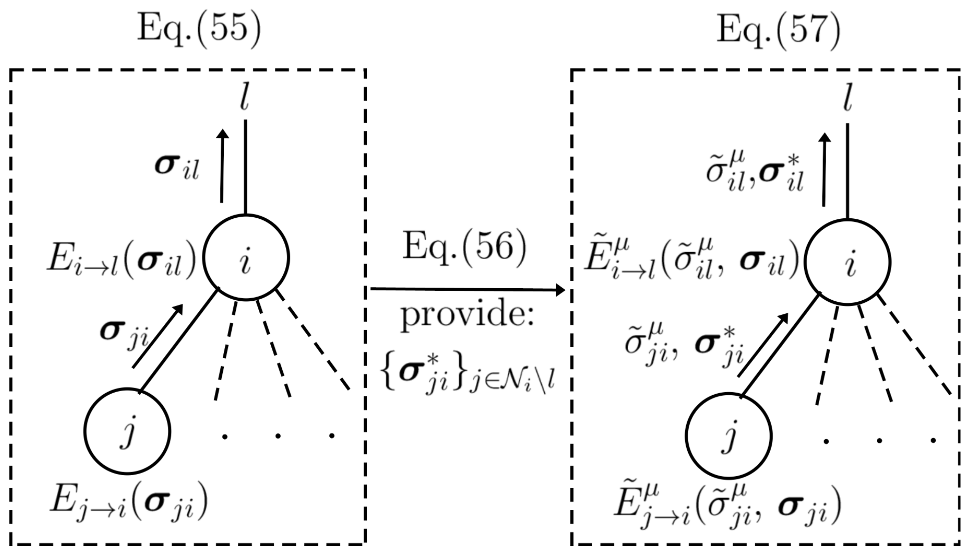

Figure 4. A two-layered diagram to illustrate the recurrence relation in Eq.(55) and Eq.(57), as well as their dependence. Both recurrence relations are iterated in parallel until the joint probability distribution $P\left[E^V, \tilde{E}^V\right]$ is converged.

of $\boldsymbol{\sigma}^*_{il}$, can be expressed as

$$\left\{\boldsymbol{\sigma}^*_{ji}\right\}_{j\in\mathcal{N}_i\backslash l} = \underset{\left\{\left\{\boldsymbol{\sigma}_{ji}\right\}_{j\in\mathcal{N}_i\backslash l}|\boldsymbol{R}_i=0\right\}}{\operatorname{argmin}} \left[\left(\sum_{\mu}\left|\sigma^{\mu}_{il}\right|\right)^{\gamma_r} + \sum_{j\in\mathcal{N}_i\backslash l} E_{j\to i}\left(\boldsymbol{\sigma}_{ji}\right)\right]. \tag{56}$$

Then, for all users μ, the energy function $\tilde{E}_{i\to l}\left(\tilde{\sigma}^{\mu}_{il}, \boldsymbol{\sigma}^*_{il}\right)$ can be written down as a recurrence relation, given by

$$\tilde{E}^{\mu}_{i\to l}\left(\tilde{\sigma}^{\mu}_{il}, \boldsymbol{\sigma}^*_{il}\right) = \min_{\left\{\left\{\tilde{\sigma}^{\mu}_{ji}\right\}_{j\in\mathcal{N}_i\backslash l}|\boldsymbol{R}_i=\boldsymbol{0}\right\}} \left[\left|\tilde{\sigma}^{\mu}_{il}\right|\left(1+\sum_{\nu\neq\mu}\left|\tilde{\sigma}^{\nu}_{il}\right|\right)^{\gamma-1} + \sum_{j\in\mathcal{N}_i\backslash l}\tilde{E}^{\mu}_{j\to i}\left(\tilde{\sigma}^{\mu}_{ji}, \boldsymbol{\sigma}^*_{ji}\right)\right], \tag{57}$$

where the exponent γ is responsible for evaluating the individual traffic cost of the vehicle μ.

Similar to the approach in Section 2.4, the message-passing procedure can be illustrated as in Fig. 4. The process is exactly the same as in the previous section: the social travel cost is minimized by Eq.(55) in the first step and the corresponding optimal path configurations identified by Eq.(56)

are passed to Eq.(57) in order to minimize individual travel costs for all users μ.

We note that the energy functions $E_{i\to l}(\boldsymbol{\sigma}_{il})$ and $\left\{\tilde{E}^{\mu}_{i\to l}\left(\tilde{\sigma}^{\mu}_{il}, \boldsymbol{\sigma}^{*}_{il}\right)\right\}_{\mu}$ are extensive and it is difficult to obtain the converged analytical solutions. Thus, the corresponding intensive quantities $E^{V}_{i\to l}(\boldsymbol{\sigma}_{il})$ and $\left\{\tilde{E}^{V}_{\mu,i\to l}\left(\tilde{\sigma}^{\mu}_{il}, \boldsymbol{\sigma}^{*}_{il}\right)\right\}_{\mu}$ are defined as

$$E^{V}_{i\to l}(\boldsymbol{\sigma}_{il}) = E_{i\to l}(\boldsymbol{\sigma}_{il}) - E_{i\to l}(\mathbf{0}), \tag{58}$$

$$\tilde{E}^{V}_{\mu,i\to l}\left(\tilde{\sigma}^{\mu}_{il}, \boldsymbol{\sigma}^{*}_{il}\right) = \tilde{E}^{\mu}_{i\to l}\left(\tilde{\sigma}^{\mu}_{il}, \boldsymbol{\sigma}^{*}_{il}\right) - \tilde{E}^{\mu}_{i\to l}(\mathbf{0},\mathbf{0}) \quad \forall\mu, \tag{59}$$

where the computations of E^{V} and $\tilde{E}^{V}_{\mu}$ are obtained by iterating Eq.(55) and Eq.(57).

In the thermodynamic limit as $N\to\infty$, the correlation of variables between any 2 nodes is assumed to vanish and the variables are independent of each other. The analytical solution of the detailed routing strategies of every vehicle, before and after the selfish rerouting takes place, can then be evaluated by the joint functional probability distribution $P\left[\left\{\tilde{E}^{V}_{\mu}(\tilde{\sigma}^{\mu}, \boldsymbol{\sigma}^{*})\right\}_{\mu}, E^{V}(\boldsymbol{\sigma})\right]$, in which the arguments of the energy functions will be omitted for a clearer presentation, denoted as $P\left[\left\{\tilde{E}^{V}_{\mu}\right\}_{\mu}, E^{V}\right]$. Making use of Eqs. (55)-(59), the self-consistent equation for $P\left[\left\{\tilde{E}^{V}_{\mu}\right\}_{\mu}, E^{V}\right]$ can then be written as

$$\begin{aligned} P\left[\left\{\tilde{E}^{V}_{\mu}\right\}_{\mu}, E^{V}\right] = &\int dk \frac{P(k)k}{\langle k\rangle} \int d\boldsymbol{\Lambda} P(\boldsymbol{\Lambda}) \prod_{j=1}^{k-1} \int dE^{V}_{j} \prod_{\nu=1}^{M} d\tilde{E}^{V}_{\nu,j} P\left[\left\{\tilde{E}^{V}_{\mu,j}\right\}_{\mu}, E^{V}_{j}\right] \\ &\times \delta\left(E^{V}(\boldsymbol{\sigma}) - \mathcal{R}^{*}\left[\left\{E^{V}_{j}\right\}, \boldsymbol{\Lambda}, \boldsymbol{\sigma}\right]\right) \\ &\times \prod_{\nu=1}^{M} \delta\left(\tilde{E}^{V}_{\nu}(\tilde{\sigma}^{\nu}, \boldsymbol{\sigma}^{*}) - \mathcal{R}^{**}\left[\left\{\tilde{E}^{V}_{\nu,j}\right\}, \boldsymbol{\Lambda}, \tilde{\sigma}^{\nu}, \boldsymbol{\sigma}^{*}\right]\right), \end{aligned} \tag{60}$$

where $\mathcal{R}^{*}$ and $\mathcal{R}^{**}$ correspond to the right hand side of the recurrence relation in Eq.(58) and Eq.(59), respectively, and where $P(k)$, $\langle k\rangle = \int P(k)kdk$ and $P(\boldsymbol{\Lambda})$ represent the probability distribution, av-

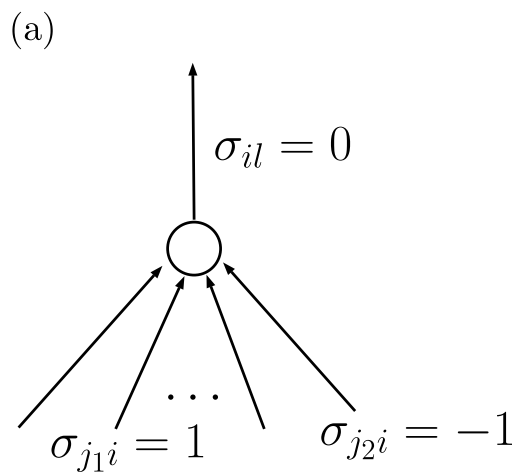

Figure 5. An illustration of how the total number of combinations of path decisions σ_{il} of the ancestor and its descendants' path σ_{ji} can be reduced. (a) For the case when $\sigma_{il} = 0$, the total number of combinations of the paths of descendants would be $2C_2^{k-1} + 1 = k(k-1) + 1$, corresponding to the sum of two sub-cases. One is $\sigma_{ji} = 0, \forall j \in \mathcal{N}_i \setminus l$, and another is selecting two descendants j_1, j_2 such that $\sigma_{j_1 i} = 1$ and $\sigma_{j_2 i} = 1$, while $\sigma_{ji} = 0$ for all other nodes j. (b) For the case when $\sigma_{il} = \pm 1$, in each of the sub-cases, the total number of combinations of the paths of descendants would be $k-1$, i.e. $2(k-1)$ in total, by selecting one descendant with $\sigma_{ji} = \pm 1$, while $\sigma_{ji} = 0$ for all other descendant nodes.

erage of the nodes degree k over the network and the probability distribution of the transportation resources, respectively.

2.5.1 Computational complexity of the exhaustive cavity method

Compared to the two-stage cavity method in Section 2.4, the computational complexity of the exhaustive cavity method is more complicated. In general, without any simplification, for each σ^μ there are three possibilities, -1, 0 and 1, thus the energy function $E^V(\boldsymbol{\sigma})$ consists of 3^M values. On the other hand, $\tilde{E}^V_\mu$ consists of 3^{M+1} values in which the optimal configuration is already found in $\tilde{E}^V_\mu$. Therefore, the computational complexity of the two-stage cavity equations is given as $O\left(\left\langle 3^{M(k-1)}\right\rangle_k\right)$, where $\langle\cdot\rangle_k$ stands for the average of the quantities inside the angular bracket over the degree distribution $P(k)$. Note that all vehicles are traveling in the same direction, so we can reduce the total combinations of $\boldsymbol{\sigma}$ from 3^M to $2^{M+1}-1$. To further simplify the total number of combinations, we can first consider all combinations of the routing decisions of one user, then consider the possible cases of $\boldsymbol{\sigma}$ when all users are combined. As shown in Fig.5, the total combinations of path decisions $\left\{\sigma_{ji}\right\}_{j\in\mathcal{N}_i}$ at any node i can be found by considering the following cases: (i) As shown in Fig.5(a), when $\sigma_{il}=0$, to ensure that $\mathcal{R}_i=0$, for all descendants j of node i except the ancestor l, σ_{ji} can be either all zero, or there exist two nodes j_1 and j_2 such that $\sigma_{j_1 i}=1$ and $\sigma_{j_2 i}=-1$. Therefore, the total combinations of this case would be $2C_2^{k-1}+1=k(k-1)+1$, denoted as a for future calculations. (ii) As shown in Fig.5(b), when $\sigma_{il}=\pm 1$, to ensure that $\mathcal{R}_i=0$, one of the descendants j of node i except the ancestor l, σ_{ji} have to be ± 1, while $\sigma_{ji}=0$ for the other descendants j. Therefore, the total number of combinations of this case would be $2C_1^{k-1}=2(k-1)$, denoted as b for future calculations. When we combine all M users, the total number of combinations when there are τ users traveling with $\sigma=1$ is given by $C_\tau^M a^{M-\tau} b^\tau$. Therefore, the total number of combinations is given as

$$2\left[\sum_{\tau=0}^{M} C_\tau^M a^{M-\tau} b^\tau\right]-a^M=2\left[(a+b)^M\right]-a^M=2\left(k^2-2k+2\right)^M-\left(k^2-3k+3\right)^M, \qquad (61)$$

where the term $-\left(k^2-3k+3\right)^M$ is to cancel the double counting of the case when $\boldsymbol{\sigma}=\mathbf{0}$. Similarly, for any selfish vehicle μ, the total number of combinations of $\tilde{\sigma}_{ji}^{\mu}$ for all neighboring nodes j of node i is $a+b=k^2-k+1$. Therefore, the computational complexity of this 2-stage cavity method can be reduced to $O\left(\left\langle k^{2M}\right\rangle_k\right)$, which is much less than the complexity before reduction.

2.5.2 Probability of selfish rerouting

After obtaining the converged joint functional probability distribution $P\left[\left\{\tilde{E}^V_\mu\right\}_\mu, E^V\right]$, we can measure the complete routing behaviors of the selfish rerouting $\tilde{\boldsymbol{\sigma}}^*$ and the optimal traffic configurations $\boldsymbol{\sigma}^*$ by computing the joint probability $p(\tilde{\boldsymbol{\sigma}}^*, \boldsymbol{\sigma}^*)$, and this probability can help us to evaluate the physical quantities we desire, including the fractional change of various costs. The probability $p(\tilde{\boldsymbol{\sigma}}^*, \boldsymbol{\sigma}^*)$ can be found by

$$\begin{aligned} p(\tilde{\boldsymbol{\sigma}}^*, \boldsymbol{\sigma}^*) = &\int dE^V_1 \prod_\nu d\tilde{E}^V_{\nu,1} P\left[\left\{\tilde{E}^V_{\mu,1}\right\}_\mu, E^V_1\right] \int dE^V_2 \prod_\nu d\tilde{E}^V_{\nu,2} P\left[\left\{\tilde{E}^V_{\mu,2}\right\}_\mu, E^V_2\right] \\ &\times \delta\left(\boldsymbol{\sigma}^* - \operatorname*{argmin}_{\boldsymbol{\sigma}}\left[E^V_1(\boldsymbol{\sigma}) + E^V_2(-\boldsymbol{\sigma}) - \left(\sum_\nu |\sigma^\nu|\right)^{\gamma_r}\right]\right) \\ &\times \prod_\nu \delta\left(\tilde{\sigma}^{\nu*} - \operatorname*{argmin}_{\tilde{\sigma}^\nu}\left[\tilde{E}^V_{\nu,1}(\tilde{\sigma}^\nu, \boldsymbol{\sigma}^*) + \tilde{E}^V_{\nu,2}(-\tilde{\sigma}^\nu, -\boldsymbol{\sigma}^*) - |\tilde{\sigma}^\nu|\left(1 + \sum_{\kappa\neq\nu}|\sigma^{\kappa*}|\right)^{\gamma-1}\right]\right), \end{aligned} \tag{62}$$

which relies on evaluating the energy changes of particular selfish rerouting.

2.5.3 Cost of rerouting

While different from $p(\tilde{\sigma}^{\mu*}, \sigma^{\mu*}, I^*)$, although the computational complexity is much higher in this approach, $p(\tilde{\boldsymbol{\sigma}}^*, \boldsymbol{\sigma}^*)$ allows us to precisely calculate the optimal traffic I^* recommended and the resulting traffic condition after selfish rerouting $\tilde{I}^*$ for any given number of selfish vehicles without any assumption and requirement. The probability of having optimal traffic on a link before rerouting $p(I^*)$ can be found easily by

$$p(I^*) = \sum_{\tilde{\boldsymbol{\sigma}}^*} \sum_{\boldsymbol{\sigma}^*} p(\tilde{\boldsymbol{\sigma}}^*, \boldsymbol{\sigma}^*) \delta\left(I^* - \sum_\nu |\sigma^\nu|\right). \tag{63}$$

Consider now that there exist Mf_s selfish users on the whole network, and define $\tilde{I}^*$ and $\tilde{m}_s^*$ as the resulting total traffic flow and the number of selfish users existing on the link after rerouting, respectively. The probability $P\left(\tilde{I}^*, \tilde{m}_s^*\right)$ can then be evaluated by

$$P\left(\tilde{I}^*, \tilde{m}_s^*\right) = \sum_{\tilde{\boldsymbol{\sigma}}^*}\sum_{\boldsymbol{\sigma}^*} p(\tilde{\boldsymbol{\sigma}}^*, \boldsymbol{\sigma}^*)\delta\left(\tilde{I}^* - \left(\sum_{\nu=1}^{Mf_s}|\tilde{\sigma}^{\nu*}| + \sum_{\nu=Mf_s+1}^{M}|\sigma^{\nu*}|\right)\right)\delta\left(\tilde{m}_s^* - \sum_{\nu=1}^{Mf_s}|\tilde{\sigma}^{\nu*}|\right), \tag{64}$$

and by marginalizing $P\left(\tilde{I}^*, \tilde{m}_s^*\right)$ over $\tilde{m}_s^*$, the probability $P\left(\tilde{I}^*\right)$ is given by

$$P\left(\tilde{I}^*\right) = \sum_{\tilde{m}_s^*=1}^{Mf_s} P\left(\tilde{I}^*, \tilde{m}_s^*\right). \tag{65}$$

Therefore, the social traffic cost before rerouting $\mathcal{H}\left(\boldsymbol{\sigma}^*(\gamma_r), \gamma\right)$, the social traffic cost after rerouting $\mathcal{H}\left(\tilde{\boldsymbol{\sigma}}^*(\gamma_r), \gamma\right)$, the travel cost averaged over all selfish users $\mathcal{H}_{\text{selfish}}\left(\tilde{\boldsymbol{\sigma}}^*(\gamma_r), \gamma\right)$ and the travel cost averaged over all compliant users $\mathcal{H}_{\text{compliant}}\left(\tilde{\boldsymbol{\sigma}}^*(\gamma_r), \gamma\right)$ are given by

$$\mathcal{H}\left(\boldsymbol{\sigma}^*(\gamma_r), \gamma\right) = \sum_{I^*} P(I^*)\,|I^*|^{\gamma}, \tag{66}$$

$$\mathcal{H}\left(\tilde{\boldsymbol{\sigma}}^*(\gamma_r), \gamma\right) = \sum_{\tilde{I}^*} P(\tilde{I}^*)\left|\tilde{I}^*\right|^{\gamma}, \tag{67}$$

$$\mathcal{H}_{\text{selfish}}\left(\tilde{\boldsymbol{\sigma}}^*(\gamma_r), \gamma\right) = \frac{1}{Mf_s}\sum_{\tilde{I}^*, \tilde{m}_s^*}\left[\tilde{m}_s^*\left|\tilde{I}^*\right|^{\gamma-1} P\left(\tilde{I}^*, \tilde{m}_s^*\right)\right], \tag{68}$$

$$\mathcal{H}_{\text{compliant}}\left(\tilde{\boldsymbol{\sigma}}^*(\gamma_r), \gamma\right) = \frac{1}{M(1-f_s)}\sum_{\tilde{I}^*, \tilde{m}_s^*}\left[\left(\left|\tilde{I}^* - \right|\tilde{m}_s^*\right)\left|\tilde{I}^*\right|^{\gamma-1} P\left(\tilde{I}^*, \tilde{m}_s^*\right)\right]. \tag{69}$$

Therefore, the fractional changes $\Delta\mathcal{H}(\gamma_r, \gamma)$, $\Delta\mathcal{H}_{\text{selfish}}(\gamma_r, \gamma)$ and $\Delta\mathcal{H}_{\text{compliant}}(\gamma_r, \gamma)$, for the global traffic cost, selfish users and compliant users, respectively, can be computed using Eq.(9).

2.5.4 Rerouting correlation

We note that the predictions in Section 2.6 of $\Delta\mathcal{H}(\gamma_r, \gamma)$, $\Delta\mathcal{H}_{\text{selfish}}(\gamma_r, \gamma)$ and $\Delta\mathcal{H}_{\text{compliant}}(\gamma_r, \gamma)$ made by the two-stage cavity method derived in Section 2.4 are less accurate compared to the results obtained from the exhaustive cavity method derived in this chapter. One of the major differences between the two methods is that the cavity method in Section 2.4 computes the probability $P\left(\tilde{I}^*, \tilde{m}_s^*\right)$ using probabilistic modeling by assuming every vehicle is acting independently and following the routing behavior $p(\tilde{\sigma}^{\mu*}, \sigma^{\mu*}, I^*)$ obtained by the average vehicle singled out; in contrast, the exhaustive cavity method captures the exact routing behaviors of every vehicle to obtain the precise probability distribution $p(\tilde{\sigma}^{\mu*}, \sigma^{\mu*}, I^*)$ even if a herd behavior exists under which selfish vehicles are more likely to switch into certain links. Therefore, the interactions and correlations between vehicles would be one of the major reasons for why the two-stage cavity method followed by probabilistic modeling produces less accurate results compared to the exhaustive cavity method. To examine the interaction between the vehicles, as well as the existence of any herd behavior, we need to define a quantity to measure the likelihood of routing behaviors between different users. We first define $\Delta\sigma = |\tilde{\sigma}^*| - |\sigma^*|$ as the change in the driving behavior of a vehicle. Now consider 2 users ν and μ traveling on the network. We define the conditional rerouting correlation, given the total traffic flow I^* on a link, as

$$\langle \Delta\sigma^{\nu}\Delta\sigma^{\mu}\rangle_{I^*} = \sum_{\left\{(ij)\in\mathbb{E}|I^*_{ij}=I^*\right\}} \frac{\Delta\sigma^{\nu}_{ij}\Delta\sigma^{\mu}_{ij}}{Z} = \sum_{\left\{(ij)\in\mathbb{E}|I^*_{ij}=I^*\right\}} \frac{\left(\left|\tilde{\sigma}^{\nu*}_{ij}\right| - \left|\sigma^{\nu*}_{ij}\right|\right)\left(\left|\tilde{\sigma}^{\mu*}_{ij}\right| - \left|\sigma^{\mu*}_{ij}\right|\right)}{Z}, \tag{70}$$

where Z is the normalization constant given by

$$Z = \sum_{\{(ij)\in\mathbb{E}|I^*_{ij}=I^*\}} \left(\delta\left(\left|\tilde{\sigma}^{\nu*}_{ij}\right| + \left|\sigma^{\nu*}_{ij}\right|\right) - 1\right)\left(\delta\left(\left|\tilde{\sigma}^{\mu*}_{ij}\right| + \left|\sigma^{\mu*}_{ij}\right|\right) - 1\right). \tag{71}$$

The normalization constant counts links that both vehicles ν and μ is traveling in either recommended and rerouting stages, so they both exist on the link and only the interaction between them is under consideration. On the other hand, the quantity $\Delta\sigma$ can be understood as the switching strategy of a user, and since $|\tilde{\sigma}|$ and $|\sigma|$ can only be 1 or 0, $\Delta\sigma$ consists of three possibilities only: (i) $\Delta\sigma = 1$ where $(|\tilde{\sigma}|, |\sigma|)$ must be $(1, 0)$, meaning that initially, the vehicle is not traveling on that particular link and switches into the link after rerouting; (ii) $\Delta\sigma = -1$ where $(|\tilde{\sigma}|, |\sigma|)$ must be $(0, 1)$, representing the case that the vehicle is traveling on the link initially, but switches out to another path after selfish rerouting; (iii) $\Delta\sigma = 0$ where $(|\tilde{\sigma}|, |\sigma|)$ can only be $(1, 1)$ as we do not consider the case that $(|\tilde{\sigma}|, |\sigma|) = (0, 0)$, which means the vehicle is not changing its decision after selfish rerouting. We further note that $\sum_{\{(ij)\in\mathbb{E}|I^*_{ij}=I^*\}} \left(\delta\left(\left|\tilde{\sigma}^{\nu*}_{ij}\right| + \left|\sigma^{\nu*}_{ij}\right|\right) - 1\right)\left(\delta\left(\left|\tilde{\sigma}^{\mu*}_{ij}\right| + \left|\sigma^{\mu*}_{ij}\right|\right) - 1\right) \geq \sum_{\{(ij)\in\mathbb{E}|I^*_{ij}=I^*\}} \left(\left|\tilde{\sigma}^{\nu*}_{ij}\right| - \left|\sigma^{\nu*}_{ij}\right|\right)\left(\left|\tilde{\sigma}^{\mu*}_{ij}\right| - \left|\sigma^{\mu*}_{ij}\right|\right)$, and thus the term $\langle\Delta\sigma^{\nu}\Delta\sigma^{\mu}\rangle_{I^*}$ must be bounded below and above by -1 and 1, providing us with a clear picture of the conditional rerouting correlation. $\langle\Delta\sigma^{\nu}\Delta\sigma^{\mu}\rangle_{I^*} < 0$ suggests that ν and μ are more likely to take opposite switching decisions. For instance, user ν initially traveling on link (ij) switches to another link after selfish rerouting, while another user μ initially not traveling on (ij) switches into (ij) after selfish rerouting. $\langle\Delta\sigma^{\nu}\Delta\sigma^{\mu}\rangle_{I^*} > 0$ suggests that ν and μ are more likely to take the same switching decisions. Moreover, if the quantity $(\langle\Delta\sigma^{\nu}\Delta\sigma^{\mu}\rangle_{I^*} < 0)$ is closer to 1, then the likelihood of the routing behavior is higher. Therefore, $\langle\Delta\sigma^{\nu}\Delta\sigma^{\mu}\rangle_{I^*}$ provides a measurement of the likelihood of any two vehicles picking similar rerouting strategies over links with the total traffic flow of I^*, allowing us to investigate which kind of links are more likely for vehicles to pick. On a macroscopic scale, we can further define the rerouting correlation as

$$\langle \Delta\sigma^{\nu}\Delta\sigma^{\mu}\rangle = \sum_{I^*} \langle \Delta\sigma^{\nu}\Delta\sigma^{\mu}\rangle_{I^*}\, P(I^*), \tag{72}$$

in order to evaluate the general level of the likelihood of choosing a similar rerouting strategy over the whole network.

To obtain the quantities defined above analytically, we evaluate the probability $p(\tilde{\sigma}^{\nu*}, \tilde{\sigma}^{\mu*}, \sigma^{\nu*}, \sigma^{\mu*} I^*)$ describing the joint probability of the routing behavior of $\nu*$ and μ over links with the total flow I^*, given as

$$p_Z(\tilde{\sigma}^{\nu*}, \tilde{\sigma}^{\mu*}, \sigma^{\nu*}, \sigma^{\mu*}, I^*) = \frac{1}{Z}\sum_{\tilde{\sigma}}\sum_{\sigma} p(\tilde{\boldsymbol{\sigma}}, \boldsymbol{\sigma})\delta\left(\tilde{\sigma}^{\mu} - \tilde{\sigma}^{\mu*}\right)\delta\left(\tilde{\sigma}^{\nu} - \tilde{\sigma}^{\nu*}\right)\delta\left(\sigma^{\mu} - \sigma^{\mu*}\right)\delta\left(\sigma^{\nu} - \sigma^{\nu*}\right), \tag{73}$$

where the normalization constant $Z = \sum_{\tilde{\sigma}}\sum_{\sigma} p(\tilde{\boldsymbol{\sigma}}, \boldsymbol{\sigma})\,(\delta\,(|\tilde{\sigma}^{\nu*}| + |\sigma^{\nu*}|) - 1)\,(\delta\,(|\tilde{\sigma}^{\mu*}| + |\sigma^{\mu*}|) - 1)$. Then the conditional rerouting correlation can be computed by

$$\begin{aligned}\langle \Delta\sigma^{\nu}\Delta\sigma^{\mu}\rangle_{I^*} = &\sum_{\{\tilde{\sigma}^{\nu*}, \tilde{\sigma}^{\mu*}, \sigma^{\nu*}, \sigma^{\mu*}\}} \Delta\sigma^{\nu}\Delta\sigma^{\mu}\, p_Z(\tilde{\sigma}^{\nu*}, \tilde{\sigma}^{\mu*}, \sigma^{\nu*}, \sigma^{\mu*}, I^*) \\ &\sum_{\{\tilde{\sigma}^{\nu*}, \tilde{\sigma}^{\mu*}, \sigma^{\nu*}, \sigma^{\mu*}\}} (|\tilde{\sigma}^{\nu*}| - |\sigma^{\nu*}|)\,(|\tilde{\sigma}^{\mu*}| - |\sigma^{\mu*}|)\, p_Z(\tilde{\sigma}^{\nu*}, \tilde{\sigma}^{\mu*}, \sigma^{\nu*}, \sigma^{\mu*}, I^*),\end{aligned} \tag{74}$$

and the rerouting correlation can be computed by

$$\langle \Delta\sigma^{\nu}\Delta\sigma^{\mu}\rangle = \sum_{I^*} \langle \Delta\sigma^{\nu}\Delta\sigma^{\mu}\rangle_{I^*}\, P(I^*). \tag{75}$$

2.6 Major results

In this section, we mainly study transportation systems under two situations with $(\gamma_r, \gamma) = (1, 2)$ and $(2, 2)$. The reason for only choosing these two scenarios to study and compare is that they represent two extreme conditions of traffic coordination, given the measurements of the social cost are the same. The case $(\gamma_r, \gamma) = (1, 2)$ represents the situation that exists in transportation systems in our daily lives in that all drivers are picking their routes independently to minimize their own traveling costs, and they can switch to other routes the next day after knowing the traffic condition on the current day. The case $(\gamma_r, \gamma) = (2, 2)$ represents a transportation network that is already optimal in social cost, and where some drivers are not following the optimal configurations and selfishly switch to other paths. In Section 2.6.1 and Section 2.6.2, we investigate the transportation networks with random regular graph structures, i.e. the graphs in which all nodes have the same connectivity k. In Section 2.6.3, we study selfish routing over England's highway network to show how our theoretical understandings develop to fit the results from a realistic system.

2.6.1 Analytical results by the two-stage cavity method and probabilistic modeling

To obtain the analytical results, we employ the derivation incorporating the distance from the destination in Section 2.4.4 into the calculation for better measurements of costs. To employ population dynamics, the functional probability distribution $P(\tilde{E}^V, E^V, D)$ is approximated by a pool of 10,000 sets of functions $\left\{\tilde{E}_{\xi}^{V}, E_{\xi}^{V}, D_{\xi}\right\}_{\xi}$, where

$$P(\mathbf{\Lambda}) = \begin{cases} \frac{1}{N}, & \text{if } \mathbf{\Lambda} = (1,0); \\ \frac{M-1}{N}, & \text{if } \mathbf{\Lambda} = (0,1); \\ \frac{1}{N}, & \text{if } \mathbf{\Lambda} = (-\infty,-\infty); \\ 1-\frac{M+1}{N}, & \text{otherwise.} \end{cases}, \tag{76}$$

and $P(k = 3) = 1$ for the graph setup of a random regular graph with connectivity of 3. Since it is computationally inefficient to measure the convergence of $P(\tilde{E}^V, E^V, D)$, we instead measure the social traffic cost $\mathcal{H}$ to determine whether the iteration process of population dynamics is converged. On the other hand, the simulation results are generated by the results after averaging over 1000 realizations, in which each is obtained by applying our cavity method to transportation networks with randomly generated random regular graph structures with network size $N = 100$ and node connectivity $k = 3$. To study the accuracy of the prediction of $p(\tilde{\sigma}^{\mu *}, \sigma^{\mu *}, I^*, D^*)$ by the cavity method, we also produce semi-analytical results by first obtaining the rerouting probability $p(\tilde{\sigma}^{\mu *}, \sigma^{\mu *}, I^*, D^*)$ from simulation results instead of Eq.(45), then inserting this empirical probability into Eqs.(46) to (50) to compute the quantities for measurement of the system's behavior. Generally, the analytical and semi-analytical results should be similar, and this would suggest that the probabilities measured by the cavity method are accurate.

As shown in Fig. 6, the analytical and semi-analytical results capture the positive and negative regimes as well as the trends of simulation results, but there are discrepancies. Note that the analytical and semi-analytical results are in good agreement, suggesting that the cavity method provides a good estimation of the rerouting probability $p(\tilde{\sigma}^{\mu *}, \sigma^{\mu *}, I^*, D^*)$ in simulations. We also note that when $(\gamma_r, \gamma) = (2, 2)$, there results in little difference between analytical and simulation results, suggesting that over a socially optimal state, Eq. (47) provides a good estimate of $P(\tilde{I}^*, \tilde{m}_s^* | I^*, D^*)$. When $(\gamma_r, \gamma) = (2, 2)$, optimal route recommendations aim to minimize the social cost, and vehicles tend to be evenly distributed over the whole network, so the routing decisions of all vehicles are similar and hence a mean-field probability $p(\tilde{\sigma}^{\mu *}, \sigma^{\mu *}, I^*, D^*)$ is sufficient to describe the routing decisions of all vehicles. When $(\gamma_r, \gamma) = (1, 2)$, however, the discrepancies are much larger, vehicles are recommended to follow their shortest paths and depending on the network topology, their routing decisions can vary greatly, hence a mean-field probability $p(\tilde{\sigma}^{\mu *}, \sigma^{\mu *}, I^*, D^*)$ is not enough to describe the routing decisions of all vehicles. Therefore, we believe that the discrepancies come from using $p(\tilde{\sigma}^{\mu *}, \sigma^{\mu *}, I^*, D^*)$ as a mean-field probability for every vehicle's routing decision. In Section 2.6.2, we show the discrepancies are reduced by applying the two-stage exhaustive cavity method.

I. *Shortest path recommendation* - $(\gamma_r, \gamma) = (1, 2)$:

To investigate the scenario when $(\gamma_r, \gamma) = (1, 2)$, we obtain the fractional change in the social travel cost averaged over all vehicles, $\Delta\mathcal{H}(1, 2)$, from all three approaches for different cases of vehicle density $\alpha = 0.1, 0.5$ and 0.9. As shown in Fig. 6(a), $\mathcal{H}(1, 2)$ is a convex curve, first decreasing to negative values and then increasing back to positive as f_s increases. This is because users are following their shortest path in the case of the shortest path recommendation. When f_s is small, the small fraction of selfish users will pick the routes that are less used (i.e. I^* is smaller) in the rerouting stage, which is beneficial to the whole system and hence $\Delta\mathcal{H}(1, 2)$ becomes negative, since the social cost is a nonlinear convex function in total traffic flow and links are less crowded after rerouting. However, when f_s further increases, the large fraction of selfish vehicles will switch into the less occupied links in the initial stage, generating more serious congestion compared to the

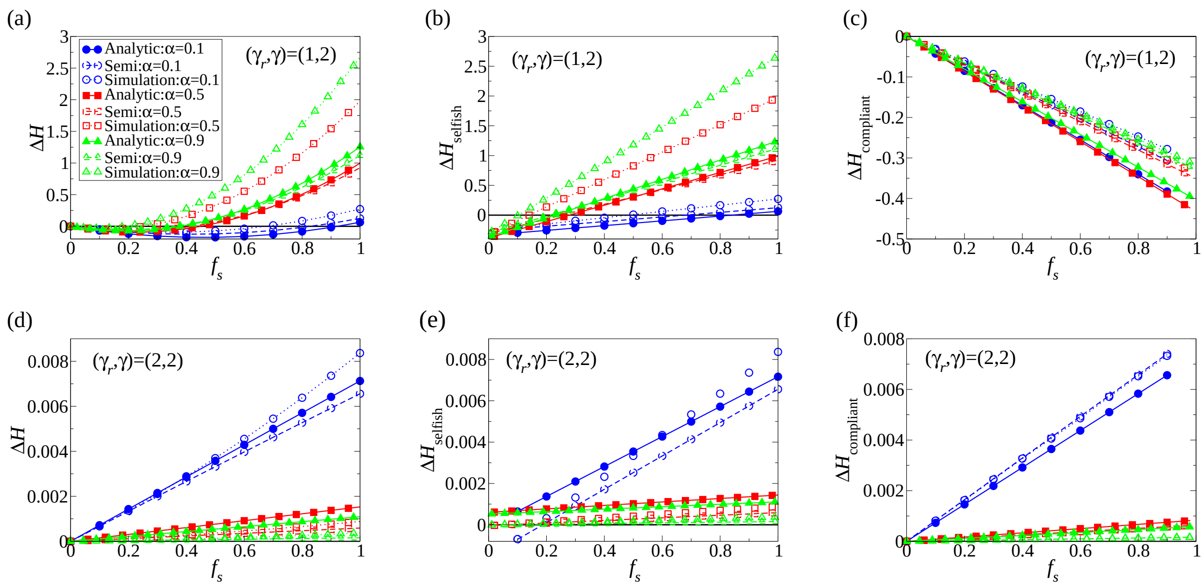

Figure 6. The fractional change obtained by the analytical, semi-analytical and simulation results, in (a) the social cost $\Delta\mathcal{H}$, (b) the traveling cost of selfish users $\Delta\mathcal{H}_{\text{selfish}}$ and (c) the traveling cost of compliant users $\Delta\mathcal{H}_{\text{compliant}}$, as a function of f_s, averaged over all selfish and compliant vehicles, respectively, for vehicle density α =0.1, 0.5 and 0.9, with $(\gamma_r, \gamma) = (1, 2)$. The corresponding fractional change in costs are shown in (d),(e) and (f) respectively for the case $(\gamma_r, \gamma) = (2, 2)$. The simulation results are obtained on transportation networks with random regular graph structures with network size $N = 100$ and node connectivity $k = 3$, averaged over 1000 realizations. The analytical results are obtained by the cavity method. The semi-analytical results are obtained by estimating the probability $P(\tilde{I}^*, \tilde{m}_s^*|I^*, D^*)$ by $p(\tilde{\sigma}^{\mu *}, \sigma^{\mu *}, I^*, D^*)$ measured in simulations.

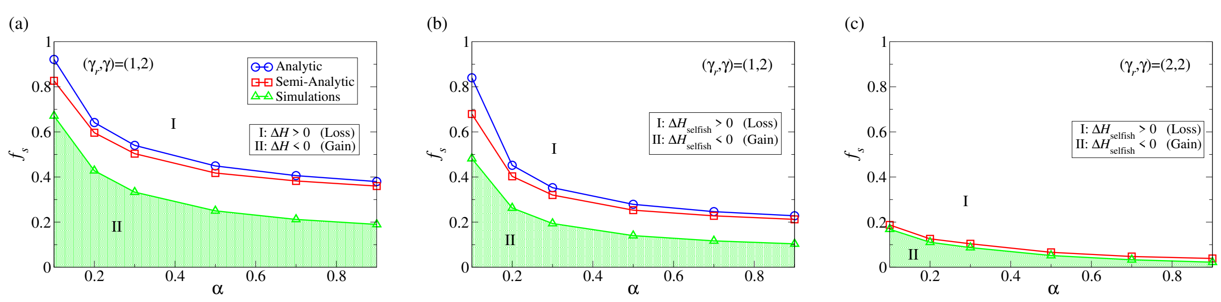

Figure 7. The positive or negative regimes by the analytical results, semi-analytical results and simulation results for (a) $\Delta\mathcal{H}(1, 2)$, (b) $\Delta\mathcal{H}_{\text{selfish}}(1, 2)$ and (c) $\Delta\mathcal{H}_{\text{selfish}}(2, 2)$ are shown in terms of the vehicle density α and the fraction of selfish drivers f_s.

initial stage and resulting in $\mathcal{H}(1,2)$ becoming positive.

Furthermore, we note that in Fig. 6(a), when the density α is smaller, the critical value of f_s at which $\Delta\mathcal{H}$ starts to become positive is larger. We show the regime of transportation system gain (i.e. $\Delta\mathcal{H} < 0$) after selfish rerouting, in terms of α and f_s, as shown in Fig. 7, in order to demonstrate the benefits brought by the selfish rerouting. The regime of gaining exists for all users and selfish users when $(\gamma_r, \gamma) = (1,2)$, while the regime exists for selfish users only when $(\gamma_r, \gamma) = (2,2)$. As we can see in Fig. 7(a), the regime of the system gaining decreases as α increases. This implies that it is beneficial to the system with a suitable value of the fraction of selfish vehicles f_s, given that all vehicles are following their shortest path initially. Similar to Fig. 6, the results from the analytical and semi-analytical approaches capture the trends, but show discrepancies when compared to the simulation results. The agreement of trends shows that in the case of $(\gamma_r, \gamma) = (1,2)$, the analytical approach provides the correct physical picture, though it does not give the exact regime.

Next, we investigate the fractional change of traveling cost over different groups of selfish and compliant users. We remark that there should be at least one selfish vehicle on the network to calculate $\mathcal{H}_{\text{selfish}}$, thus $\frac{1}{M}$ is the smallest value of f_s for $\Delta\mathcal{H}_{\text{selfish}}$. As shown in Fig. 6(b), when f_s increases, the fractional change in the traveling cost of selfish users, $\Delta\mathcal{H}_{\text{selfish}}$, increases from a negative value to positive. When the fraction of selfish vehicles f_s is smaller, the value of $\Delta\mathcal{H}_{\text{selfish}}$ is more negative in value, suggesting that selfish users can better make use of the less-used links and gain more from rerouting when there are fewer selfish drivers. Nevertheless, when f_s increases, the gain of the selfish users will disappear because there are more selfish vehicles traveling on the less-used links in the initial stage which incur congestion. In Fig. 7(b), we can see that the critical value of f_s at which the selfish users start to lose decreases as the vehicle density α increases. Remarkably, Fig. 6(c) shows that $\Delta\mathcal{H}_{\text{compliant}} < 0$ for any $f_s > 0$ and the magnitude of $\Delta\mathcal{H}_{\text{compliant}}$ increases as f_s

increases. This suggests that the compliant users that are following the recommendations always benefit from the presence of selfish users, and when there are more selfish users, the compliant users gain more. This is because when the selfish drivers are switching into the less-used links, the links that are originally crowded will be less occupied and thus the travel cost of compliant users decreases.

II. *Socially optimal recommendation* - $(\gamma_r, \gamma) = (2, 2)$:

In this scenario, since the optimal configuration is suggested to drivers, the social traffic cost is minimized in the initial stage and after selfish rerouting, the social cost can only be unchanged or increased. Therefore, we can see that $\Delta\mathcal{H} > 0$ for all f_s and α in Fig. 6(d), and $\Delta\mathcal{H}$ increases as f_s increases, meaning the more selfish users, the higher the social cost. On the other hand, we can see that in terms of magnitude, the fractional change of costs for the case $(\gamma_r, \gamma) = (2, 2)$ is much less than the case $(\gamma_r, \gamma) = (1, 2)$, as shown in Fig. 6. This suggests that over an optimal configuration, there are no or very few specific less-used routes that can benefit most users, thus after rerouting, the correlations and congestion caused only slightly affect the system. Interestingly, better than the case when $(\gamma_r, \gamma) = (1, 2)$ in Fig. 6(a), we can see that the analytical and semi-analytical results show good agreement with the simulation results. This may because when the social traffic cost is optimized, the traffic load is balanced already and the heterogeneity of links is reduced, thus fewer links are attractive to selfish vehicles, which will be discussed more in Section 2.6.2 by the rerouting correlation, and therefore the cavity method measures the probabilities better in this case. We notice an interesting property that although transportation must lose for any changes made to the system, selfish drivers may gain in their individual travel costs by harming the system and compliant users, as shown in Fig. 6(e). When the fraction of selfish users f_s is small, $\Delta\mathcal{H}_{\text{selfish}}$ is negative and $\Delta\mathcal{H}_{\text{selfish}}$ increases and becomes positive as f_s increases. This suggests that a small fraction of selfish users are able to take advantage of the less-used routes, yet this strategy backfires due to congestion and correlations when f_s further increases. In Fig. 7(c), we show the parameter regime in which the selfish users gain from rerouting, and the boundary of the regime shows the critical value of f_s at which selfish users start to lose if f_s further increases, for a given density α. We can see that the critical value of f_s decreases as α increases, suggesting that when the density of vehicles α increases, the fraction of selfish vehicles that can gain is smaller. Furthermore, we can see that the regime where $\Delta\mathcal{H}_{\text{selfish}} < 0$ for the case $(\gamma_r, \gamma) = (2, 2)$ is much less than the case $(\gamma_r, \gamma) = (1, 2)$, as shown in Fig. 7(b) and (c). This suggests that compared to the uncoordinated system in which $\gamma_r = 1$, fewer selfish drivers can gain from rerouting in an originally optimized system in which $\gamma_r = 1$. This is because compared to the uncoordinated system, the traffic load in the originally optimized system is more balanced and selfish users have difficulty finding alternative paths to improve individual travel costs. On the other hand, in contrast to the case when $(\gamma_r, \gamma) = (1, 2)$, compliant users always lose for all $f_s > 0$, and $\Delta\mathcal{H}_{\text{compliant}}$ increases as f_s increases, but not to a large degree. This may because the correlation is diminished in the socially optimal transportation system and there are very few favorable less-used routes that attract selfish users, resulting in very few links being less occupied and thus the individual travel costs of compliant users are not decreased.

To conclude the case with $(\gamma_r, \gamma) = (2, 2)$, we can see that in the case when the social traffic cost is initially minimized, rerouting by the selfish drivers is increasing the social traffic cost, increasing the individual costs of compliant users, while selfish users may gain if they are in the minority in the system.

In Section 2.6.1.I and 2.6.1.II, the analytical results successfully reveal the properties of the dynamics of path switching and the corresponding impact to the system, such as the regimes of gaining and losing for different costs of interest. Compared to the conventional transportation studies that mainly focus on the equilibrium of selfish routing (Fotakis, Kontogiannis, Koutsoupias, Mavronicolas, and Spirakis 2002; Roughgarden and Tardos 2002), it is more complex to study the dynamics of routing and its impact. Therefore, in an unexplored aspect of selfish routing studies, the two-stage cavity method with probabilistic modeling provides a new set of tools, as well as a new understanding.

III. *Critical values of γ_r for phase transition of gaining and losing*:

We observe that in Fig. 6(a), when $\gamma_r = 1$, in which drivers initially follow their shortest paths, $\Delta\mathcal{H} < 0$ if f_s is small, meaning that if only a small fraction of selfish vehicles exist on the system, all users gain on average; while in Fig. 6(d), when $\gamma_r = 2$, in which drivers initially follow the optimal route configuration, $\Delta\mathcal{H} > 0$ for all $f_s > 0$, meaning that all users always lose on average when selfish users exist. On the other hand, as shown in Fig. 6(c) and (f), when $\gamma_r = 1$, $\Delta\mathcal{H}_{\text{compliant}} < 0$ for all $f_s > 0$, i.e. compliant users always gain; while when $\gamma_r = 2$, $\Delta\mathcal{H}_{\text{compliant}} > 0$ for all $f_s > 0$, i.e. compliant users always lose. The reason is that when γ_r is small, the original traffic load is distributed unevenly, thus selfish users are shifting as a group from the originally over-used links to the originally less-used links, causing the originally over-used links to become less occupied after rerouting and beneficial to the compliant users; on the other hand, when γ_r is large, the traffic load is already distributed evenly in the initial stage, resulting in no favorable less-used links to provide an incentive for selfish users to shift as a group, very few links become less occupied after rerouting and, hence, the compliant users lose.

To further investigate the observation, we identify the critical values of γ_r for which the fractional change of costs is equal to zero, denoted as γ_r^*, beyond which the system or compliant users start to lose. Given a small fraction of selfish users $f_s = 0.1$, the corresponding values of γ_r^* for which

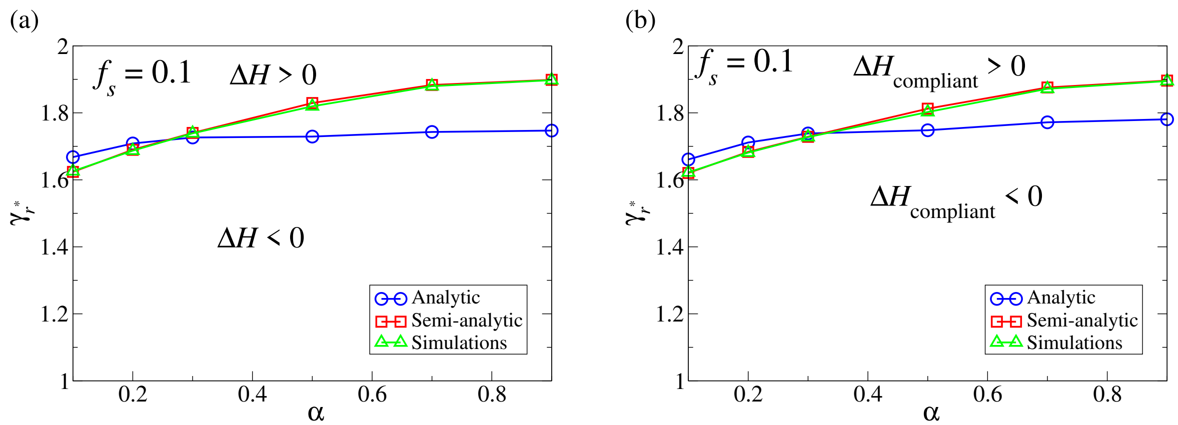

Figure 8. The critical values γ_r^* for which (a) $\Delta\mathcal{H} = 0$ and (b) $\Delta\mathcal{H}_{\text{compliant}} = 0$, as a function of the vehicle density α. The regimes in which $\Delta\mathcal{H}$ and $\Delta\mathcal{H}_{\text{compliant}}$ are positive and negative are also indicated in (a) and (b), respectively. The simulation results are obtained on transportation networks with random regular graph structures with network size $N = 100$ and node connectivity $k = 3$, averaged over 1000 realizations. The analytical results and semi-analytical results are also obtained and shown.

$\Delta\mathcal{H} = 0$ and $\Delta\mathcal{H}_{\text{compliant}} = 0$ identified by the analytical, semi-analytical and simulation results are shown in Fig. 8(a) and (b), respectively. We observe that in Fig. 8, for both groups of users, the critical values γ_r^* increase as the vehicle density α increases. When the density α increases, a larger value of γ_r is needed to distribute the traffic load evenly so that very few favorable less-used links exist on the network, and therefore the critical values γ_r^* beyond which compliant users lose increased. In our setup, since f_s is small, most drivers are compliant and hence the critical values γ_r^* beyond which all users lose on average increases as α increases, which is similar to Fig. 8(b), as shown in Fig. 8(a).

2.6.2 Analytical results by the exhaustive cavity method

To illustrate that our exhaustive cavity method derived in Section 2.5 provides an accurate analytic solution to path switching behavior, compared to the previous cavity method derived in Section 2.4.4, we focus on the same two scenarios as in Section 2.6.1, where the initial path configurations are computed based on $\gamma_r = 1$ and 2, and individual vehicles then reroute according to $\gamma = 2$. Due to the high computational complexity of this exhaustive approach, we examine transportation networks with a different density $\alpha = M/N$ by fixing the number of vehicles to be $M = 8$ and vary the number of nodes N. To employ population dynamics, the functional probability distribution of $P(\tilde{E}^V, E^V)$ is approximated by a pool of 2000 sets of functions $\left\{\tilde{E}^V_\xi, E^V_\xi\right\}_\xi$, where

$$P(\mathbf{\Lambda}) = \begin{cases} \frac{1}{N}, & \text{if } \exists \mu \text{ s.t. } \Lambda^\mu = 1, \text{ and } \Lambda^\nu = 0 \text{ for all } \nu \neq \mu; \\ \frac{1}{N}, & \text{if } \Lambda^\nu = -\infty, \text{ for all } \nu; \\ 1 - \frac{M+1}{N}, & \text{otherwise.} \end{cases}, \tag{77}$$

and $P(k = 3) = 1$ for the graph setup of a random regular graph with connectivity of 3. As in Section 2.6.1, instead of measuring the convergence of $P(\tilde{E}^V, E^V, D)$, we measure the social cost $\mathcal{H}$ for checking the convergence of the iteration process. On the other hand, the simulation results are generated by the results after averaging over 1000 realizations, in which each is obtained by transportation networks with randomly generated random regular graph structures with a different density $\alpha = M/N$ by fixing the number of vehicles to be $M = 8$ and varying the number of nodes N, with node connectivity $k = 3$. We then compare the analytic solutions obtained by our exhaustive approach with those obtained by the previous approach and the simulation results.

As shown in Fig. 9, for both scenarios of $(\gamma_r, \gamma) = (1, 2)$ and $(2, 2)$, our exhaustive approach agrees much better with simulation results than the first approach in Section 2.4 in terms of the fractional change in the social traffic cost $\mathcal{H}$ and the individual travel costs $\mathcal{H}_{\text{selfish}}$ and $\mathcal{H}_{\text{compliant}}$ of selfish and compliant users. As in Section 2.6.1, the cavity method provides a good estimate of $\mathcal{H}_{\text{selfish}}$ and

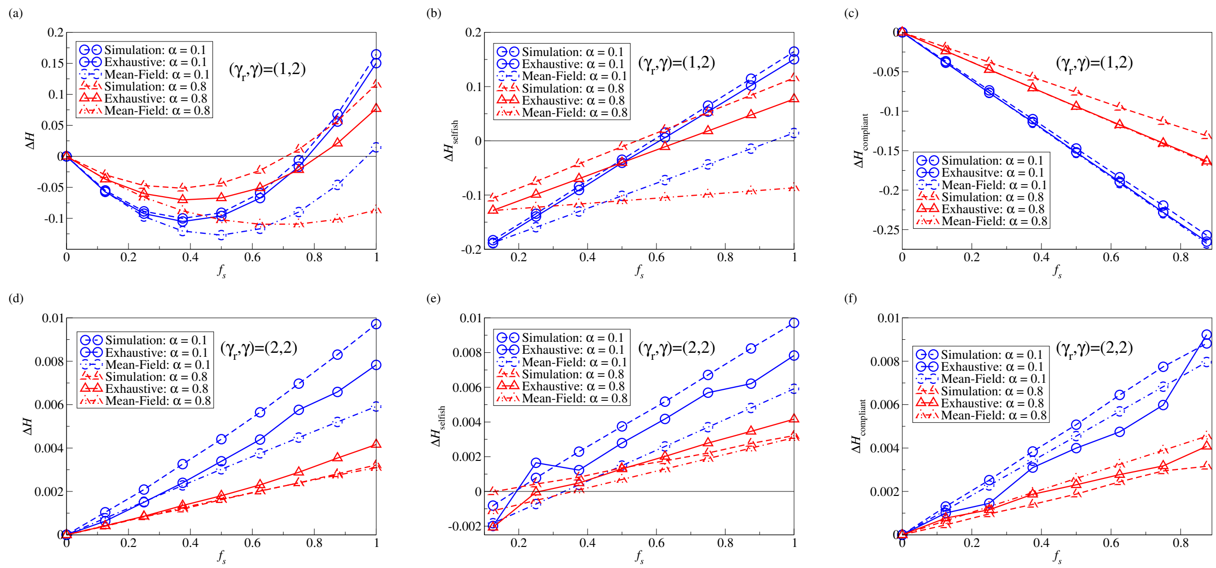

Figure 9. The fractional change in (a) the social cost $\Delta\mathcal{H}$, (b) the traveling cost of selfish users $\Delta\mathcal{H}_{\mathrm{selfish}}$ and (c) the traveling cost of compliant users $\Delta\mathcal{H}_{\mathrm{compliant}}$, as a function of f_s, averaged over all selfish and compliant vehicles, respectively, for the vehicle density α =0.1 and 0.8, with $(\gamma_r, \gamma) = (1, 2)$. The corresponding fractional changes in costs are shown in (d),(e) and (f) respectively for the case $(\gamma_r, \gamma) = (2, 2)$. The simulation results are obtained by averaging 1000 realizations on random regular graphs with a fixed number of vehicles $M = 8$ and $k = 3$ for density $\alpha = M/N = 0.1$ and 0.8. The analytical results obtained by the exhaustive cavity method and the first approach in Section 2.4 are also shown.

$\mathcal{H}_{\mathrm{compliant}}$, yet it yields a smaller value of $\mathcal{H}$ compared to simulations but still captures the trend. This suggests that if one prefers accurate analytical results describing the rerouting behavior, the exhaustive approach which articulates all route choices in Eq. (55) and Eq. (57) for a small group of vehicles is a better option, compared to the first approach in Section 2.4 which is capable of analyzing a system with a larger number of vehicles.

I. *Herd behavior in rerouting*:

The discrepancies between the results obtained by the exhaustive and the probabilistic modeling methods imply that the latter method cannot capture some fundamental mechanisms in selfish

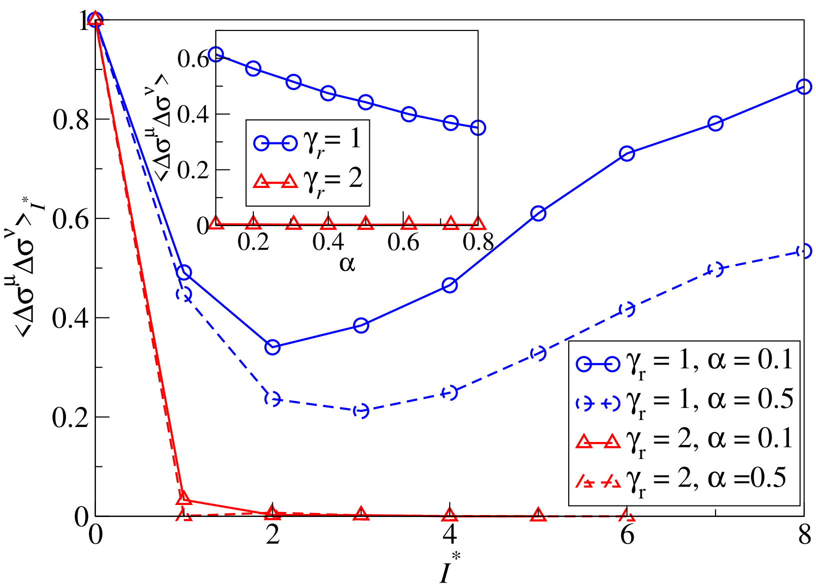

Figure 10. The conditional rerouting correlation $\langle \Delta\sigma^{\nu}\Delta\sigma^{\mu} \rangle_{I^*}$ as a function of I^* for $\gamma_r = 1$ and 2, $\alpha = 0.1$ and 0.5. Insets: The overall rerouting correlation $\langle \Delta\sigma^{\nu}\Delta\sigma^{\mu} \rangle$ as a function of α for $\gamma_r = 1$ and 2. The results are the analytical solutions obtained by the exhaustive cavity method.

rerouting. We first note that in the probabilistic modeling approach, the traffic condition after rerouting is estimated by computing the rerouting choice of a specific vehicle, which leads to a mean-field switching probability for all vehicles, assuming all of them make an independent rerouting decision. The discrepancies thus come from the invalidity of this mean-field assumption, suggesting a correlation underlying the rerouting decisions of individual vehicles. For instance, a route may be favorable to most users and hence they are correlated and switch into those favorable links, which can be considered as a herd behavior in path switching.

To examine herd behavior in rerouting, we compute the conditional rerouting correlation $\langle \Delta\sigma^{\nu}\Delta\sigma^{\mu} \rangle_{I^*}$ in Eq. (74) and the overall rerouting correlation $\langle \Delta\sigma^{\nu}\Delta\sigma^{\mu} \rangle$ in Eq. (75), as shown in Fig. 10 and its inset, respectively. We observe that when $\gamma_r = 2$, where the path configurations optimizing the social traffic cost are initially recommended to all users, the values of $\langle \Delta\sigma^{\nu}\Delta\sigma^{\mu} \rangle_{I^*}$ and $\langle \Delta\sigma^{\nu}\Delta\sigma^{\mu} \rangle$ are very small for all α and $I^* \neq 1$. We also note that when $I^* = 0$, $\langle \Delta\sigma^{\nu}\Delta\sigma^{\mu} \rangle = 1$

since $|\sigma^*| = 0$ and hence $|\tilde{\sigma}| = 1$ if $|\tilde{\sigma}| + |\sigma^*| \neq 0$. This suggests that over a globally optimized transportation network, when traffic flows tend to be evenly distributed on the whole network, roads that are favorable to most vehicles do not exist and hence rerouting strategies among selfish vehicles tend to be uncorrelated. This also explains that when $\gamma_r = 2$, $\mathcal{H}$ obtained by the probabilistic modeling approach gives a better estimation than that obtained when $\gamma_r = 1$, as shown in Fig. 6 and Fig. 9, since rerouting is less correlated in the former.

On the other hand, in the case of $\gamma_r = 1$ with $\alpha = 0.1$ or 0.5, $\langle \Delta\sigma^\nu \Delta\sigma^\mu \rangle_{I^*} > 0$ for all I^* as shown in Fig. 10, and in particular, $\langle \Delta\sigma^\nu \Delta\sigma^\mu \rangle_{I^*}$ first decreases then increases as I^* increases. When the initially recommended traffic flow I^* on a link is small, it is trivial that $|\sigma^*| \approx 0$ and hence $\Delta\sigma = |\tilde{\sigma}| - |\sigma^*| > 0$ implies $|\tilde{\sigma}| > 0$ in most cases, suggesting the two vehicles tend to switch into the same link that they initially do not travel on. Therefore, $\langle \Delta\sigma^\nu \Delta\sigma^\mu \rangle_{I^*} > 0$ implies that selfish vehicles consider the road to be relatively less-used and favorable to travel, so they switch to the road together. Then, when I^* increases, $\langle \Delta\sigma^\nu \Delta\sigma^\mu \rangle_{I^*}$ decreases as the switching options become more even, and selfish vehicles can either stay or leave the recommended road to minimize their individual costs, since the link they are traveling already has low total traffic flow. Finally, when I^* further increases, since the shortest paths are recommended to vehicles in the case of $\gamma_r = 1$ and a large portion of vehicles are already traveling on the link, and hence the remaining options for the selfish vehicles are to stay ($\Delta\sigma = 0$) or to leave ($\Delta\sigma = -1$) the road. Therefore, in such cases the most possible values of $\Delta\sigma^\nu \Delta\sigma^\mu$ would be either 1 or 0. An increasing $\langle \Delta\sigma^\nu \Delta\sigma^\mu \rangle_{I^*}$ therefore implies that more selfish vehicles choose to leave the road together, leading to herd behavior in switching.

Next, we examine the dependence of herd behavior on vehicle density. As shown in the inset of Fig. 10, the overall rerouting correlation $\langle \Delta\sigma^\nu \Delta\sigma^\mu \rangle$ decreases as the density of vehicles α increases.

This can be understood as when the vehicle density is small, most vehicles are recommended to travel on a limited number of paths, leading to under-loaded roads and multiple selfish vehicles tend to switch to these roads which lead to a relatively higher $\langle \Delta\sigma^{\nu}\Delta\sigma^{\mu} \rangle$ than the case with high vehicle density α.

The above results show that there is a high correlation when vehicles reroute, leading to herd behavior and thus sub-optimal route configurations, suggesting why the cavity method in Section 2.4 is unable to estimate the transportation costs as accurately as the exhaustive cavity method. We remark that the computational complexity of the exhaustive approach is much higher than that of the probabilistic modeling approach. On the other hand, the exhaustive approach provides an accurate theoretical solution that can only predict small systems, however the mean-field approach is less accurate but is workable on large systems and is able to capture the clear physical properties of the system. Therefore, it is a trade-off between system size and precision for deciding which approach to employ.

2.6.3 England highway network: selfish routing case

To study the impact of selfish rerouting in a realistic transportation system, we simulate the mathematical model we derived on England's highway network that consists of 395 nodes, representing the starting or ending highway junctions based on the data in *Highways Agency network journey time and traffic flow data* 2018, and for simplicity we assign the weights of all links to be identical. We also create a node in the location of London and define it as the universal destination as shown in Fig. 11(b). To visualize the simulation, an example of the transportation flow on this highway network before selfish rerouting, with $M = 11$ vehicles are following the shortest path configuration($\gamma_r = 1$), is shown in Fig. 11(b); the resulting transportation flow after all vehicles

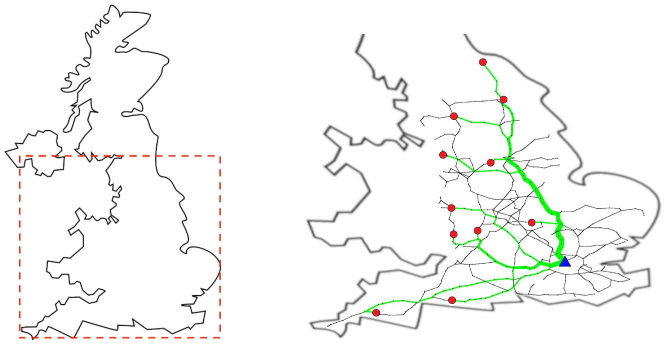

Figure 11. (a) The region of the England highway network we use in simulation, enclosed by the rectangle. England's highway network consists of 395 nodes, and each node is representing the starting point or the ending point of the junction of roads. (b) An example of the initial traffic condition consisting of $M = 11$ users following their shortest paths and traveling from their origin, denoted as red filled circles, to the universal destination in London, denoted as the blue triangle. (c) The updated traffic flow after selfish rerouting of all users, by considering the traffic condition in (b). The users switch to the less-used roads in the initial stage, leaving the originally over-loaded roads empty.

rerouted is shown in Fig. 11(c). Similar to the example shown, the origins of users are randomly selected and the universal destination is fixed at London for every realization of the simulation. All users are initially following the recommended configuration obtained based on the value of γ_r, and a fraction of selfish users are switching to other paths to optimize their individual traveling costs by considering the recommended configuration.

In Fig. 12, we show the fractional change in the social cost $\Delta\mathcal{H}$ averaged over all users, the traveling cost $\Delta\mathcal{H}_{\text{selfish}}$ and $\Delta\mathcal{H}_{\text{compliant}}$ averaged over selfish and compliant users respectively, with 500 realizations of simulations. The corresponding regimes to indicate when all users and selfish users gain after selfish rerouting are shown in Fig. 13. We note that England's highway network and random regular graphs have very different topological characteristics. For instance, the England highway network has many loops and is not in a treelike structure. But remarkably, the results

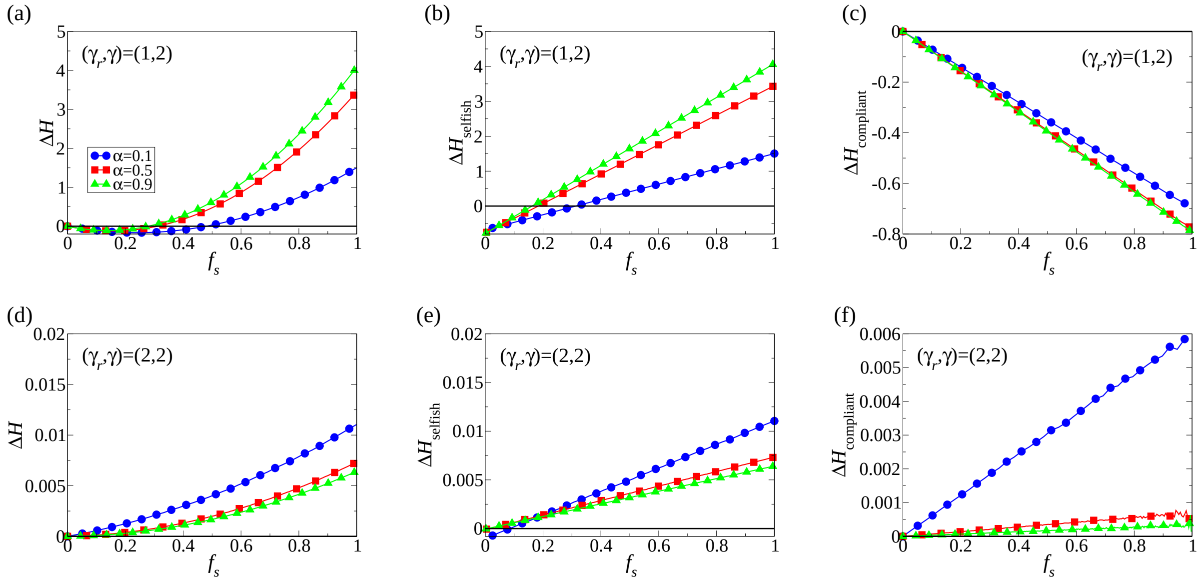

Figure 12. The fractional change in (a) the social cost $\Delta\mathcal{H}$, (b) the traveling cost of selfish users $\Delta\mathcal{H}_{\text{selfish}}$ and (c) the traveling cost of compliant users $\Delta\mathcal{H}_{\text{compliant}}$, as a function of f_s, averaged over all selfish and compliant vehicles, respectively, for the vehicle density α =0.1, 0.5 and 0.9, with $(\gamma_r, \gamma) = (1, 2)$. The corresponding fractional changes in costs are shown in (d), (e) and (f) respectively for the case $(\gamma_r, \gamma) = (2, 2)$. The simulation results are obtained by averaging 500 realizations on England's highway networks.

obtained from simulation results on the network are similar to those we predicted via the analytical results of the probabilistic modeling and exhaustive approaches, as well as the simulation results on random regular graphs, for both $(\gamma_r, \gamma) = (1, 2)$ and $(2, 2)$, as shown in Fig. 6, Fig. 7 and Fig. 9. This implies that although the analytical results obtained by the probabilistic modeling and exhaustive approaches in Section 2.4 and Section 2.5 are derived based on tree structures, these methods are able to qualitatively capture the impact of selfish rerouting in realistic transportation networks.

2.7 Summary

In this chapter, we derived theoretical frameworks by employing the cavity method developed for the study of spin glasses to study transportation systems in which optimized paths are suggested

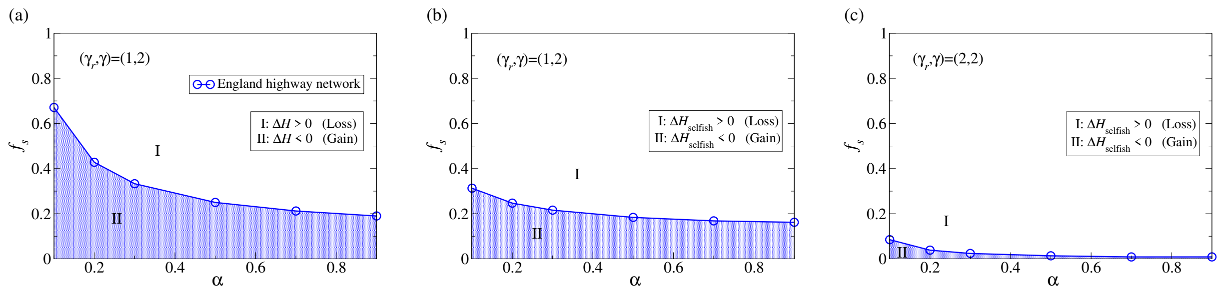

Figure 13. The positive or negative regimes for (a) $\Delta\mathcal{H}(1,2)$, (b) $\Delta\mathcal{H}_{\mathrm{selfish}}(1,2)$ and (c) $\Delta\mathcal{H}_{\mathrm{selfish}}(2,2)$ obtained by simulation results on England's highway network are shown in terms of the vehicle density α and the fraction of selfish drivers f_s.

to users initially, while some of them would choose alternative paths in order to minimize their individual costs instead of following the suggestions.

Both analytical and simulation results show that, in the case of transportation networks in which vehicles are initially following their shortest paths, a small fraction of selfish users are beneficial to the whole system due to the reduction of social traffic cost. The individual traffic costs of the selfish users are also reduced by switching to the less-used links and yet, when the fraction of selfish users further increases, the social cost and the individual costs of selfish users increase, due to the congestion caused by the rerouting. Remarkably, for compliant users who do not switch to other paths, their individual costs always decrease for any values of the fraction of selfish users. On the other hand, in the case when all users are recommended with the optimal configuration of paths, the social cost of the whole system as well as the individual costs of the compliant users are increased due to the selfish rerouting. For selfish users, they may gain from rerouting if they are only a minority in the system, but they may lose if the size of their group increases.

Using the exhaustive cavity method and computing the rerouting correlation, we also studied the correlation between users over the transportation networks. We showed that in the case of vehicles that are initially following their shortest paths, selfish users are highly correlated while rerouting, which leads to the failure of the probabilistic modeling approach. This phenomenon can be understood as the herd behavior of users. While in the case when all users are recommended with the optimal configuration of paths, the correlation is small and both the probabilistic modeling and exhaustive approach have good agreement with simulations.

The mean-field cavity method we derived is capable of studying systems of large size and successfully captures the trend as well as the features of transportation networks after path switching, but it can only provide a rough estimate of the numerical values of the rerouted system. In contrast, the exhaustive cavity method can only work on small networks due to high computational complexity, but it can precisely analyze the impact of rerouting, as well as identifying the detailed routing behavior of each user on the network, and carry out correlation analysis. Therefore, it is a trade-off between system size and precision in choosing which method to use.

Chapter 3: Nash equilibrium of multiple rounds of a selfish routing game over transportation networks

3.1 Iterative approach to reach Nash equilibrium

In Section 2.6, we showed that the transportation system may benefit after one round of rerouting. In this chapter, we aim to investigate the Nash equilibrium state (Osborne and Rubinstein 1994) of the system. If a system is in its Nash equilibrium state, then the corresponding strategies (path decisions) of each player (vehicle) are in its local optimal point that no player can gain their payoff (reduction of individual travel cost) by changing their own strategy while other players remain unchanged. Therefore, in such a state, all players (vehicles) in the system will no longer switch to other paths in selfish rerouting, making the system effective and stable. Nevertheless, in our transportation network problem, it is almost impossible to list all possibilities of routing decisions of all users. Instead, we investigate a transportation system with multiple rounds of selfish rerouting via simulation. If all vehicles no longer change their routing strategies for certain time steps, then that is the Nash equilibrium state of the system.

In this chapter, we employ the same mathematical model developed in Section 2.1 and we define $\boldsymbol{\sigma}_t = \left\{{}^{t}\sigma^{\nu}_{ij}\right\}_{\forall\nu,(ij)}$ as the routing configuration of all vehicles at time step t. At time $t = 0$, all users are following their recommended paths $\boldsymbol{\sigma}^*$ that are minimizing $\mathcal{H}(\boldsymbol{\sigma}_t|\gamma_r)$, i.e. $\boldsymbol{\sigma}^* = \mathrm{argmin}_{\boldsymbol{\sigma}_t}\,\mathcal{H}(\boldsymbol{\sigma}_t|\gamma_r)$. When $\gamma_r = 1$, vehicles are following their shortest paths, and they are following the path configurations that minimize the social cost $\mathcal{H}$ when $\gamma_r = 2$. Afterward, for any time $t > 0$, a fraction f_s of selfish users are randomly selected, then every selfish user μ is switching to a path that minimizes their individual travel cost $\mathcal{H}_\mu(\tilde{\boldsymbol{\sigma}}^{\mu *}_t|\boldsymbol{\sigma}^*_{t-1}(\gamma_r), \gamma)$ instead of the recommended path, based on the traffic condition $\boldsymbol{\sigma}^*_{t-1}(\gamma_r)$ at time $t - 1$.

3.2 Simulation results

Consider an example of multiple rounds of selfish rerouting on a transportation network of size $N = 30$ with $M = 14$ users, such that all users are traveling to the common destination by their shortest paths under 2 different scenarios: (i) the fraction of selfish users $f_s = 0.5$, as shown in Fig. 14(a), (b) and (c); and (ii) the fraction of selfish users $f_s = 1$, as shown in Fig. 14(a), (d) and (e). As shown in the example with $f_s = 0.5$ in Fig. 14(a), (b) and (c), we find that when the fraction of selfish users f_s is small, the path configuration converges to the Nash equilibrium state very quickly after a few iterations, in which no selfish users further switch afterward. On the other hand, when f_s is large, the dynamics of the path configuration may become a limit cycle that fluctuates repeatedly between certain states, when all users are switching simultaneously. For instance, drivers are departing at the same time for work on their daily commute. As shown in the example of Fig. 14(a), (d) and (e) with $f_s = 1$, users are following their shortest paths at $t = 0$ and leaving some links that are relatively less occupied. At $t = 1$, most users reroute to those less occupied links at $t = 0$, leaving the highly occupied links at $t = 0$ to become less occupied at $t = 1$. At the next time step $t = 2$, users switch back to those underloaded links at $t = 1$. The above process is then continued and switching back and forth repeatedly between the path configurations at time $t = 1$ and $t = 2$. Therefore, in this example with $f_s = 1$, the system never converges to a Nash equilibrium state.

In Fig. 15, we show the time series of the social traffic cost $\mathcal{H}$ for exemplar instances, in order to further investigate the convergence and alternating rerouting behavior we observed in Fig. 14, over different cases of vehicle density α. We show in Fig. 15(a) that, in the cases when the vehicle density is low with $\alpha = 0.1$, the social cost $\mathcal{H}$ converges in the instances with $f_s = 0.1$ and 0.5 when

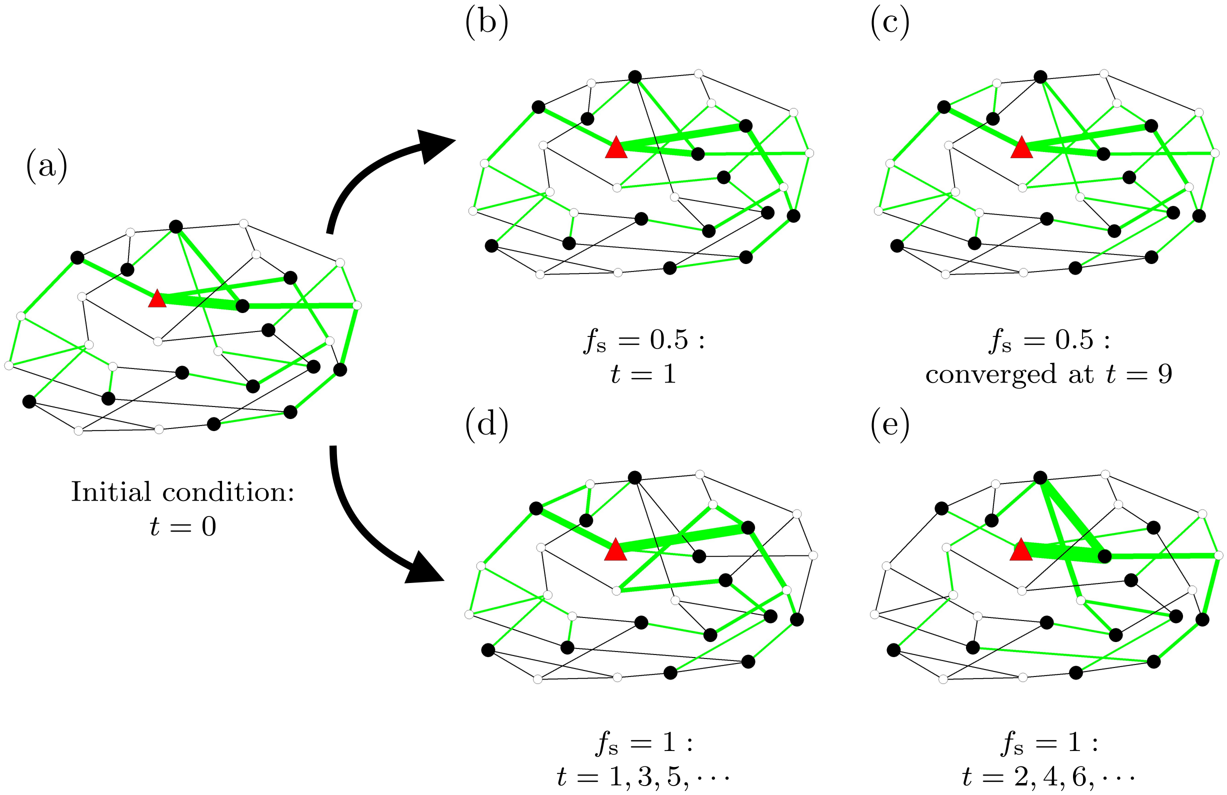

Figure 14. An example of multiple rounds of selfish rerouting on a transportation network comprising $N = 30$ nodes with $M = 14$ vehicles, under 2 scenarios with different fractions of selfish users, $f_s = 0.5$ ((a), (b) and (c)) and $f_s = 1$ ((a), (d) and (e)). The origin of vehicles and the universal destination are indicated as black filled circles and red triangle, respectively. Links with non-zero traffic flow are indicated in green and the width of links are proportional to the volume of flow. (a) Initially at $t = 0$, all users are traveling to the destination by their shortest paths, (b) shows that when $f_s = 0.5$, half of the users reroute at $t = 1$ to minimize their individual travel costs, and (c) shows the system reaching a Nash equilibrium state at $t = 9$. While in the case when $f_s = 1$, (d) shows all vehicles reroute at $t = 1$ and some links near to the common destination have very low or zero volume, (e) shows that at $t = 2$, all users are switching to the less-used links at $t = 1$, resulting in the other links being underloaded. The system is then switching back and forth between the path configurations in (d) and (e) repeatedly and never reaches a Nash equilibrium state.

$(\gamma_r, \gamma) = (1, 2)$, and; all instances with $f_s = 0.1$, 0.5 and 0.9 when $(\gamma_r, \gamma) = (2, 2)$. To investigate the convergence of social cost in general, we show in Fig. 15(c) the fraction of instances for which the social cost is unchanged in the last 2500 steps in a simulation of a total of 5000 steps over 1000 realizations. We observe that almost all instances converge except the instances with a larger fraction of selfish users $f_s = 0.9$ when $(\gamma_r, \gamma) = (1, 2)$, which is possibly due to the large amount of selfish rerouting simultaneously. The time series of $\mathcal{H}$ of an example in this case is shown in Fig. 15(a). When $f_s = 0.9$ and $(\gamma_r, \gamma) = (1, 2)$, $\mathcal{H}$ robustly fluctuates at high values relative to its initial value, which is similar to the example we show in Fig. 14(a), (d) and (e). These results imply that when the density α is low, most cases of the transportation system converge to a Nash equilibrium by selfish rerouting, no matter whether the users are following the global optimal or the shortest path configuration.

On the other hand, we show the time series of the social cost $\mathcal{H}$ from instances in Fig. 15(b), for the cases when the vehicle density is high with $\alpha = 0.9$. For the instances of $f_s = 0.5$ and 0.9 when $(\gamma_r, \gamma) = (1, 2)$, we can see that the time series of $\mathcal{H}$ fluctuates more seriously than the corresponding instances in Fig. 15(a). As shown in Fig. 15(d), for the cases with $(\gamma_r, \gamma) = (2, 2)$, although the convergence is marginally lower than the case when $\alpha = 0.1$, most instances still converge. Nevertheless, for the cases with $(\gamma_r, \gamma) = (1, 2)$, the ratio of convergence starts to drop rapidly after $f_s = 0.1$, which is completely different from the cases with low vehicle density. The above results imply that the higher the vehicle density α, the more difficultly the transportation system has in converging to a Nash equilibrium state by selfish rerouting, especially for the case in which the users are following their shortest paths in the initial step. The results also imply that the globally optimal route coordination provided in the initial step plays an important role in facilitating the convergence of Nash equilibrium.

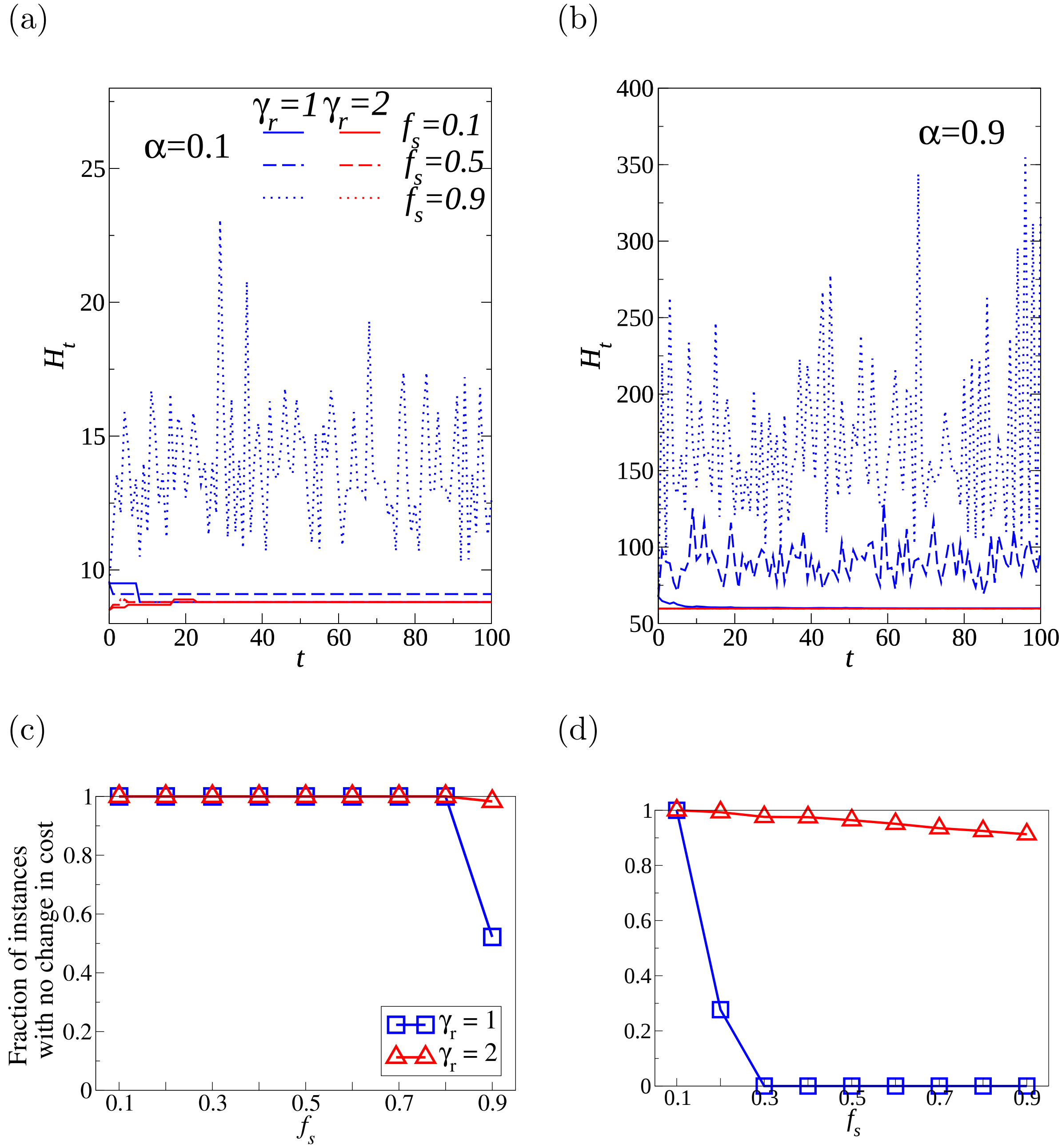

Figure 15. (a) and (b) are the time series of the social cost $\mathcal{H}$, where the time t is the number of rounds for selfish rerouting on specific instances of a random regular graph with $N = 3$, $k = 3$, $(\gamma_r, \gamma) = (1, 2)$ and $(2, 2)$ and various values of f_s, for (a) $\alpha = 0.1$ and (b) $\alpha = 0.9$. (c) and (d) are the fraction of instances which have no change in social traffic cost $\mathcal{H}$ in the last 2500 steps in a simulation of 5000 iteration steps, for $\alpha = 0.1$ and 0.9 respectively, over 1000 realizations. The simulation results are obtained on random regular graphs with size $N = 100$ and degree $k = 3$, averaged over 1000 realizations.

Apart from the convergence, we also aim to examine how much the system gains or loses after multiple rounds of selfish rerouting. Since the social cost $\mathcal{H}$ might fluctuate over time for the cases with different choices of parameters, we measure the time-averaged social traffic cost $\langle\mathcal{H}\rangle_t = \frac{1}{100}\sum_{101}^{200}\mathcal{H}(\boldsymbol{\sigma}_t|\gamma)$ instead of the social cost of a state in a fixed time step, then we define ψ as the fractional change of cost, given by

$$\psi = \frac{\langle\mathcal{H}\rangle_t - \mathcal{H}(\boldsymbol{\sigma}^*(\gamma)|\gamma)}{\mathcal{H}(\boldsymbol{\sigma}^*(\gamma)|\gamma)}, \tag{78}$$

in order to compare the time-averaged social traffic cost after multiple rounds of selfish rerouting with the social traffic cost in the initial step $t = 0$. The fractional change quantity ψ as a function of the fraction of selfish users f_s and the vehicle density α, is shown in Fig. 16. As shown in the figure, in both cases of $(\gamma_r, \gamma) = (1, 2)$ and $(2, 2)$, ψ exhibits similar behaviors with respect to f_s and α, while the magnitude of ψ is much larger for the case when $(\gamma_r, \gamma) = (1, 2)$. Remarkably, we observed that in general, ψ increases as f_s and α increase, starting from $\psi \approx 0$. This suggests that for a transportation system with a small vehicle density and a small fraction of selfish vehicles, the system is reaching a Nash equilibrium state that is close to the optimal state, regardless of the initial state of the system. On the other hand, if the vehicle density or the fraction of selfish users is large, for the case when the vehicles are initially following their shortest path ($(\gamma_r, \gamma) = (1, 2)$) at time step $t = 0$, it is difficult for the system to reach a Nash equilibrium state, and possibly fluctuating between largely suboptimal states. While for the case of optimal recommendation ($(\gamma_r, \gamma) = (2, 2)$), the system can still converge to a suboptimal Nash equilibrium state that is not far from the optimal solution in most cases, when compared to the shortest path case. The results show that initial route coordination not only facilitates the convergence to Nash equilibrium, but also reduces the impact

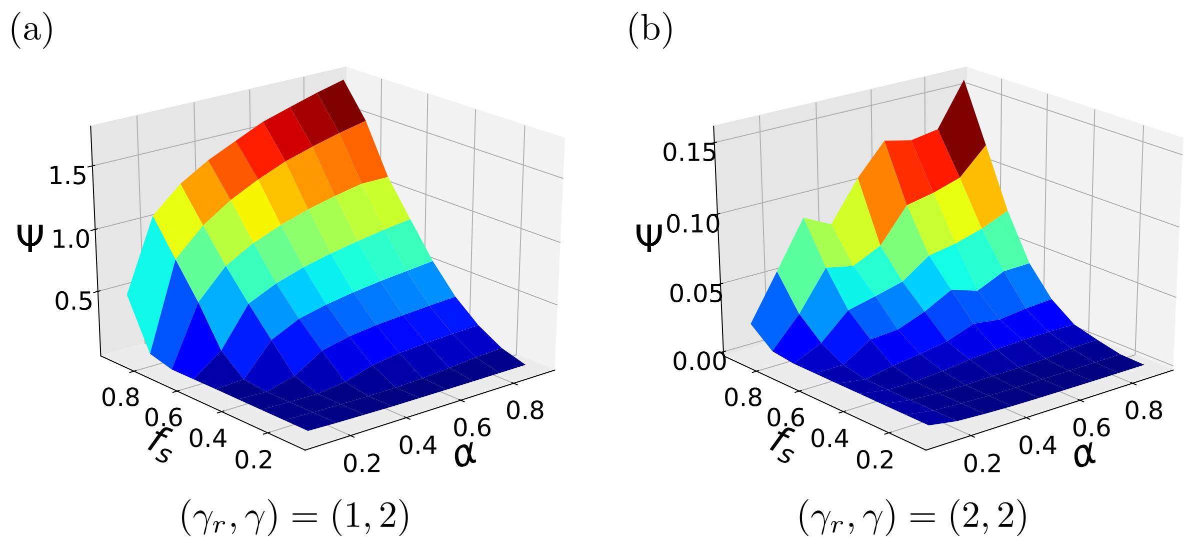

Figure 16. The fractional change ψ between the social traffic cost $\mathcal{H}$ after multiple rounds of selfish rerouting and the socially optimal traffic cost, as a function of α and f_s, for $(\gamma_r, \gamma) = (1, 2)$ and $(\gamma_r, \gamma) = (2, 2)$, respectively. The smaller the value of ψ, the social cost of the final state of the system is closer to its optimal configuration. The simulation results are obtained on random regular graphs with size $N = 100$ and degree $k = 3$, averaged over 1000 realizations.

of selfish rerouting.

3.2.1 England's highway network: Multiple rounds of selfish rerouting

Similar to Section 2.6.3, we show the simulation results on the same England highway network as in Fig. 17 and Fig. 18, in order to study the impact of multiple rounds of selfish rerouting over a realistic network. Remarkably, just like the one-step selfish rerouting case in Section 2.6.3, as shown in Fig. 17 and Fig. 18 these simulation results on the England network have similar behaviors to the random regular graphs case as shown in Fig. 15 and Fig. 16. This suggests that our approach not only works on artificial graph structures, but is also capable of studying realistic transportation networks. Nevertheless, as we can see in Fig. 17(a) and (b), over specific realistic network topology, more instances have a fluctuating time series of $\mathcal{H}$ value, suggesting it is more difficult for multiple rounds of self-rerouting to converge to a Nash equilibrium state. Moreover, the fraction of instances with no change in cost shown in Fig. 17(c) and (d) suggest that in general, the fraction of instances with no change in cost is much lower than that in the random regular graphs case. In particular, for the case with $(\gamma_r, \gamma) = (1, 2)$, we can see that even when the vehicle density is as low as $\alpha = 0.1$, the convergence starts to drop significantly after $f_s = 0.3$; while when $\alpha = 0.9$, almost no instance can converge to a Nash equilibrium state. On the other hand, for the case with $(\gamma_r, \gamma) = (2, 2)$, in both cases when $\alpha = 0.1$ and 0.9, the convergence is much larger than the corresponding case with $(\gamma_r, \gamma) = (1, 2)$. The results suggest that route coordination in the initial step also plays an important role in facilitating the convergence of Nash equilibrium in a realistic network, validating the efficacy of our approach in artificial network topologies. As shown in Fig. 18, similar to what we observed in the random regular graphs, ψ increases with f_s and α in both cases of $(\gamma_r, \gamma) = (1, 2)$ and $(2, 2)$, suggesting that when the vehicle density and the fraction of selfish users are small, the average social cost of the system will be close to the optimal social cost. These results suggest that the qualitative behavior of multiple rounds of selfish rerouting is valid against realistic network topologies.

3.3 Summary

In this chapter, we adopted the mathematical model we derived in Chapter 2, and extended the one-step selfish rerouting on transportation networks into multiple rounds of selfish rerouting via numerical simulations. We showed that after multiple rounds of selfish rerouting, the transportation system may converge to Nash equilibrium states, where users do not further benefit from switching to other paths. Remarkably, when the vehicle density and the fraction of selfish users are small, the social traffic costs at the Nash equilibrium states are close to the optimal social cost. Furthermore, we observe similar results on simulations of the England highway network, showing that our

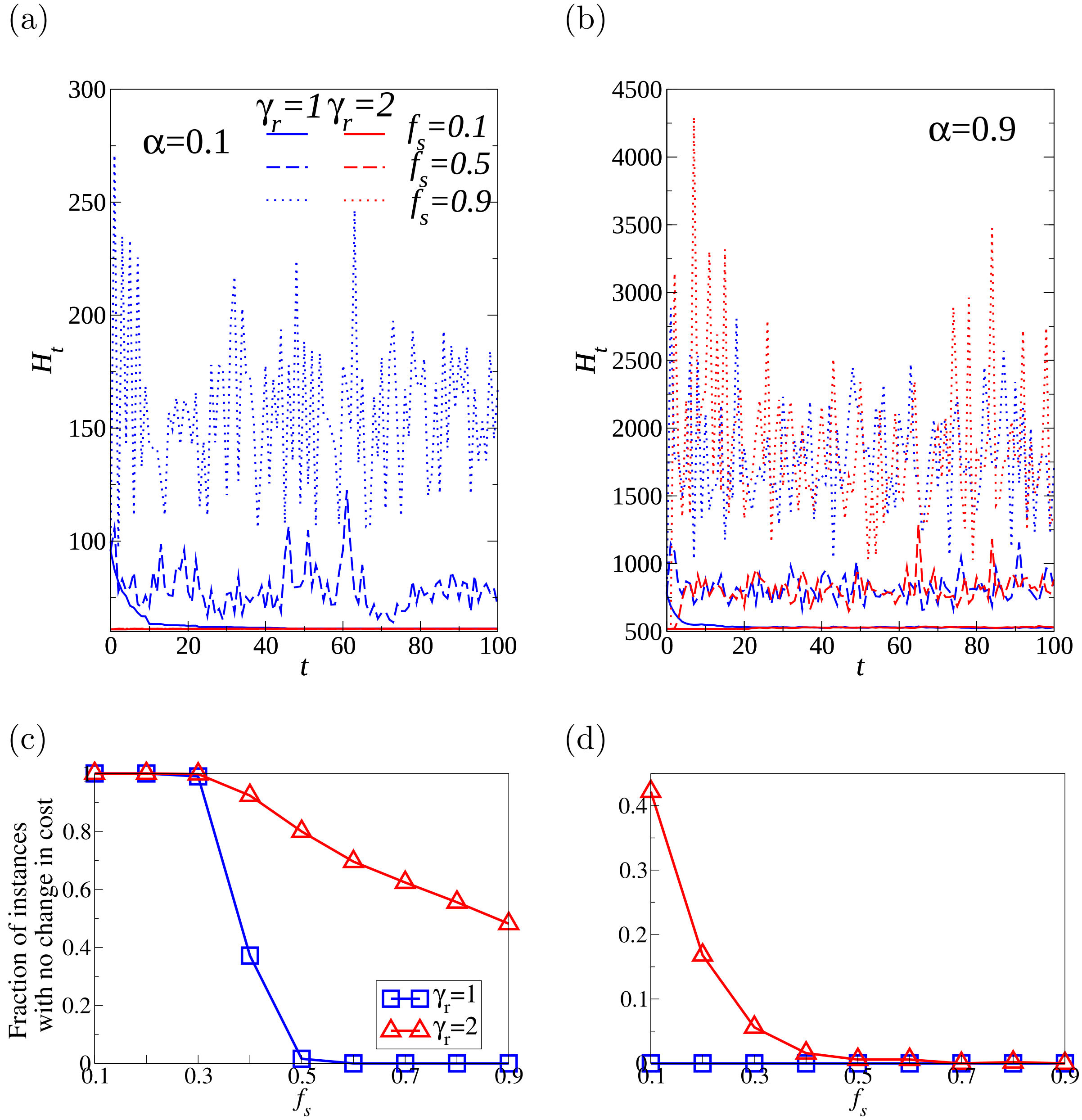

Figure 17. (a) and (b) show the time series of the social cost $\mathcal{H}$ on the England highway network, measured on instances with $(\gamma_r, \gamma) = (1, 2)$ and $(2, 2)$ and different values of $\alpha = 0.1$ and 0.9 respectively. (c) and (d) are the fraction of instances which have no change in social traffic cost $\mathcal{H}$ in the last 500 steps in simulations of 1000 iteration steps, for $\alpha = 0.1$ and 0.9 respectively, over 500 realizations. The simulation results are obtained on the England highway network averaged over 500 realizations.

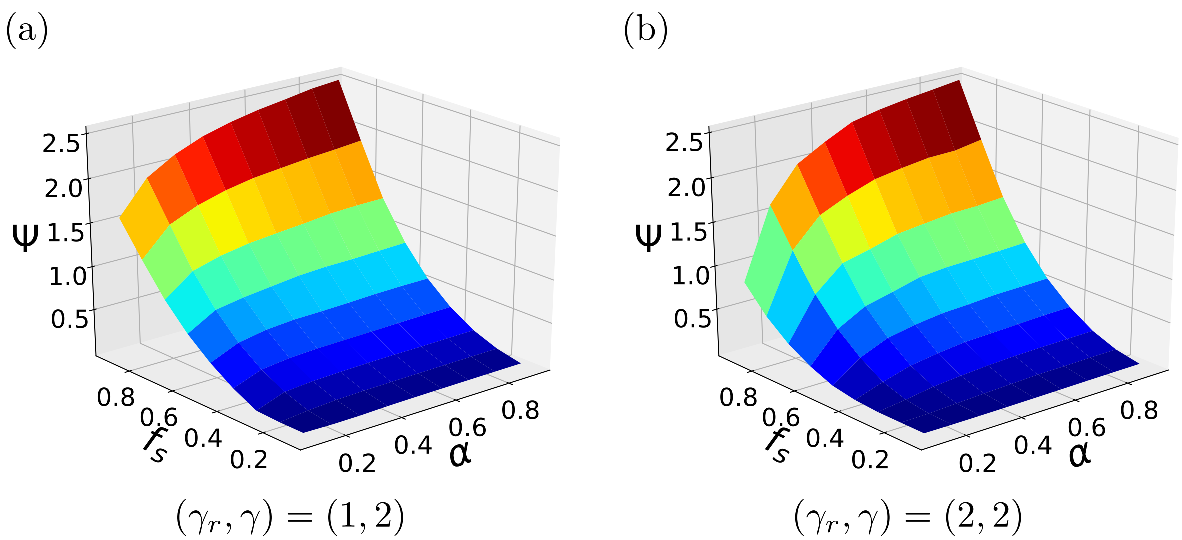

Figure 18. The fractional change ψ between the social traffic cost $\mathcal{H}$ on the England highway network before and after multiple rounds of selfish rerouting, as a function of α and f_s, for $(\gamma_r, \gamma) = (1, 2)$ and $(\gamma_r, \gamma) = (2, 2)$ respectively. The simulation results are obtained on the England highway network averaged over 500 realizations.

approach also works on realistic transportation networks.

Chapter 4: Complete realization of energy landscape and trapping dynamics in optimization processes in spin glasses and combinatorial optimization problems

In this chapter, we introduce a methodology for revealing the complete energy landscape of complex disordered systems that allows us to perform detailed and exact analysis. We first introduce the disordered system models in Section 4.1. We then introduce our approach and obtain the coarse-grained energy landscape (CEL) of the disordered systems of small size in Section 4.3, and discuss the physical properties we obtain. In Section 4.4, we compute the non-equilibrium dynamics analytically using the obtained energy landscapes, at arbitrary temperature and an arbitrarily long time that is out of reach of simulations due to computational capability. Finally, in Section 4.5, we obtain the partial coarse-grained energy landscape (PCEL) of the disordered systems with large system size by introducing a variant of the method we used in Section 4.3.

4.1 Models studied

In general, we consider a system that consists of N Boolean variables $s_i = \pm 1$, for $i = 1, 2, \ldots, N$. We denote the vector $\vec{s} = (s_1, s_2, \ldots, s_N)$ as the variable configuration, and the corresponding energy or the objective function of the system is denoted as $E(\vec{s})$. In this chapter, we investigate two glassy systems as examples of our approach, which are (i) spin glasses (Mézard et al. 1987b) and (ii) K-satisfiability problems (Malik and Zhang 2009).

4.1.1 Spin glasses

For the problem of spin glasses, we consider a spin system with N Ising spins, characterized by the Boolean variable $s_i = \pm 1$ for $i = 1, 2, \ldots, N$. The interactions between any two spins i and j

are denoted as $J_{ij} = \pm 1$. The graph topology of the spin system is characterized by the adjacency matrix (a_{ij}), where $a_{ij} = 1$ if i and j are interacting with each other, and $a_{ij} = 0$ otherwise. Then, given a configuration of Ising spins $\vec{s}$, the corresponding energy $E(\vec{s})$ of the spin system, is given by

$$E(\vec{s}) = \frac{1}{2} \sum_{i<j} a_{ij} J_{ij} s_i s_j, \tag{79}$$

where the interaction $J_{ij} = +1$ with a probability f_+ and $J_{ij} = 0$ otherwise. Unlike the common definition used in studies of spin glasses, we introduce the factor $\frac{1}{2}$ into the energy function so that a single flip of a spin leads to a unit change in energy for each active interaction. The spin system exhibits different phases, such as paramagnetic, ferromagnetic and spin glass phases (Mézard et al. 1987b; Nishimori 2001; Sherrington and Kirkpatrick 1975), which depend on the topology, the temperature and the probability distribution of J_{ij}.

4.1.2 K-satisfiability problems

The K-satisfiability (K-Sat) problem consists of N Boolean variables $s_i = \pm 1$, for $i = 1, 2, \ldots, N$ subject to M constraints called the clauses. Every clause ζ_l, $l = 1, 2, \ldots, M$, is a logical formula of OR($\vee$), of exactly K randomly selected Boolean variables $\{s_{i_r}\}_{r=1,\ldots,K}$, in which each of the variables is being negated ($\neg$) with a probability of $\frac{1}{2}$, such as $\zeta_i = (s_{i_1} \vee s_{i_2} \vee \neg s_{i_3})$. The K-Sat problem is to identify if there exists at least one configuration $\vec{s}$ of the variables such that all M clauses are satisfied. Given a configuration $\vec{s}$, the energy of each clause ζ_l is given by

$$E_l(\vec{s}) = \prod_{r=1}^{K} \frac{1 - J_{l_r} s_{l_r}}{2}, \tag{80}$$

where $J_{l_r} = -1$ if the r-th variable in the clause ζ_l is negated, and $J_{l_r} = 1$ otherwise. The energy $E_l(\vec{s}) = 0$ if the clause is satisfied and $E_l(\vec{s}) = 1$ if the clause is violated. The total energy $E(\vec{s})$ of the whole system is then given by

$$E(\vec{s}) = \sum_{l=1}^{M} E_l(\vec{s}), \tag{81}$$

which is equivalent to the number of violated clauses. Therefore, when $E(\vec{s}) = 0$, all clauses are satisfied and the system is in the ground state. Varying the value of the controllable ratio $\alpha = \frac{M}{N}$, the system exhibits different phases including the Easy-SAT phase, Hard-SAT phase and the UNSAT phase as α increases (Mézard and Zecchina 2002).

4.2 Full energy landscape(FEL)

In the above systems, there are N Boolean variables and each variable can only have 2 possible values, either 1 or -1. Therefore, the total number of different variable configurations is 2^N, and the configuration space is a $N-$dimensional discrete space. Next, consider two configurations $\vec{s}_x = \{s_i^x\}$ and $\vec{s}_y = \{s_i^y\}$, the Hamming distance between $\vec{s}_x$ and $\vec{s}_y$, denoted as $||\vec{s}_x - \vec{s}_y||_H$, is the number of variables they differ by, i.e.

$$||\vec{s}_x - \vec{s}_y||_H = \sum_{i=1}^{N} \left(1 - \delta_{s_i^x, s_i^y}\right), \tag{82}$$

and we consider that the two configurations $\vec{s}_x$ and $\vec{s}_y$ are connected to each other if the Hamming distance $||\vec{s}_x - \vec{s}_y||_H = 1$. Thus, the configuration space is indeed an $N-$dimensional hypercube.

Since the disorders J and the variables we defined in the above systems are integers, the resulting energy of these systems are also integral, which leads to discrete energy levels, allowing us to

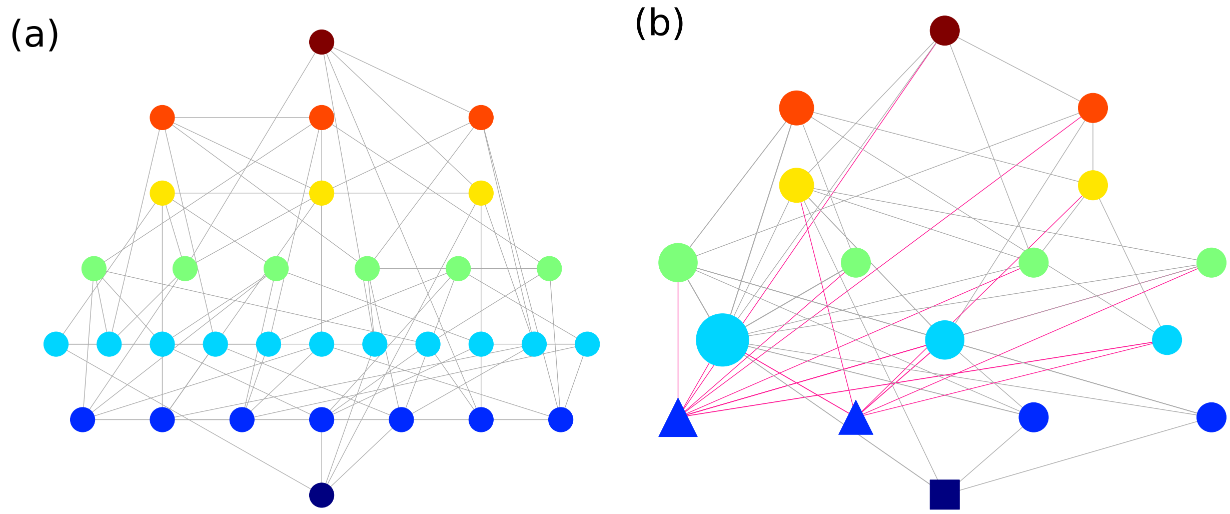

Figure 19. (a) The FEL of an example with $2^N = 32$ configurations from $E = 0$ at the bottom to $E = 6$ at the top, from a 3-Sat problem with the number of variables $N = 5$ and $\alpha = 4$. (b) The corresponding CEL with the number of clusters $C = 17$. The global minima and the local minima of the system are shown as squares and triangles, respectively. The node size is proportional to the number of configurations within the clusters. The connections between any cluster and the local minima are shown as red links.

present this hypercube as an energy landscape which can be shown as a network. Each variable configuration $\vec{s}$ is represented as a node on the network, and any two nodes are connected with a link if their Hamming distance is 1. Then all nodes with the same energy are arranged on the same horizontal level in the network, and where the configurations with lower energy are at a lower level. We call this network layout the full energy landscape (FEL). To give a clear illustration of this completely new approach, we show the FEL of a small 3-Sat problem with $N = 5$ and $\alpha = 4$ in Fig. 19(a) as an example. As shown in the figure, we can see how the $2^N = 32$ variable configurations are arranged on the FEL at different energy levels starting from $E = 0$ at the bottom, and how they are connected with their neighboring configurations. Note that the total number of variable configurations increases exponentially with N, and thus illustrating that the configuration

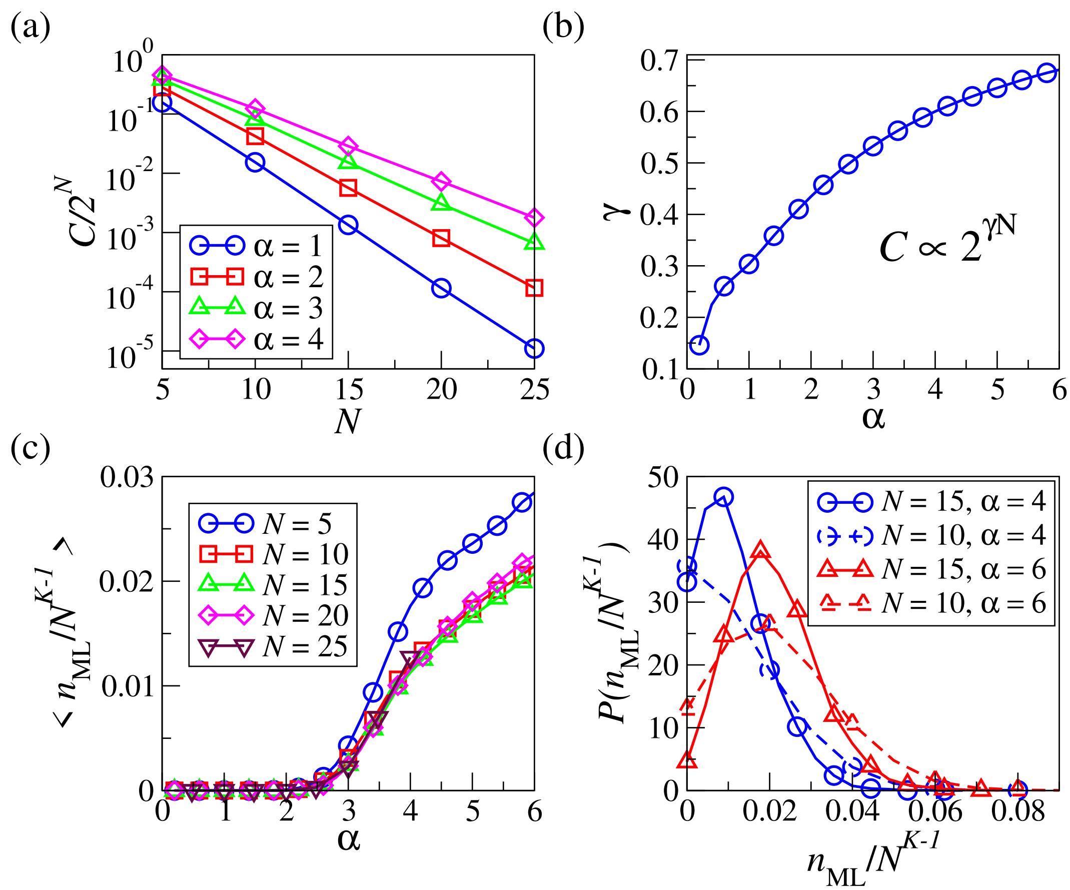

Figure 20. The number of clusters in the CEL divided by the total number of variable configurations, $C/2^N$, as a function of N, for different values of α. (b) The exponent γ in the relation $C \propto 2^{\gamma N}$, as a function of α. (c) The rescaled average number of local minima in the CEL, $\langle n_{\mathrm{ML}}/N^{K-1}\rangle$ of the $K-$Sat problem as a function of α for different size N with $K = 3$. (d) The rescaled probability distribution of the number of local minima in the CEL, $N^{K-1}P(n_{\mathrm{ML}}/N^{K-1})$, as a function of n_{ML}/N^{K-1}. The simulation results are obtained by averaging more than 10000 instances for $N \leq 20$ and more than 700 instances for $N \leq 25$.

space by FEL will quickly become computationally infeasible and hard to visualize as there are too many links and nodes on the network. Therefore, we need to introduce another approach to simplify and present the energy landscape in a clear visualization.

4.3 Coarse-grained energy landscape (CEL)

To simplify the FEL, we define a simplified energy landscape as a new network $\mathcal{G}$ such that every node in $\mathcal{G}$ represents a cluster on the original FEL, with each cluster containing the connected nodes that are on the same energy level. Therefore, each cluster in this simplified energy landscape $\mathcal{G}$ represents a connected sub-graph in the FEL in which all nodes in the cluster are of the same energy. The total number of clusters in $\mathcal{G}$ is denoted as C. Two clusters a and b are connected with a link (ab) in $\mathcal{G}$, if there exists at least one variable configuration in a is connected with at least one variable configuration in b in the FEL. Every link (ab) in $\mathcal{G}$ is assigned with a weight w_{ab}, where w_{ab} is the total number of links in the FEL that connect a variable configuration in a to one in b. We name such a simplified energy landscape $\mathcal{G}$ the coarse-grained energy landscape (CEL). For illustration, in Fig. 19(b) we show the corresponding CEL of the FEL in Fig. 19(a), where the number of variable configurations is reduced from $2^N = 32$ nodes in the FEL to $C = 17$ clusters in the CEL.

To examine the size reduction effect of the CEL, we take the $K-$Sat problem with $K = 3$ as an example, showing the ratio of the total number of clusters to the total number of variable configurations, i.e. $\frac{C}{2^N}$ in Fig. 20(a). Remarkably, the ratio $\frac{C}{2^N}$ decreases exponentially as the number of variables N increases linearly, suggesting that the reduction effect of grouping variable configurations in the CEL is increasing with N. Furthermore, from Fig. 20(a), we have the relation $\log_2\left(\frac{C}{2^N}\right) = mN + d$ for some constant d and $m < 0$, implying that the total number of clusters $C \propto 2^{\gamma N}$, i.e. $C = A2^{\gamma N}$ for some constant A and reduction exponent $\gamma < 1$, and the value of γ as a function of α is shown in Fig. 20(b). As shown in the figure, the exponent γ increases as α increases, suggesting that the structure of the energy landscape is more complicated when the value of α is larger. This result is

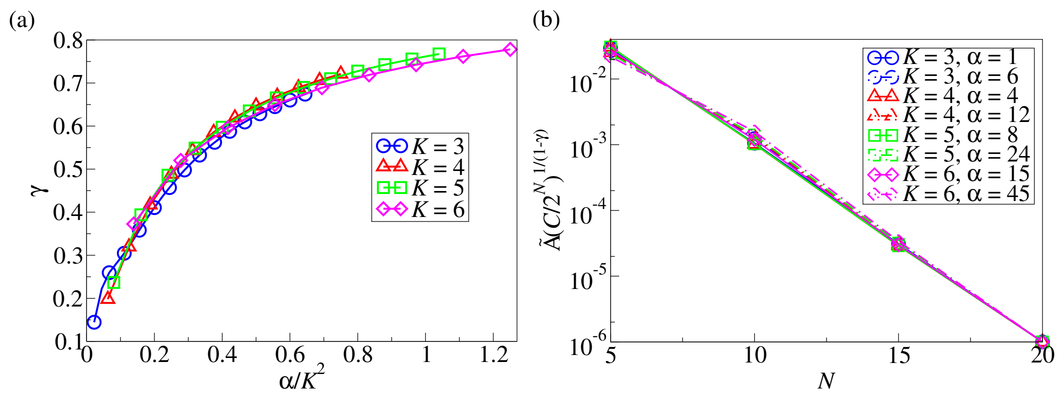

Figure 21. (a) The reduction exponent γ as a function of $\frac{\alpha}{K^2}$ for the $K-$Sat system with different values of $K = 3, 4, 5$ and 6. (b) The scaled ratio $\tilde{A}\left(\frac{C}{2^N}\right)^{\frac{1}{1-\gamma}}$ as a function of N, where $\tilde{A} = A^{\frac{1}{1-\gamma}}$, for different values of K and α.

consistent with the existing understanding of $K-$Sat systems that the structure of the solution space is more complicated in the Hard-SAT phase than that in the Easy-SAT phase at small α (Krzakała et al. 2007; Mézard and Zecchina 2002).

4.3.1 Reduction effect of the CEL

We further investigate the reduction effect of the CEL by studying the number of clusters in the CEL for the $K-$Sat problem with $K = 3, 4, 5$ and 6. Remarkably, as shown in Fig. 21(a), the reduction exponent γ collapses onto a common function of $\frac{\alpha}{K^2}$ for different values of K. The result implies that the reduction effect of decreasing the number of nodes by the clustering in CEL is universal for different values of K, N and α. On the other hand, as shown in Fig. 21(b), the scaled ratio $\tilde{A}\left(\frac{C}{2^N}\right)^{\frac{1}{1-\gamma}}$ collapses onto a common function which decreases exponentially with N, for different values of K and α, which further validates this universal reduction effect. The effect allows us to estimate the total number of clusters in the CEL of a $K-$Sat problem with any given values of K, N and α.

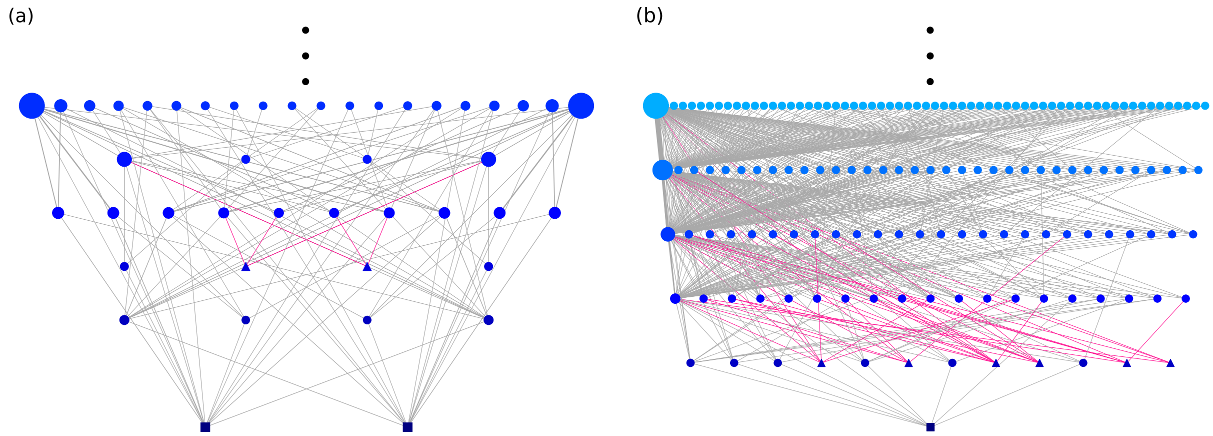

Figure 22. The low-energy part of the exemplar CELs for an instance of (a) spin glasses on a random regular graph with $f_+ = 0.5$ and; (b) $K-$Sat problem with $K = 3$ and $\alpha = 4$. The number of variables in both instances is $N = 15$. The node size corresponds to the number of variable configurations inside the clusters; the global and local minima are shown as squares and triangles respectively; the red links correspond to the connections to the local minima.

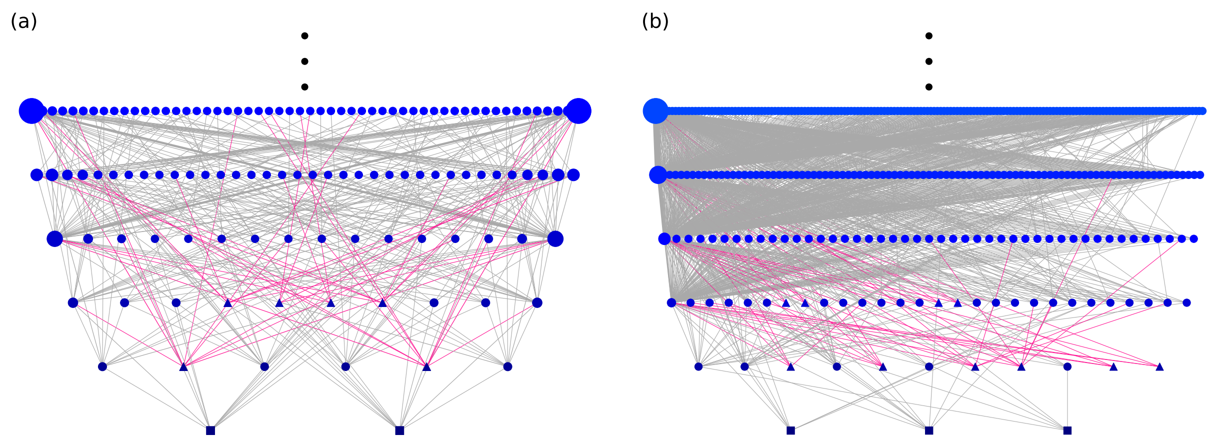

Figure 23. Another example of CELs showing the low-energy part for an instance of (a) spin glasses on a random regular graph with $f_+ = 0.5$ and; (b) $K-$Sat problem with $K = 3$ and $\alpha = 4$. The number of variables in both instances is $N = 20$. The node size corresponds to the number of variable configurations inside the clusters; the global and local minima are shown as squares and triangles respectively; the red links correspond to the connections to the local minima.

4.3.2 Identification of CEL local minima

Besides reducing the size of the energy landscape, another important advantage of CEL is to identify the local minima of the energy landscape. In FEL, it is nontrivial and difficult to identify if a variable configuration is at local minimum, and then we have to prove that all paths connecting the configuration to any other configurations with lower energy must pass through at least one configuration with higher energy. In CEL, since all connected variable configurations that have the same energy are formed into clusters, the CEL with L different levels of energy is indeed a $L-$partite graph, i.e. the CEL can be partitioned into L independent sets by energy, in which every node in the CEL is only connecting to nodes on different energy levels. Therefore, for any nodes in the CEL, the energies of its neighboring nodes can either be higher or lower, and hence the local minima in the CEL are the nodes where all neighbors are of higher energies, which can be identified easily. In the CEL in Fig. 19(b), there exist two local minima with energy $E = 1$ that are shown as triangles as an example. The low-energy part of another exemplar CEL of spin glasses on a random regular graph with $f_+ = 0.5$ and $N = 15$ is shown in Fig. 22(a). Note that for any variable configuration $\vec{s}$ in the spin system, the configurations $\vec{s}$ and $-\vec{s}$ must have the same energy by Eq. (79), which leads to an energy landscape with a symmetric structure as shown in Fig. 22(a), with a pair of local minima of $E = 3$. On the other hand, another example of a $K-$Sat problem with $K = 3$, $N = 15$ and $\alpha = 4$, in which the corresponding CEL consists of six local minima at $E = 1$, is shown in Fig. 22(b). We also show two more CEL examples in Fig. 23 with a larger number of variables N.

Since we can easily identify the local minima in the CEL, we are allowed to study the statistics of local minima. We show in Fig. 20(c) the scaled average number of local minima, $\langle n_{\mathrm{LM}}/N^{K-1}\rangle$, as a function of α, for the $K-$Sat problem with $K = 3$ and different values of N. We observe that the local minima become non-zero and start to rise for $\alpha > \alpha_{\text{LM}} \approxeq 2.5$, suggesting that the system starts to become hard to be solved. This is consistent with the phenomenon that the algorithmic hardness of $K-$Sat systems increases as α increases. Remarkably, as shown in Fig. 20(c), the number of local minima n_{LM} scales with N^{K-1}, suggesting that the scaled number of local minima as a function of α is universal for different system sizes. Furthermore, as shown in Fig. 20(d), we can see that from the probability distribution of n_{LM}/N^{K-1}, as the system size N increases, the distribution becomes narrower, suggesting the larger the system size, the more stable the distribution. We remark that most previous studies on small combinatorial systems with an exhaustive approach focus on the ground states only (Ardelius and Zdeborová 2008), therefore our results are different from these studies and provide a new physical picture about combinatorial optimization problems.

4.4 Markov chain Monte Carlo (MCMC) dynamics through optimization

According to common belief, a probably impractically long time is required for glassy systems to converge to their equilibrium, due to the complex energy landscape that local minima may define (Vincent, Hammann, Ocio, Bouchaud, and Cugliandolo 1997), and yet the full picture of the energy landscape has seldom been studied. Now, the CEL can largely reduce the number of nodes and identify the local minima of glassy systems. Therefore, we are able to reveal the complete non-equilibrium dynamics of these glassy systems which are trapped in the local minima, at an arbitrary temperature for an arbitrarily long time.

Consider a combinatorial system with energy function $\vec{s}$. Following the Boltzmann distribution (HASTINGS 1970; Metropolis, Rosenbluth, Rosenbluth, Teller, and Teller 1953), at equilibrium, the probability that a system is in a variable configuration $\vec{s}$ is given by

$$P(\vec{s}) = \frac{1}{Z} e^{-\beta E(\vec{s})}, \tag{83}$$

where $\beta = 1/T$ is the inverse temperature and $Z = \sum_{\vec{s}} e^{-\beta E(\vec{s})}$ is the normalization constant to ensure that $\sum_{\vec{s}} P(\vec{s}) = 1$. When the system is in its equilibrium, it follows the principle of detailed balance where the transition of variable configurations is reversible. To be precise, consider a reversible Markov process of the transition of configurations, given an equilibrium probability distribution of configurations $\vec{P} = (P_1(\vec{s_1}), P_2(\vec{s_2}), \ldots, P_{2^N}(\vec{s}_{2^N}))$, for any time steps t, and for any two connecting variable configurations $\vec{s_i}$ and $\vec{s_j}$, we have

$$P_i T_{i\to j} = P_j T_{j\to i}, \tag{84}$$

where $T_{i\to j} = P(X_{t+1} = \vec{s_j} | X_t = \vec{s_i})$ is the transition probability and X_t is the configuration of the system at time step t. Then, using the CEL, we can describe the Markov chain Monte Carlo (MCMC) dynamics of the system by formulating the transition probabilities $T_{a\to b}(\beta)$ from a cluster a to another cluster b. Given the inverse temperature β, for any variable configuration $\vec{s_i}$ within the cluster a, with a flip of a single variable, it can either be transiting to its neighboring configurations in a cluster b with probability $T_{a\to b}(\beta)$, or staying at its current cluster with probability $T_{a\to a}(\beta)$ which can be either rejecting the flip or transiting to another configuration with the same cluster a.

Therefore, given the inverse temperature β, the transition probability $T_{a\to b}(\beta)$ for $a \neq b$ is given by

$$T_{a\to b}(\beta) = \frac{w_{ab}}{n_a N}\frac{e^{-\beta\Delta E_{a\to b}}}{e^{-\beta\Delta E_{a\to b}}+1}, \text{ and}$$
$$T_{a\to a}(\beta) = 1 - \sum_{b\in\partial a} T_{a\to b}, \tag{85}$$

where $\Delta E_{a\to b} = E_b - E_a$ is the energy difference between the clusters a and b, and n_a is the number of variable configurations in cluster a. The quantity $n_a N$ is the total possible number of links in the FEL connecting the variable configurations with the cluster a, which includes those links connecting to the configurations within the clusters internally. Therefore, the quantity $w_{ab}/n_a N$ represents the probability of choosing a particular variable to flip, while the quantity $e^{-\beta\Delta E_{a\to b}}/(e^{-\beta\Delta E_{a\to b}}+1)$ is the probability that the flip is accepted, and the system is then transiting from cluster a to b. To reveal the MCMC dynamics, we denote $\vec{P}_t = (P^t_1, P^t_2, \ldots, P^t_C)$ as the probabilities of the system in a variable configuration within different clusters at time step t, and we have

$$\vec{P}_t = \mathcal{T}_\beta \vec{P}_{t-1} = \mathcal{T}^t_\beta \vec{P}_0, \tag{86}$$

where $\mathcal{T}_\beta = [T_{a\to b}(\beta)]_{C\times C}$ for $a, b = 1, 2, \ldots, C$, is the transition probability matrix. We note that if there exists an eigenvalue λ of $\mathcal{T}_\beta$ with $\lambda = 1$ and its corresponding eigenvector is $\vec{P}^*$, then we have $\lambda\vec{P}^* = \vec{P}^* = \mathcal{T}_\beta\vec{P}^*$, and thus the eigenvector $\vec{P}^*$ is the equilibrium probability distribution of configurations for the system. Furthermore, by the matrix decomposition of $\mathcal{T}_\beta$, we have

$$\mathcal{T}_\beta = Q_\beta D_\beta Q^{-1}_\beta, \tag{87}$$

where $D_\beta = \mathrm{diag}(\Lambda_\beta)$ with $\Lambda_\beta = (\lambda_1(\beta), \lambda_2(\beta), \ldots, \lambda_C(\beta))$ and $\lambda_i(\beta)$ is the $i-$th largest eigenvalue of $\mathcal{T}_\beta$, which can be found by spectral analysis, and Q_β is a $C \times C$ matrix in which the $i-$th column is the corresponding eigenvector of $\mathcal{T}_\beta$. Therefore, we can compute $\mathcal{T}_\beta^t$ efficiently by

$$\mathcal{T}_\beta^t = Q_\beta D_\beta^t Q_\beta^{-1}, \tag{88}$$

where $D_\beta^t = \mathrm{diag}(\Lambda_\beta^t)$, with $\Lambda_\beta^t = (\lambda_1^t(\beta), \lambda_2^t(\beta), \ldots, \lambda_C^t(\beta))$. Alternatively, to calculate $\mathcal{T}_\beta^t$, one can first break down into powers of 2, i.e. represents t in the form $\sum_{i=0}^{\lfloor \log_2(t) \rfloor} a_i 2^i$ for some $\{a_i\}_{i=1,\ldots,\lfloor \log_2(t) \rfloor}$, and thus,

$$\mathcal{T}_\beta^t = \prod_{i=0}^{\lfloor \log_2(t) \rfloor} \mathcal{T}_\beta^{a_i 2^i}. \tag{89}$$

Noted that all the terms $\mathcal{T}_\beta^{2^i} = \mathcal{T}_\beta^{2^{i-1}} \cdot \mathcal{T}_\beta^{2^{i-1}}$ can be computed by one induction process with at most $\lfloor \log_2(t) \rfloor$ matrix multiplications being needed. This induction method would be better than the matrix diagonalization method when the eigenvalues of the matrix are too complicated to find. Thus, the term $\mathcal{T}_\beta^t$ in Eq. (86) can be computed easily and efficiently, hence the dynamics $\vec{P}_t$ can be revealed at an arbitrary temperature for an arbitrarily long time, which is out of reach of simulations using modern computational capability.

For any specific instance with an inverse temperature β, we can compute the eigenvalues of the transition probability matrix $\mathcal{T}_\beta$ as described above, and we denote $\lambda_i(\beta)$ to be the $i-$th largest eigenvalue of $\mathcal{T}_\beta$. The first ten eigenvalues $\lambda_1(\beta), \lambda_2(\beta), \ldots, \lambda_{10}(\beta)$, for different inverse temperature β for the instances of spin glass and $3-$Sat shown in Fig. 22(a) and (b) are shown in Fig. 24(a) and (b), respectively. Interestingly, due to the symmetric structure of the energy landscape, we

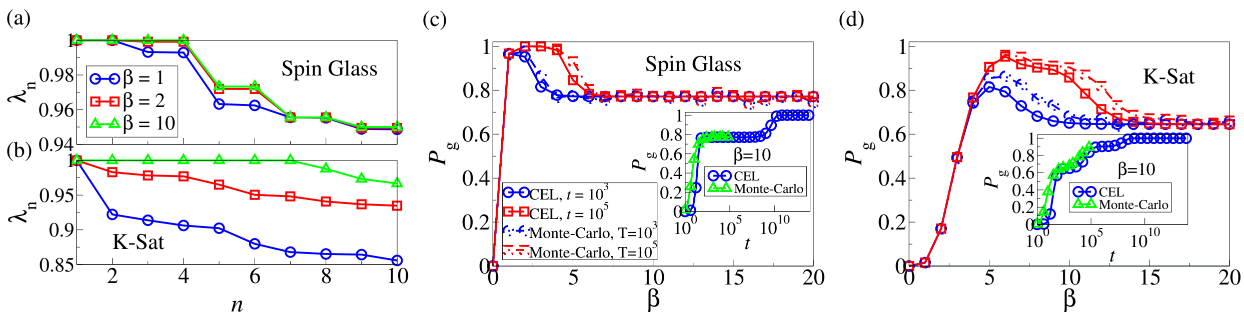

Figure 24. (a, b) The first ten eigenvalues $\lambda_1(\beta), \lambda_2(\beta), \ldots, \lambda_{10}(\beta)$ of the transition probability matrix $\mathcal{T}_\beta$, with different values of $\beta = 1, 2, 10$, of the spin glass and the 3−Sat problem instances shown in Fig. 22(a) and (b) respectively. (c, d) The corresponding probability of finding the ground states, P_g, of the instances as a function of β, obtained by Eq. (86), for $t = 10^3$ and 10^5 iteration steps, compared with the MCMC simulation results. Insets: The time series of P_g.

can see that the eigenvalues of the spin glass instance are in pairs. Another interesting result is that the λ_i differ more when β is small, while some eigenvalues after λ_1 are approaching 1 as β increases. The number of λ_i approaching 1 is equal to the number of local minima in the CEL of the corresponding instance. In particular, in the spin glass instance, λ_3 and λ_4 correspond to the two symmetric local minima at $E = 3$ in Fig. 22(a). On the other hand, in the 3−Sat instance, λ_2 to λ_7 correspond to the six local minima at $E = 1$ in Fig. 22(b). That the eigenvalues are approaching 1 as β increases also implies that trapping of MCMC dynamics in local minima are increasing, similar to the trapping in global minima in which the corresponding eigenvalue $\lambda_1 = 1$. This raises an important question as to whether at zero temperature as $\beta \to \infty$, the equilibrium of the system is at the ground states. It is because $\lambda_i \to 1$ at the local minima as $\beta \to \infty$, which is equivalent to the largest eigenvalue $\lambda_1 = 1$ at the ground states, and hence the equilibrium condition $\vec{P'} = \mathcal{T}_\beta \vec{P'}$ is satisfied for any $\vec{P'} = (P'_1, \ldots, P'_C)$ with $\sum_{i=1}^{C} P'_i = 0 = 1$ and $P'_i = 0$ for all clusters i that are not local and global minima.

With the transition probability matrix and using Eq. (86), we can compute the complete dynamics at any given inverse temperature for an arbitrarily long time. Starting with a uniform distribution $\vec{P}_0$, i.e. $P_i = 1/C$ for all clusters i, we obtain the probability P_g being in the ground states after $t = 10^3$ and 10^5 iteration steps as a function of β, for the spin glass and $3-$Sat instances, as shown in Fig. 24(c) and (d) respectively. As expected, we observe that P_g firstly increases as β increases, but remarkably P_g decreases when β further increases, which is due to the trapping of local minima. We further notice that, for a given fixed β, P_g after $t = 10^5$ iterations is higher than that after 10^3. The MCMC simulation results are in good agreement with the theoretical predictions by CEL and Eq. (86). These results suggest that given a random initial condition, the trapping of dynamics at the local minima becomes more significant as the inverse temperature β increases after some specific values, implying that it is more difficult to locate the ground states within a short period of time.

We show the time series of P_g in the insets of Fig. 24(c) and (d) to further investigate the trapping of dynamics at the local minima, and we can see that P_g increases with t as expected. Nevertheless, multiple jumps and plateaus are observed as P_g increases, suggesting that the local minima are trapping the system and occupying some probability, but these trappings start to vanish at different time steps t at which P_g starts to increase again. This phenomenon can be explained by the eigenvalues of the transition probability matrix $\mathcal{T}_\beta$. Note that the eigenvalues $\lambda_i(\beta)$ of the local minima are close to 1 and the value of $\lambda_i^t(\beta)$ is sufficiently less than 1 only when t is sufficiently large, which can stop the trapping of local minima. This also suggests that the values of $\lambda_i(\beta)$ of the local minima are affecting their ability in trapping the system, in which the values may depend on the network topology of the CEL. The closer $\lambda_i(\beta)$ is to 1, the trapping effect of the local minima is stronger and, hence, by examining $\lambda_i(\beta)$, one can estimate the characteristics of the system.

To further validate our theory, we show another instance of a $3-$Sat problem in the Easy-Sat phase having a simple CEL in Fig. 25, which is contrary to the cases we showed in the above. We can

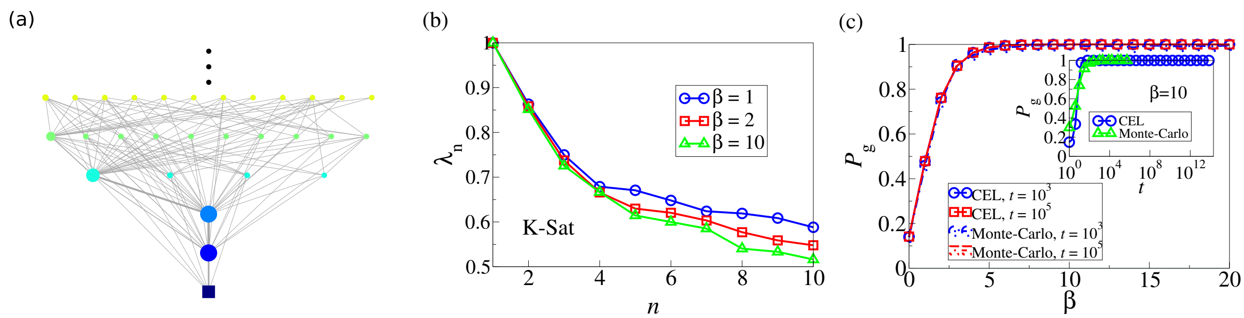

Figure 25. (a) The low-energy part of a less complex CEL for an instance of a 3−Sat problem with $\alpha = 1$ that is in the Easy-Sat phase. (b) The corresponding first ten eigenvalues $\lambda_1(\beta), \ldots, \lambda_{10}(\beta)$ of the transition probability matrix $\mathcal{T}_\beta$, with different values of $\beta = 1, 2, 10$. (c) The corresponding probability of finding the ground states, P_g, of the instances as a function of β, obtained by Eq. (86), for $t = 10^3$ and 10^5 iteration steps, compared with the MCMC simulation results. Insets: The time series of P_g.

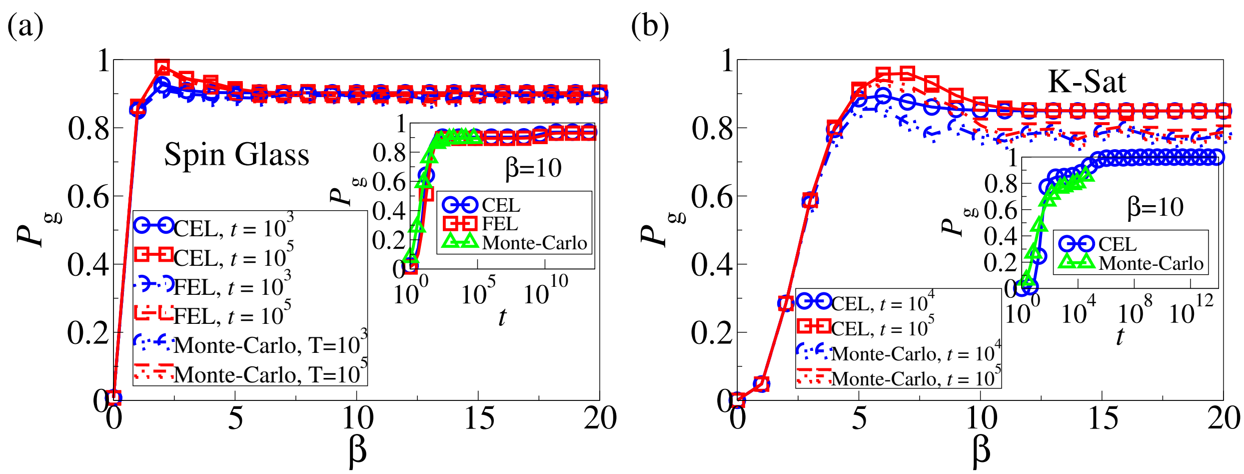

Figure 26. The sample averaged probability P_g of finding the ground states as a function of the inverse temperature β, obtained by Eq. (86), for $t = 10^4$ and 10^5 iteration steps, compared with the MCMC simulation results for (a) both CEL and FEL of the spin glass on random regular graphs with $N = 10$ and $f_+ = 0.5$, and (b) 3-Sat problems with $N = 15$ and $\alpha = 4$.

see that in Fig. 25(b), for an instance without local minima, only the largest eigenvalue $\lambda_1 = 1$ and the next eigenvalues will not approach 1 as β increases, as shown in Fig. 25(b). Furthermore, as shown in Fig. 25(c), we notice that P_g is a strictly increasing function with β; and the time series of P_g is also strictly increasing with t without any jump and plateau, as shown in the inset. These results imply that the existence of local minima is the key to the trapping of the MCMC dynamics. On the other hand, we also show the sample averaged results for both the theoretical predictions by Eq. (86) and MCMC simulations in Fig. 26, showing that the sample averaged P_g exhibits similar behavior to that we observed in the single instances, and the theoretical predictions obtained from CEL, FEL and the sample averaged MCMC simulation results are in good agreement, including the jumps and plateaus in the time series of P_g, and the drop of P_g with β, while the differences between the MCMC simulations and the theoretical predictions may come from the mean-field nature of the transition probability within the clusters in Eq. (86).

4.4.1 Implications for simulated annealing

Aside from revealing the non-equilibrium dynamics, the eigenvalues of the transition probability matrix $\mathcal{T}_\beta$ from the CEL also have implications for the importance of the cooling schedule in simulated annealing (SA) (Kirkpatrick, Gelatt, and Vecchi 1983). SA is a physics-inspired meta-heuristic algorithm to find the global optimal configuration of a system by gradually decreasing the temperature. At each step, the SA heuristic compares the energies between the current variable configuration $\vec{s}$ and the neighboring configuration $\vec{s'}$ after flipping one variable, respecting the detailed balance condition, and the system is transiting to $\vec{s'}$ with probability $e^{-\beta\left(E(\vec{s'})-E(\vec{s})\right)}$ or else staying at the current configuration. The temperature is decreasing throughout the iterating process and, in general, it is believed that the system is converging to the global optimal configuration after an extended iteration time.

Recall that as in Fig. 24(c) and (d), the system can identify the global minima from the local minima when β is small, in which the differences among the eigenvalues are large enough that λ_1 of the global minima are much larger than the λ_i of the local minima. Nevertheless, the differences between the eigenvalues decrease as β increases, regardless of the initial condition, implying that the global and local minima are similar in nature. Starting from a high temperature in SA, the system is not in a randomly selected configuration at each cooling stage. Instead, throughout the cooling process, the system is biased towards the global minima induced by the difference between the largest eigenvalue λ_1 and the other eigenvalues λ_i of the local minima, in which the difference diminishes as the temperature decreases. This suggests that comparing with the fixed-temperature non-equilibrium dynamics, SA is more effective in identifying the global optimal variable configuration. Nevertheless, if the system is trapped in a local minimum configuration, further cooling in SA only lowers the transiting probability, which is unable to help the system escape from the trapping. To escape from the local minima in the dynamics, one may only rely on an extremely slow cooling schedule, which is computationally infeasible. Remarkably, since we are able to obtain the optimal value of β when the probability P_g is maximum in the non-equilibrium dynamics, one can design a cooling schedule based on this optimal β to boost the crossing of the energy barrier. For instance, the cooling schedule can increase from $\beta = 0$ and stop at the optimal β for a long period of time until a solution is found. Therefore, the transition probability matrix $\mathcal{T}_\beta$ from the CEL and the eigenvalue analysis we discussed provide a new set of tools, allowing us to study the trapping of local minima in both the non-equilibrium dynamics and the dynamics in SA analytically, in order to accelerate the energy barrier crossing.

4.4.2 Other applications revealing non-equilibrium dynamics of glassy systems

We remark that revealing the CEL and the non-equilibrium dynamics of a glassy system is not limited to finding the probability of being in the ground states. Indeed, since the probabilities and the energies of all states are known, one can measure any extra quantities in the non-equilibrium dynamics at finite temperature, such as the average energy and the magnetization of the system. In particular, since all states a_i within the cluster a have the same energy E_a and hence the probabilities of being in these states are all identical, i.e. the probability being in each state within the cluster is equal to P_a/n_a. This convenient property allows us to measure any physical quantities of a glassy system simply by obtaining the expected value of the mean value of clusters. For instance, the average energy of the system $\langle E \rangle$ can be found by

$$\langle E \rangle = \sum_i P_i E_i = \sum_a \sum_{a_i} P_{a_i} E_{a_i} = \sum_a P_a E_a. \tag{90}$$

Taking magnetization as another example, the magnetization m can be evaluated by

$$m = \frac{1}{N} \sum_i P_i ||\vec{s}_i|| = \frac{1}{N} \sum_a \sum_{a_i} P_{a_i} ||\vec{s}_{a_i}|| = \frac{1}{N} \sum_a P_a \sum_{a_i} \frac{||\vec{s}_{a_i}||}{n_a} = \frac{1}{N} \sum_a P_a \langle ||\vec{s}|| \rangle_a , \tag{91}$$

where $||\vec{s}_i|| = \sum_{j=1}^{N} s_j^i$ and $\langle ||\vec{s}|| \rangle_a$ is the average value of $||\vec{s}_{a_i}||$ of all states a_i in the cluster a. Therefore, the method of revealing CEL and the non-equilibrium dynamics not only aims at finding the probability of being in ground states, but also able to access various physical quantities using the probabilities of being at different clusters.

4.5 Partial coarse-grained energy landscape (PCEL)

For systems with large variable size N, it becomes infeasible to compute the CEL of the system since there are in total 2^N variable configurations to examine. Instead of the complete CEL, we introduce a method to obtain the partial-grained energy landscape (PCEL) for large systems, which focuses on the configurations with low energies. In this method, variable configurations are sampled in the MCMC simulations of the non-equilibrium dynamics at a given sampling inverse temperature

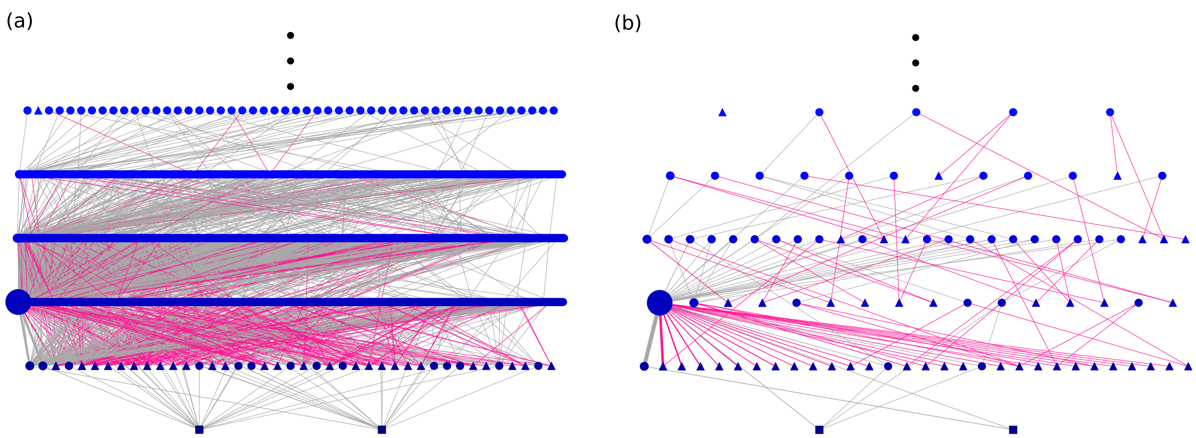

Figure 27. (a) An example of PCEL showing the low-energy part for a 3-Sat problem instance with variable size $N = 50$ and $\alpha = 4$, configurations are sampled with $T = 10^5$ at $\beta_s = 5$ with 10 restarts. (b) The corresponding simplified PCEL which keeps only one of the shortest paths between any two minima. The node size corresponds to the number of variable configurations inside the clusters; the global and local minima are shown as squares and triangles respectively; the red links correspond to the connections to the local minima.

β_s for a given time steps T, then the sampling process is restarted with randomly selected initial conditions for multiple rounds. All the sampled variable configurations are recorded and the PCEL is constructed with these configurations, following the same procedures as in CEL. Thus, any specific part of the landscape can be extracted by choosing a suitable value of β_s. For instance, with moderately large β_s, we can extract the low-energy part of the energy landscape.

Note that the PCEL is only an approximation of the energy landscape by MCMC simulations with finite time T which can only sample a small fraction of all 2^N configurations, and even the number of configurations sampled can already be much larger than the number of configurations examined for small systems we showed above. Moreover, some clusters of the same energy in the PCEL may be contained in a larger cluster because some of the intermediate configurations between two clusters can be unvisited in the MCMC simulation. An example of PCEL showing the low-energy

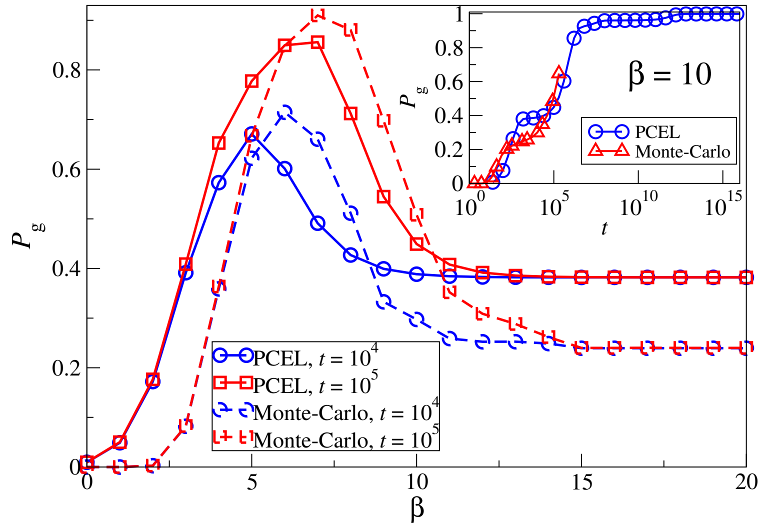

Figure 28. The probability P_g of finding the ground state as a function of β for the 3-Sat problem instance in which the simplified PCEL is shown in Fig. 27. The theoretical predictions are obtained by Eq. (86) with the transition probability matrix from the simplified PCEL sampled with $T = 10^5$ at $\beta_s = 5$ with 10 restarts, for $t = 10^4$ and 10^5 iteration steps, compared with the simulation results. Insets: the time series of P_g, where the time t in the theoretical predictions are multiplied by the factor $\ln\left(\frac{2^N}{n(\vec{s}_{\mathrm{PCEL}})}\right)$ where $n(\vec{s}_{\mathrm{PCEL}})$ is the number of variable configurations in the PCEL, in order to rescale the size between the PCEL and the original system.

part for a 3-Sat problem instance with $N = 50$ is shown in Fig. 27(a). Since the glassy behaviors of the non-equilibrium dynamics are mainly contributed by the global and local minima as we discussed above, we further simplify the energy landscape by leaving only a single shortest path between minima in the PCEL to obtain a simplified transition probability matrix $\tilde{\mathcal{T}}_\beta$ and a simplified PCEL as shown in Fig. 27(b). In our studies, we found that the results obtained by $\tilde{\mathcal{T}}_\beta$ are similar to the results without simplification.

We remark that the major advantage of analyzing the dynamics of the systems by PCEL is that one can obtain the dynamics of the system at any temperature and for any arbitrarily long iteration time that is out of the reach of simulations, by simply obtaining the PCEL with a single MCMC

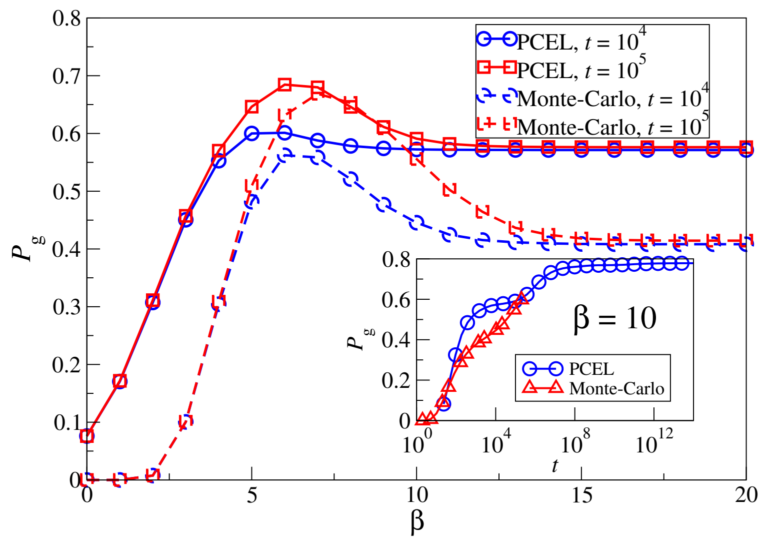

Figure 29. The sample averaged probability P_g of finding the ground state as a function of β, for the 3-Sat problems with $N = 50$ and $\alpha = 4$, obtained by Eq. (86) with the transition probability matrix from the simplified PCEL sampled with $T = 10^5$ at $\beta_s = 5$ with 10 restarts, for $t = 10^4$ and 10^5 iteration steps, averaged over 50 realizations, compared with the MCMC simulation results. Insets: the time series of the sample averaged P_g, where the time t in the theoretical predictions are multiplied by the factor $\ln\left(\frac{2^N}{n(\vec{s}_{\text{PCEL}})}\right)$ where $n(\vec{s}_{\text{PCEL}})$ is the number of variable configurations in the PCEL.

procedure at a single sampling temperature β_s. We show in Fig. 28 the non-equilibrium dynamics of an instance of a 3−Sat problem with $N = 50$ and $\alpha = 4$, which is obtained by Eq. (86) with the transition probability matrix from the simplified PCEL shown in Fig. 27 sampled at a single $\beta_s = 5$. Since the number of variable configurations sampled in the PCEL, denoted as $\vec{s}_{\text{PCEL}}$, is just a small portion of all 2^N variable configurations in the original system, the non-equilibrium dynamics using the corresponding transition probability matrix would be much faster than that of the original system as there are much fewer possible transitions between clusters. Thus, to compare the theoretical predictions with the MCMC simulations, we rescale the time series of the theoretical predictions by multiplying the time t by the factor $\ln\left(\frac{2^N}{n(\vec{s}_{\text{PCEL}})}\right)$. As we can see in Fig. 28, the theoretical and simulation results are in good agreement for different values of β except when β is small, which is because the sampling of PCEL focuses on the variable configurations with low energies and high-energy configurations are explored when β is small. Remarkably, as is the case in small systems, the same phenomenon can be observed in the non-equilibrium dynamics obtained using PCEL for large systems, in which: (1) P_g firstly increases then decreases as the inverse temperature increases; and (2) multiple jumps and plateaus exist in the time series of P_g. We also show in Fig. 29 the corresponding sample averaged P_g against β, and we can see that similar behaviors are observed as the case in the single instance. These results imply that the findings in small systems obtained using the CEL can also be observed using the PCEL in large systems. This shows that CEL and PCEL provide a new set of tools and a platform for revealing the non-equilibrium dynamics over an arbitrary long time for combinatorial systems.

4.6 Limitations of the CEL and PCEL

Although in our example, the PCEL works very well in the cases of systems with $N = 50$, it might not be the case in extreme large systems containing millions of variables. When the number of variables is large, the number of total possible configurations will be extremely large. In such cases, even though the number of configurations sampled in the MCMC simulations is very large, it would still be a very small portion of all total possible configurations. Thus the PCEL constructed would only be a small part of the whole energy landscape and the non-equilibrium dynamics obtained might not be representing the true system. To tackle this problem, one has to design a method to create a PCEL that can represent the whole picture of the true energy landscape, which will be one of the directions in our future studies.

Another disadvantage of our proposed methods is that the CEL and PCEL can only work on combinatorial systems with discrete energy functions. Note that to construct the CEL, one has to group the connected configurations with the same energy into the same cluster. Nevertheless, if the energy function is a continuous function, then it is almost impossible to find two connected configurations with the same energy and hence it is very difficult to construct a CEL with high size reduction effect. Similarly, for any systems in which the variables are not discrete, it is also very difficult to construct the FEL and CEL.

4.7 Summary

In this chapter, we introduced a method to reveal the complete energy landscapes of combinatorial systems with small size, namely the coarse-grained energy landscape (CEL). This novel method provides advantages not only in exploring the energy landscape, but also provides a new understanding of glassy systems. The innovative part of the method is that by obtaining the transition probability matrix using the CEL of the system, we can obtain the non-equilibrium dynamics of the system analytically at any arbitrary temperature for any arbitrary time steps, which is computationally infeasible by MCMC simulations. On the other hand, to tackle the problem of too many configurations in large systems, we propose a variant of the CEL approach to reveal the partial coarse-grained energy landscape (PCEL) by single MCMC simulation at a single sampling temperature, in which the same analysis as in the small systems can also be done.

In terms of providing new understanding, our method unveils the complete physical picture about how glassy systems are trapped in local minima, including the property that the probability of finding the ground states decreases as temperature increases, as well as the existence of jumps and plateaus in the time series of the ground states probability. To conclude, our method contributes a new set of tools to analyze the non-equilibrium dynamics of complex systems at any temperature for any long period of time, allowing us to obtain new understandings and insights theoretically that existing methods are computationally unable to provide.

Chapter 5: Conclusion

In this thesis, we applied knowledge and techniques from statistical physics to study two interdisciplinary problems. In particular, we studied the problem of selfish routing over optimized transportation networks in Chapters 2 and 3, and we studied the problem of revealing the complete energy landscape of disordered systems in Chapter 4.

In the first part of the thesis, we studied transportation systems in which some selfish users choose alternative routes that minimize their own costs instead of following the optimal configuration of paths suggested to them. We derived two theoretical two-stage message-passing frameworks by employing the cavity method developed for studying spin glasses (Mézard and Zecchina 2002) to study the impact and behaviors of selfish rerouting in the system. The frameworks are the two-stage cavity method followed by probabilistic modeling, and the two-stage exhaustive cavity method. The former approach captures the rerouting behaviors and impacts of the rerouting of selfish users using a probability estimation in which the energy functions can be relatively simple in terms of computational complexity. Therefore, the method is capable of studying systems of large size with a good estimate of trends and features. On the other hand, the exhaustive cavity method derived exhaustive energy functions which measure the detailed routing decisions of every user before and after rerouting accurately, and thus can provide precise measurements of the impacts and behaviors of selfish rerouting, as well as carrying out correlation analysis. Nevertheless, the computational complexity is extremely high and only small systems can be studied. Therefore, we provide two sets of tools that serve different needs, and it is a trade-off between system size and precision for choosing which method to use.

Using both methods, we demonstrated how they can be applied to study the impacts of selfish rerouting on various groups of users, including the compliant users, selfish users and the whole system. In particular, we showed that over uncoordinated transportation networks, a small fraction of selfish users are beneficial to the whole system. Interestingly, we discovered that compliant users always gain in the uncoordinated transportation network and selfish users may gain under some conditions in the optimized systems. We also showed that the discrepancies between the results obtained by the probabilistic modeling approach and the simulation results come from the highly correlated routing behaviors between selfish users, which are assumed to be independent in the probabilistic modeling approach. We remark that the cavity methods we presented are not limited to considering two steps of dynamics; one can extend the frameworks by introducing more layers of energy functions to fit the use of other problems. Furthermore, they can be generalized to study iterative game-theoretical problems by deriving new mathematical models and the corresponding energy functions.

Next, we extended this single round selfish rerouting problem into the scenario of multiple rounds selfish rerouting, and this problem was studied via simulations. We showed that when the fraction of selfish users and the vehicle density are small, the system can easily converge to its Nash equilibrium after multiple rounds of selfish rerouting, in which the social cost is close to the global optimum.

In the second part of the thesis, we focused on studies of the energy landscapes of glassy systems, including the spin glasses and $K-$satisfiability problems. While various conventional approaches omit some features of the energy landscape, such as the connectivity between configurations or the dimensions of the configuration space are reduced, we proposed methods using the techniques of grouping connecting configurations with the same energy to obtain the coarse-grained energy landscape (CEL) for small systems and the partial coarse-grained energy landscape (PCEL) for large systems. Such methods can completely reveal the landscape, showing the detailed connectivity of each cluster and identifying the local minima. Furthermore, using the CEL and PCEL, we derived the transition probability matrix analytically, allowing us to reveal the non-equilibrium dynamics of glassy systems at any temperature and for any extended time that would be infeasible via simulations. Additionally, we provided a new understanding of how glassy systems are trapped by the local minima in the non-equilibrium dynamics. We found that below the suitable range of temperature, the probability of finding the ground states decreased as the temperature further decreased. Remarkably, by revealing the whole non-equilibrium dynamics, we observed jumps and plateaus in the time series of the ground states probability, which may be caused by the trapping of local minima. We remark that the contribution of this work is not limited to providing new physical pictures about $K-$satisfiability and spin glasses; more importantly, this research provides a new set of tools to study complex disordered systems which can generate results and insights that are currently computationally infeasible by simulations.

In conclusion, two interdisciplinary problems were studied in this thesis using the techniques and knowledge developed in statistical physics. The cavity method, originally developed for studying spin glasses, is employed in the first problem to reveal the impact of selfish rerouting in transportation systems. In the second problem, we introduced a set of tools that can be used to study complex disordered systems including spin glasses, and showed how the non-equilibrium dynamics are trapped by the local minima, which can be applied to any combinatorial systems. All these studies show how the techniques and knowledge from statistical physics can be broadly applied to problems in different areas, and the newly developed results can also provide fresh understanding in the conventional fields of physics.

References

Anshelevich, E., & Ukkusuri, S. 2009. Equilibria in dynamic selfish routing. In *International symposium on algorithmic game theory* (pp. 171–182).

Ardelius, J., & Zdeborová, L. 2008. Exhaustive enumeration unveils clustering and freezing in the random 3-satisfiability problem. *Physical Review E*, *78*(4), 040101.

Ballard, A. J., Das, R., Martiniani, S., Mehta, D., Sagun, L., Stevenson, J. D., & Wales, D. J. 2017. Energy landscapes for machine learning. *Physical Chemistry Chemical Physics*, *19*(20), 12585–12603.

Barbehenn, M. 1998. A note on the complexity of dijkstra's algorithm for graphs with weighted vertices. *IEEE transactions on computers*, *47*(2), 263.

Bayati, M., Borgs, C., Braunstein, A., Chayes, J., Ramezanpour, A., & Zecchina, R. 2008a. Statistical mechanics of steiner trees. *Physical review letters*, *101*(3), 037208.

Bayati, M., Borgs, C., Braunstein, A., Chayes, J., Ramezanpour, A., & Zecchina, R. 2008b, Jul. Statistical mechanics of steiner trees. *Phys. Rev. Lett.*, *101*, 037208. Retrieved from `https://link.aps.org/doi/10.1103/PhysRevLett.101.037208` doi: 10.1103/PhysRevLett.101.037208

Becker, O. M., & Karplus, M. 1997. The topology of multidimensional potential energy surfaces: Theory and application to peptide structure and kinetics. *The Journal of chemical physics*, *106*(4), 1495–1517.

Biswas, K., & Katzgraber, H. G. 2020. Adding color: Visualization of energy landscapes in spin glasses. *arXiv preprint arXiv:2004.12431*.

Bollobás, B. 2001. *Random graphs* (2nd ed.) (No. 73). Cambridge University Press.

Buldyrev, S., Dokholyan, N., Goldberger, A., Havlin, S., Peng, C.-K., Stanley, H., & Viswanathan, G. 1998. Analysis of dna sequences using methods of statistical physics. *Physica A: Statistical Mechanics and its Applications*, *249*(1-4), 430–438.

Cao, Y., Ding, L., Wang, G., Bao, Z., & Han, Z. 2009. Analysis on cascading failure and self-organized criticality in evolving power grids. *Autom Electr Power Syst*, *33*(5), 1–6.

Cole, R., Dodis, Y., & Roughgarden, T. 2006. How much can taxes help selfish routing? *Journal of Computer and System Sciences*, *72*(3), 444–467.

Correa, J. R., Schulz, A. S., & Stier-Moses, N. E. 2004. Selfish routing in capacitated networks. *Mathematics of Operations Research*, *29*(4), 961–976.

Directorate-General for Mobility and Transport. 2021. *Clean transport, urban transport, urban mobility.* https://ec.europa.eu/transport/themes/urban/urban_mobility_en.

Dobrin, R., & Duxbury, P. M. 2001, May. Minimum spanning trees on random networks. *Phys. Rev. Lett.*, *86*, 5076–5079. Retrieved from https://link.aps.org/doi/10.1103/PhysRevLett.86.5076 doi: 10.1103/PhysRevLett.86.5076

Erdös, P., & Rényi, A. 1959. On random graphs i. *Publicationes Mathematicae Debrecen*, *6*, 290.

Ferguson, T. S. 2020. *A course in game theory*. World Scientific.

Fischer, S., & Vöcking, B. 2004. On the evolution of selfish routing. In *European symposium on algorithms* (pp. 323–334).

Fotakis, D., Kontogiannis, S., Koutsoupias, E., Mavronicolas, M., & Spirakis, P. 2002. The structure and complexity of nash equilibria for a selfish routing game. In *International colloquium on automata, languages, and programming* (pp. 123–134).

Gabrié, M., Dani, V., Semerjian, G., & Zdeborová, L. 2017. Phase transitions in the q-coloring of random hypergraphs. *Journal of Physics A: Mathematical and Theoretical*, *50*(50), 505002.

Gō, N. 1983. Protein folding as a stochastic process. *Journal of Statistical Physics*, *30*(2), 413–423.

HASTINGS, W. 1970. Monte carlo sampling methods using markov chains and their applications. *Biometrika*, *57*(1), 97–109.

Highways agency network journey time and traffic flow data. 2018. (https://data.gov.uk/dataset/)

Kirkpatrick, S., Gelatt, C. D., & Vecchi, M. P. 1983. Optimization by simulated annealing. *science*, *220*(4598), 671–680.

Krivov, S. V., & Karplus, M. 2004. Hidden complexity of free energy surfaces for peptide (protein) folding. *Proceedings of the National Academy of Sciences*, *101*(41), 14766–14770.

Krzakała, F., Montanari, A., Ricci-Tersenghi, F., Semerjian, G., & Zdeborová, L. 2007. Gibbs states and the set of solutions of random constraint satisfaction problems. *Proceedings of the National Academy of Sciences*, *104*(25), 10318–10323.

Lei, J., & Huang, K. 2010. Protein folding: A perspective from statistical physics. *arXiv preprint arXiv:1002.5013*.

Lien, J. W., Mazalov, V. V., Melnik, A. V., & Zheng, J. 2016. Wardrop equilibrium for networks with the bpr latency function. In *International conference on discrete optimization and operations research* (pp. 37–49).

Lokhov, A. Y., Mézard, M., Ohta, H., & Zdeborová, L. 2014. Inferring the origin of an epidemic with a dynamic message-passing algorithm. *Physical Review E*, *90*(1), 012801.

Lokhov, A. Y., & Saad, D. 2017. Optimal deployment of resources for maximizing impact in spreading processes. *Proceedings of the National Academy of Sciences*, *114*(39), E8138–E8146.

Malik, S., & Zhang, L. 2009. Boolean satisfiability from theoretical hardness to practical success.

Communications of the ACM, *52*(8), 76–82.

Marino, R., Parisi, G., & Ricci-Tersenghi, F. 2016. The backtracking survey propagation algorithm for solving random k-sat problems. *Nature communications*, *7*(1), 1–8.

Mead, A. 1992. Review of the development of multidimensional scaling methods. *Journal of the Royal Statistical Society: Series D (The Statistician)*, *41*(1), 27–39.

Metropolis, N., Rosenbluth, A. W., Rosenbluth, M. N., Teller, A. H., & Teller, E. 1953. Equation of state calculations by fast computing machines. *The journal of chemical physics*, *21*(6), 1087–1092.

Mézard, M., Parisi, G., & Virasoro, M. 1987a. Sk model: The replica solution without replicas. *SPIN GLASS THEORY AND BEYOND: AN INTRODUCTION TO THE REPLICA METHOD AND ITS APPLICATIONS. Edited by MEZARD M ET AL. Published by World Scientific Press*, 232–237.

Mézard, M., Parisi, G., & Virasoro, M. A. 1987b. *Spin glass theory and beyond: An introduction to the replica method and its applications* (Vol. 9). World Scientific Publishing Company.

Mézard, M., & Zecchina, R. 2002. Random k-satisfiability problem: From an analytic solution to an efficient algorithm. *Physical Review E*, *66*(5), 056126.

Nesti, T., Sloothaak, F., & Zwart, B. 2020. Emergence of scale-free blackout sizes in power grids. *Physical Review Letters*, *125*(5), 058301.

Nishimori, H. 2001. *Statistical physics of spin glasses and information processing: an introduction*. Oxford; New York: Oxford University Press.

Noh, J. D., & Rieger, H. 2002, Dec. Stability of shortest paths in complex networks with random edge weights. *Phys. Rev. E*, *66*, 066127. Retrieved from https://link.aps.org/doi/10.1103/PhysRevE.66.066127 doi: 10.1103/PhysRevE.66.066127

Osborne, M. J., & Rubinstein, A. 1994. *A course in game theory*. MIT press.

Pastor-Satorras, R., & Vespignani, A. 2001. Epidemic spreading in scale-free networks. *Physical review letters*, *86*(14), 3200.

Po, H. F., & Yeung, C. H. 2021. Complete realization of energy landscape and non-equilibrium trapping dynamics in spin glass and optimization problem. *(submitted to Physical Review Letters and under review), arXiv preprint arXiv:2106.05330*.

Po, H. F., Yeung, C. H., & Saad, D. 2021. Futility of being selfish in optimized traffic. *Physical Review E*, *103*(2), 022306.

Po, H. F., Yeung, C. H., Zeng, A., & Wong, K. M. 2017. Evolving power grids with self-organized intermittent strain releases: An analogy with sandpile models and earthquakes. *Physical Review E*, *96*(5), 052312.

Prato, C. G. 2009. Route choice modeling: past, present and future research directions. *Journal of choice modelling*, *2*(1), 65–100.

Ricci-Tersenghi, F., & Semerjian, G. 2009. On the cavity method for decimated random constraint satisfaction problems and the analysis of belief propagation guided decimation algorithms. *Journal of Statistical Mechanics: Theory and Experiment*, *2009*(09), P09001.

Roughgarden, T., & Tardos, É. 2002. How bad is selfish routing? *Journal of the ACM (JACM)*, *49*(2), 236–259.

Sella, G., & Hirsh, A. E. 2005. The application of statistical physics to evolutionary biology. *Proceedings of the National Academy of Sciences*, *102*(27), 9541–9546.

Sherrington, D., & Kirkpatrick, S. 1975. Solvable model of a spin-glass. *Physical review letters*, *35*(26), 1792.

Shiftan, Y., Bekhor, S., & Albert, G. 2011. Route choice behaviour with pre-trip travel time information. *IET intelligent transport systems*, *5*(3), 183–189.

United States. Bureau of Public Roads. 1964. *Traffic assignment manual for application with a large, high speed computer* (Vol. 37). Washington, D.C. : U.S. Department of Commerce, Bureau of Public Roads, Office of Planning, Urban Planning Division : For sale by the Superintendent of Documents, U.S. Government Printing Office.

Vincent, E., Hammann, J., Ocio, M., Bouchaud, J.-P., & Cugliandolo, L. F. 1997. Slow dynamics and aging in spin glasses. In *Complex behaviour of glassy systems* (pp. 184–219). Springer.

Xu, Y.-Z., Po, H. F., Yeung, C. H., & Saad, D. 2021a. Scalable node-disjoint and edge-disjoint multi-wavelength routing. *(submitted to Physical Review X and under review). arXiv preprint arXiv:2107.00609*.

Xu, Y.-Z., Po, H. F., Yeung, C. H., & Saad, D. 2021b. Scalable node-disjoint and edge-disjoint multi-wavelength routing. *arXiv preprint arXiv:2107.00609*.

Yeung, C. H. 2019. Coordinating dynamical routes with statistical physics on space-time networks. *Physical Review E*, *99*(4), 042123.

Yeung, C. H., & Saad, D. 2012. Competition for shortest paths on sparse graphs. *Physical review letters*, *108*(20), 208701.

Yeung, C. H., Saad, D., & Wong, K. M. 2013. From the physics of interacting polymers to optimizing routes on the london underground. *Proceedings of the National Academy of Sciences*, *110*(34), 13717–13722.

Yeung, C. H., Wong, K. M., & Li, B. 2014. Coverage versus supply cost in facility location: Physics of frustrated spin systems. *Physical Review E*, *89*(6), 062805.

Zdeborová, L., & Krząkała, F. 2007. Phase transitions in the coloring of random graphs. *Physical Review E*, *76*(3), 031131.